NEWDUMP

Nuclear Energy Waste Disposal Using Massdriver Propulsion

A Student Design Project
Department of Aerospace Engineering
The University of Michigan
Winter Term 1979

Cover drawn by Dennis Melvin

enm

UNR8150

PROJECT PERSONNEL

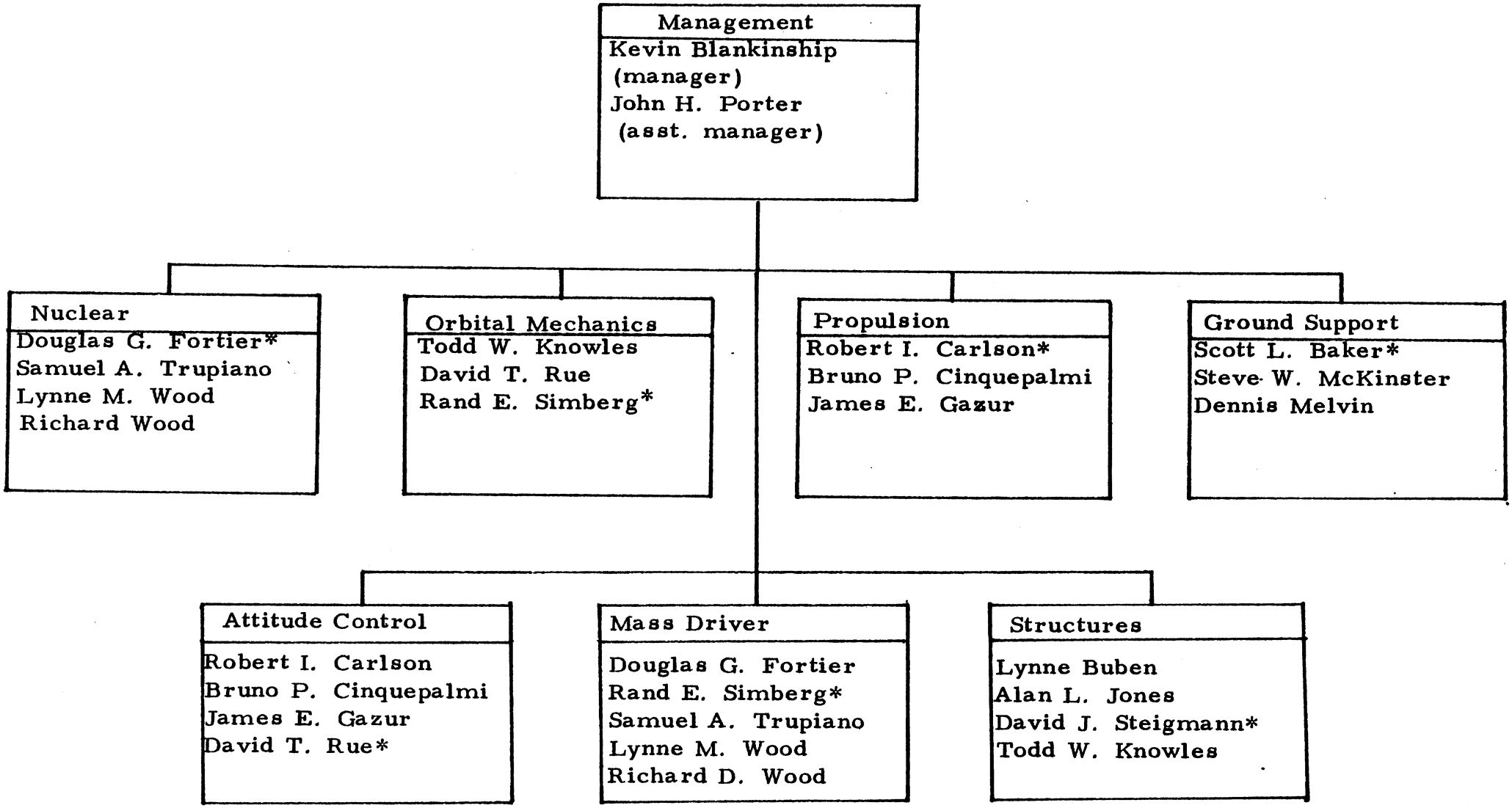

*Group Leaders

Foreword

Project NEWDUMP is the twenty-second in a series of senior design studies carried out by students in Aerospace Engineering 483: "Aerospace System Design." Originated in 1965 by Professor Wilbur C. Nelson, this course has been taught regularly since that time. It is offered in parallel with Aerospace Engineering 481: "Airplane Design," and 482: "Design of Rocket and Air-Borne Remote Sensing Probes," to accommodate the full spectrum of interest of the aerospace engineering students.

The preliminary design study presented here is of a system to affect removal of nuclear waste material into space. The wastes generated in nuclear powerplants are sent to reprocessing facilities to remove less toxic and even desirable raw materials and incidentally to reduce the total mass to manageable amounts. The resulting waste products are transported to a launch site where they are launched by the Space Shuttle to a space station in earth parking orbit.

The next phase of the disposal sequence (the earth parking orbit is not considered a suitable permanent depository) was the subject of an intense study in the early phases of the project. Debated were the closely related subjects of the propulsive system to be used and the eventual destination of the wastes. The decision reached was to use a mass-driver as a propulsive device. A mass-driver, still in the early stages of development, is an electromagnetic gun capable of imparting efficiently large speed increments to payload packages. This concept allowed the team to consider deep space as an attainable destination for the nuclear wastes.

The students of the Aerospace System Design Course are organized into a management and several engineering groups, one for each of the main subsystems.

Technical assistance is obtained through the cooperation of engineering faculty members as well as in consultation with technical and management staff members in Government and Industry.

The one semester's work of each group is integrated into this final report.

Professor Harm Buning
April 1979

TABLE OF CONTENTS

1
INTRODUCTION

1.1 PERSPECTIVES ON THE NUCLEAR WASTE PROBLEM

With the recent incident at the Three-Mile Island nuclear plant, the public debate over the future of nuclear energy is expected to heat up, resulting in new, more stringent requirements for nuclear reactor construction and the handling of nuclear waste.

The Interagency Review Group (IRG), consisting of representatives from 15 government agencies, is presently evaluating possible methods of waste disposal in an attempt to resolve differences in previous studies and present a solution acceptable to the public. The IRG is expected to produce several options as to the best solution to the nuclear waste problem. These options will include storage/disposal methods such as underground storage, sea bed storage, and reprocessing methods.

The effectiveness of each method is reflected in their philosophies regarding what level of safety is desired by the public. Evaluation of the different methods is contingent upon what can be regarded a safe level of toxicity and the capability of maintaining stability of storage over the consequential time periods. Views as to the minimum tolerable level of toxicity differ widely and are reflected in a variety of comparative criteria. These criteria include considerations such as the relation to the toxicity of natural ores, radiation effects on people, ecological considerations, etc. Most methods consequently shoot for target periods of safe storage on the order of 100,000 years.

Stability of storage is an equally debatable issue. Most assessments developed rely on a mix of empirical evidence and statistical modeling. An experimental test site for assessing the stability of salt-mine storage in Asse, West Germany, where experiments in waste placement are currently underway. Although the Asse facility offers first-hand information regarding effectiveness of deep-underground disposal, it will require a substantial time baseline before the reliability of this method is accurately ascertained.

Viewing the problem of disposal from an economics standpoint, social costs can be associated with alternative activities and the possible hazards. By enumerating the social costs, a perspective can be developed by which an optimum solution is found. Social costs can be categorized as follows:

1. Cost of diverting resources from other uses for handling and storage of nuclear waste.

2. Cost of provision of facilities for work storage/disposal.

3. Social cost of system failure (real costs in terms of property damage, radiation-related illnesses, etc.).

Although the first category cannot easily be quantified, it is recognized that the rate of nuclear waste production (dependent upon the number of reactors in operation) and the required storage duration constitute the major cost drivers. The second cost is more accountable, reflecting the R&D, construction, and operating costs. The third category, since it reflects the real costs of failure is a subject of values and the degree of risk-aversity of the public.

From these considerations, it is evident tradeoffs between long-run cost and safety result for each method of storage/disposal. In the context of this study, the goal is to provide a disposal system offering an improved tradeoff of long-run costs with safety providing growth potential and allowing for more risk-averse disposal practices.

1.2 STUDY GROUNDRULES

The groundrules developed followed from a respect for safety in transporting and handing nuclear waste and a consciousness of costs. The following groundrules were followed throughout the study:

1. Disposal of only Light Water Reactor (LWR) waste.

2. Disposal system should be capable of transporting all LWR waste currently produced and through to the year 2000.

3. Present state-of-the-art technology should be used wherever possible.

4. Shuttle to be used as the baseline transportation system to earth orbit.

5. Nuclear waste mix disposed of should consist of materials which have little or no industrial usage and are hazardous to man and the environmen

6. Waste mix should be processable by current means.

7. System simplicity preferred for high reliability.

8. Prime concern is safety. Slight reductions in safety are acceptable when resulting in large cost reduction.

1.3 INITIAL STUDIES/CONVENTIONAL SPACE DISPOSAL

Initially, conventional methods of space disposal were examined in an effort to produce a design concept representing the optimum mix of destination, nuclear waste mix, shielding, and spacecraft configuration for producing a safe, cost-effective method of disposal. The initial studies included:

1. Destination
2. Nuclear waste mix for disposal
3. Reprocessing methods
4. Ground transportation/launch site selection
5. Packaging for space transportation
6. Shuttle bay cooling
7. Environmental impact study
8. Reliability of space disposal operations
9. Long-term disposal safety.

The conventional study represented the achievable using current technology. The results of this effort is summarized in Table I.

The conventional study served as a baseline for comparison with the mass driver concept. Results are presented in their appropriate sections.

Table I. Conventional Space Disposal Study Results

Destination: Circular solar orbit at .86 AU.

Waste Mix: Mix 4A (see Nuclear report for description).

Weight Waste/Flight: 4000 lbs

Orbital Long-Term Stability: 10^{-2} earth reentries per 10^{6} year

Deployment: Shuttle to low earth orbit with two nuclear waste spacecraft. Two shuttle flights for upper stages. Upper stage required for earth escape. Requires kick motor for circularization.

1.4 THE MASS DRIVER

In this application, the mass-driver constitutes the primary element in an orbiting nuclear waste disposal facility where canisters, containing high-level radioactive waste are transported to the facility in low earth orbit and accelerated by the mass-driver to speeds on the order of 12 km/sec for solar system escape.

Use of an orbiting station using a mass-driver for nuclear waste disposal was first proposed jointly by Alan Friedlander of Science Applications, Inc. and Rand Simberg of the NEWDUMP project team.

The mass-driver first appeared in the early 1970's as a device called the 'Magneplane,' a joint project conducted by MIT and the Raytheon Corporati Later, the device gained notoriety as a propulsion system in the space manufacturing/space colony studies conducted at the NASA Ames Research Center. During this stage, the mass driver evolved from on-paper studies to laboratory test models. Research is presently underway at the Francis K. Bitter National Laboratories at MIT and at the Physics Department at Princeton. A comprehensive report on this research will be released in late April of which preliminary copies were procured for the NEWDUMP project.

The NEWDUMP orbiting facility was made possible via several technological advances in the following areas:

1. Large Space Structure Technology: Construction techniques have been developed at NASA Marshal Space Flight Center including extravehicular activity simulations at the water tank facility. A 'Beam Builder' machine has been constructed by Grumman Aerospace Corporation for construction of beams from aluminum sheets fed into the machine. Structural testing of different aluminum beams has been performed at the NASA Johnson Space Center (JSC). Research into the development of beam builders for large composite structures is presently underway at NASA JSC, Grumman, McDonnell-Douglas, and General Dynamics.

2. Mass-Driver Technology: Much theoretical work has been accomplished during the NASA Ames Research Center studies, and at MIT and Princeton. This work proceeded in parallel with the development of two laboratory test models.

3. Economical Space Transportation: The Space Shuttle has substantially reduced the cost of space transportation since the Apollo project, with possible improvements for even greater economy.

The mass driver promises numerous advantages over both conventiona space disposal and burial/reprocessing methods. The primary advantage of the mass-driver is that it allows for permanent disposal of nuclear waste. Once the radioactive waste container attains the minimum velocity required for escape, it will never return. This eliminates the plethora of long-term storage problems with their associated costs.

This does not necessarily conflict with the present frontrunner for nuclear disposal--salt-mine storage. Salt-mine storage would be appropriate as a temporary storage until an orbiting nuclear waste disposal facility is developed.

1.5 GROWTH POTENTIAL

Another advantage of the mass-driver accelerated solar system escape system lies in its growth potential. A study by Rockwell International has shown that the payload capability of the shuttle can be increased by 50% and the cost per pound reduced by as much as 40% by the development of liquid rocket boosters. Heavy Lift Launch Vehicles (HLLV's) offer greater cost effectiveness, eventually cutting the cost/lbm by a factor of 5.

Technical growth will also affect the mass-driver systems. The major areas of growth are expected to be in the power system and in the use of computers, where substantial weight savings can be realized. These areas include: semiconductor technology improvements for high-power applications, improved efficiency of solar cells, and lightweight, high frequency power storage devices.

The largest savings in cost and weight is expected in the use of composites. The NEWDUMP design, with its associated weights and costs was performed using aluminum throughout the structure, relying on current technical knowledge. The use of composites for reducing thermal stresses will result in a secondary impact on weight savings, resulting in a smaller, lighter structure due to reduced stress requirements.

1.6 CONCLUSIONS

The viewpoint taken in the study is to provide a technically feasible alternative offering a low long-run cost with the potential for inexpensive operating costs for nuclear disposal.

Although the cost of constructing an orbiting disposal facility is large, the firing rate accommodated by a single mass-driver is sufficient for the disposal need through the year 2000, based on projected growth in the rate of nuclear waste production. Due to the necessarily large scale of an orbiting waste disposal facility, a national commitment would be required for development.

Since the linear-synchronous motor technology of the mass-driver is still at the laboratory test-model stage, further research work, especially in the experimental area with larger test models having higher acceleration capability is mandated.

2
NUCLEAR

2.1 INTRODUCTION

Today, nuclear power plants provide 14% of the entire electrical power produced in the United States. For every pound of Uranium burned in a nuclear plant, it requires 2,700,000 pounds of coal to produce an equivalent amount of electricity in a conventional, coal-burning, power plant. Nuclear plants also put fewer pollutants into the atmosphere than do their counterpart, coal plants. The drawback with nuclear plants, however, lies in the solid waste produced. It is highly radioactive and remains so for many years.

This section is devoted to the description of radiation, its effect upon man, and the considerations which must be taken into account in order to make the option of space disposal feasible.

2.2 RADIATION EFFECTS

The effects of radiation on man are dependent upon the strength of radiation, length of exposure, distance from source, and the biological proper of the tissue absorbing radiation.

Radiation consists of alpha particles, beta particles, and gamma rays. The alpha particles are fast moving Helium nuclei (^4_2He) that are non-penetrat and are stopped in a fraction of a millimeter in the superficial tissue. Beta particles are electrons and can be stopped within one centimeter of tissue. Th most penetrating are the gamma rays which can traverse the entire body.

All types of radiation have one property in common, the ability to eject electrons orbiting around the nucleus from the atoms of any material through which they pass. The charged particles (alpha and beta) ionize directly and in qualitatively similar ways. Gamma radiation causes ionization by the product of secondary electrons.

The ionization tracks of the particles differ considerably. The ionization tracks of gamma radiation are long and sparsely ionized; beta particle tracks are shorter and more densely ionized: alpha particles are even shorte straight, broad and densely ionized. The densely ionizing particles have a greater relative biological effectiveness than the less densely ionizing particle

Particles	Range		Ionizing Power
	air (ft)	Tissue (cm)	
Alpha	.1	.01	10,000
Beta	10	1	100
Gamma	1000	10	1

Table 2.1 Relative Comparison of Radiation

For radiation to be biologically effective, ionization must take place within the cell nucleus. The ionization produced at various depths of the body will depend on the penetrating power of radiation. The biological effects are related to the quantity of ionization produced in the tissue or the dose of radiation absorbed.

The energy absorbed in a particular material from a radiation flux, without reference to the type and energy of radiation, is defined as a unit of absorbed dose or rad. Biological effects of equal absorbed doses in rads of different kinds of radiation are not the same. Hence, the unit rem or dose equivalent is defined where: dose in rems = dose in rads x Relative Biological Effectiveness (RBE). The RBE of radiation is the absorbed dose of 250,000 volts or x-ray radiation which produces the same biological effect as one rad of the radiation in question. For gamma rays and beta particles, RBE's are approximately one. For alpha particles, the RBE can be as high as ten.

Biological effects of ionizing radiation depend on the energy absorbed and on various modifying factors. Since the penetration of gamma rays is much greater than that of the alpha and beta particles, the absorbed dose will be primarily dependent upon the gamma rays, whose RBE is equal to one. Therefore, the dose equivalent in rem and the absorbed dose in rads are numerically equal.

Radiation affects man by causing ionization within the cell, the main damages being in the reproductive processes due to chromosome disturbances. This affects tissues that require high rates of new cell production, including skin, intestines, spleen, bone marrow, eyes, gonads, and lymph nodes causing lower immunity, blood clotting, reduced oxygen transport, sterility, dermatities, ulcers, and cataracts.

The does of a radionuclide is inversely proportional to the square of the distance from the source. Dependent upon the dosage, a person could suffer a slight loss of hair to third degree burns. Fluctuations in the blood count are the result of changes in production and destruction as well as the life span of a particular cell line. One of the first late effects of radiation is increased likelihood of cancer in the affected organs.

Very subtle genetic changes are likely to occur. Assuming a dose of 100 rads, the probability of a new mutation in the immediate offspring is one in twenty-five hundred.

Dose	Effects and Conditions
100,000 rem	spastic seizures; death in seconds
10,000 rem	disruption of central nervous and cardiovascular systems; death in minutes to hours
1,000 rem	necroses of progenitive tissue; death 30-60 days
100 rem	mild irradiation symptoms in few cases
10 rem	few or no detectable effects
10 rem/day	debilitation 3-6 weeks; death 3-6 months
1 rem/day	debilitation 3-6 months; death 3-6 years
.1 rem/day	permissable dose range; no effect
.01 rem/day	permissable dose range; no effect
.001 rem/day	natural radiation; no effect

Table 2.2 The Effects Upon Man Exposed to Various Doses of Radiation

2.3 CONSIDERATIONS FOR SPACE DISPOSAL

Spent fuel, in the form as it is removed from the reactor, has a large mass. In order to fit into our scenario of disposal and meet present economic standards, it is necessary to reduce the mass of this spent fuel and at the same time retrieve the usable fissile material (that which is capable of producing a fission reaction). Without the extraction of the useful material a Uranium shortage would occur by the year 2000 as predicted by current nuclear power projections (Reference 15)(see Table 2.3). Therefore, it is necessary that these spent fuel elements be reprocessed.

Other aspects of the research included shielding considerations, heat generation, as well as magnetic and other physical properties of the reprocess waste.

Absorption of neutrons by fission products interferes with the chain reaction to the point where it is necessary to remove the fuel elements from the reactor core, even though they still contain a large amount of unburned fissible material.

These spent fuel assemblies, as they are removed from the reactor, are what are referred to as reactor wastes. Reactor wastes, as a whole, are

Date (Year)	Power (G. W(e))	Total Spent Fuel (Metric Tonnes)	Total Amount of Mix 4A (Kg)
Backlog			110,532.2
1979	56.3	1.88×10^3	32,010.0
1980	60.1	2.00×10^3	34,991.4
1981	70.1	2.34×10^3	38,092.0
1982	81.6	2.72×10^3	41,172.8
1983	92.8	3.09×10^3	45,983.8
1984	109.4	3.65×10^3	52,637.0
1985	126.8	4.25×10^3	60,561.8
1986	140.8	4.69×10^3	70,357.6
1987	153.7	5.12×10^3	79,665.4
1988	166.3	5.54×10^3	87,604.6
1989	179.8	5.99×10^3	95,083.6
1990	194.8	6.49×10^3	102,638.2
1991	210.7	7.02×10^3	110,728.6
1992	227.5	7.58×10^3	119,367.0
1993	244.3	8.14×10^3	128,395.8
1994	263.2	8.77×10^3	137,632.6
1995	283.0	9.43×10^3	147,409.8
1996	302.8	10.09×10^3	158,051.2
1997	322.6	10.75×10^3	168.863.2
1998	342.4	11.41×10^3	179,571.2
1999	362.2	12.07×10^3	190,138.8
2000	380.2	12.67×10^3	200,490.8

Table 2.3 Yearly Power, Spent Fuel, and Mix 4A Predictions
(See Appendix A.2 for Mix 4A Calculations)

further broken down into mixes. Each mix (Reference 2) is numbered with reference to the materials which are chemically extracted. A consideration of prime importance was minimizing total mass while staying within current technical and economic boundaries.

The mix that was chosen, termed "mix 4A", deals with the extraction from the total reactor waste the following elements: uranium, plutonium, xenon, krypton, iodine, bromine, zirconium, molybdenum, and niobium. The elements which are removed consist of those which are rare or can be used by industry and those of short half lives which can be stored in existing geological areas and pose little hazard to the populace.

The extraction of these elements as well as the cladding hulls constitut a 97.88% reduction in total mass. The remainder of the reactor waste will make up the payload (21.2 kilograms from 1 Tonne of reactor waste).

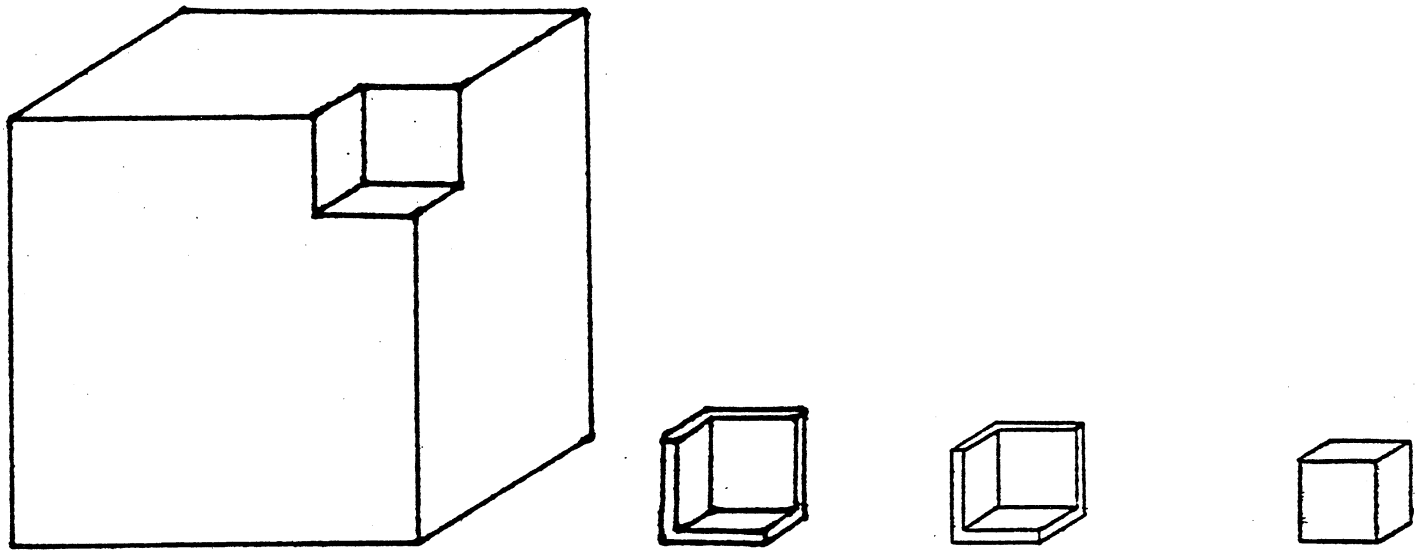

Step 1: Removal of U and Pu (965 kg) from 1000 kg of spent fuel (1000kg)

Step 2: Removal of Xe, Kr, Br, I from waste remaining after step 1 (35kg)

Step 3: Removal of Mo, Nb, Zr from waste remaining after step 2 (30kg)

Step 4: Mix 4A (23kg)

DIAGRAM 2.1: GRAPHIC VIEW OF THE REMOVAL OF CERTAIN ELEMENTS FROM 1000 KILOGRAMS OF SPENT FUEL TO PRODUCE MIX 4A

2.4 REPROCESSING PROCEDURE

These spent fuel assemblies are sent to specialized reprocessing plants where they are mechanically chopped into small pieces (so the fuel will no longer be protected by the cladding) and dissolved in a solution of 2-3 molar Nitric acid ($Al(NO_3)_3$) (see diagram 2.2). Both uranium and plutonium (the useful fissile material) are extracted (99.5%) together in a Tributyl Phosphate solution. These two actinides are then separated from each other by either ion exchange or selective oxidation and solvent extraction methods. The plutonium (valued at $5000 a pound) can be used as a reactor fuel by adding it to natural uranium, thereby eliminating the costly and energy intensive enrichment process (Reference 4). Uranium is recycled for re-enrichment or blending with other fuel materials.

The aqueous solution remaining is termed the high level waste. The next step is to remove some usable materials; zirconium (Zr), niobium (Nb), and molybdenum (Mo) which constitute a 21% further weight reduction of the remaining solution.

A 100% Tributyl Phosphate solution is then used for extraction of Nb and Zr from the aqueous solution. The Mo is separated (99%) using solvent extraction or sublimation technique.

Xenon and krypton are effluent gasses and are removed (100%) by standard gas handling techniques. Iodine and bromine are removed by virtue of their low boiling points, or, as in the case of iodine, by its reaction with silver to form silver iodide.

Iodine removal presents a special health hazard in that its radioactive half life is 1.7×10^7 years and is concentrated in the thyroid gland of living organisms. This could be considered as a single payload for disposal (Reference 2).

Bromine is not radioactive after a very short time and can be treated as a chemically toxic waste. Krypton is radioactive and has a half life of 10.6 years. It may be stored or used industrially. Xenon is non-radioactive and chemically inert. It may be stored, used industrially, or dispersed. Zirconium is used extensively in industry in corrosion prevention, refractory material, and in making super conducting magnetics ($5/lb). Molybdenum and niobium are also used extensively in industry ($15/lb).

2.5 MIX CHARACTERISTICS

The method for disposal dictates the form that the waste should be in either liquid or solid form. For the purpose of space disposal, a solid in the form of an oxide was chosen.

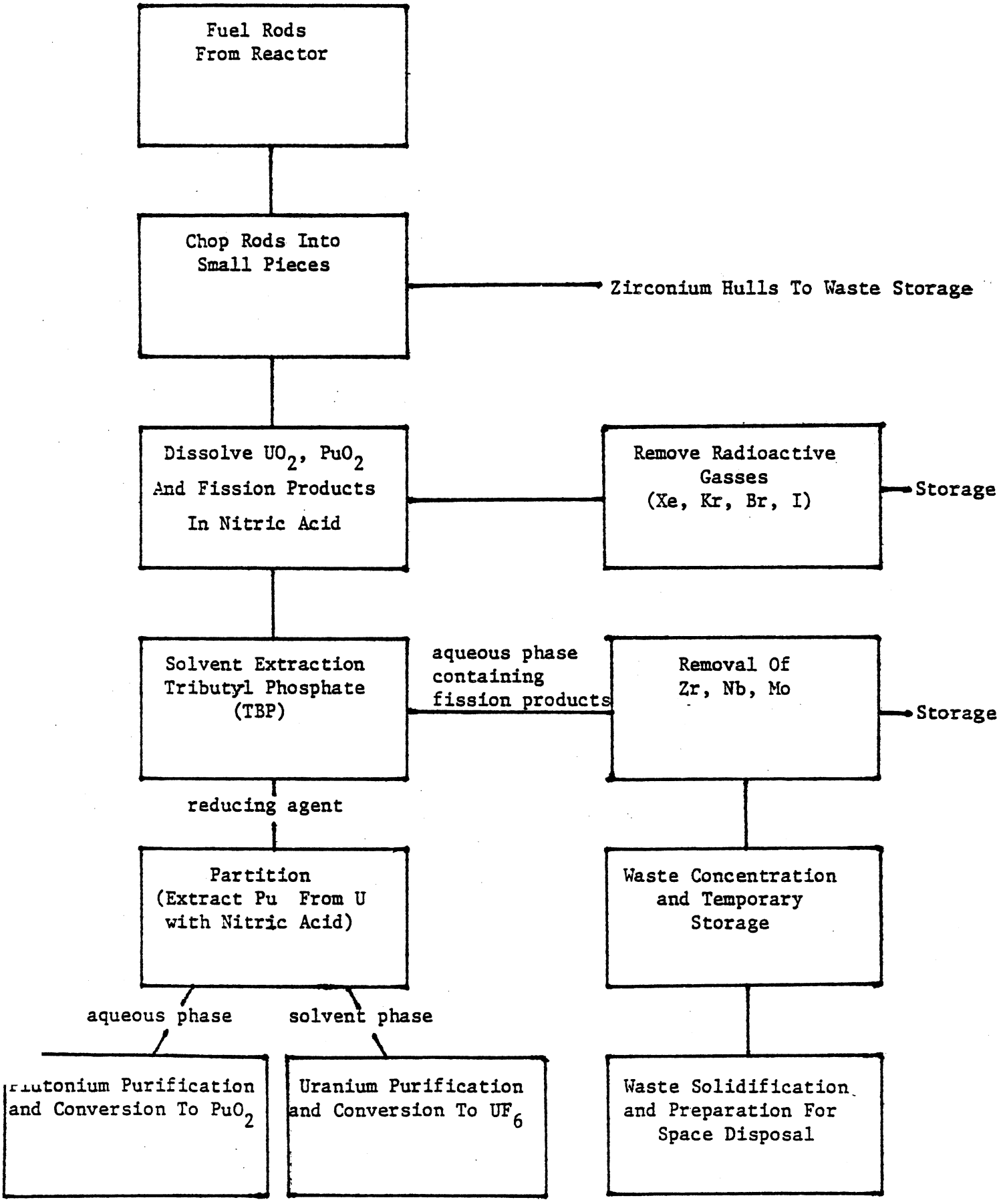

DIAGRAM 2.2: REPROCESSING FLOW DIAGRAM FOR MIX 4A

Melting point	1273 K
Thermal conductivity	.6 - 1.8 W/m K
Thermal density	.0398 W/g
Density	4.0 g/cm^3

Table 2.4 Oxide Characteristics
(Values from Reference 2)

Due to high heat generation, it is suggested that spent fuel assemblies be stored in cooling tanks at power or reprocessing plants for ten years before being prepared for space disposal. This will also decrease the amount of radioactivity and in essence the amount of shielding needed, hence, a reduction in weight for disposal purposes.

Looking at the magnetic susceptibility of the mix, (see Appendix A.1), it was determined that no interaction between the waste mix and the magnetic fields produced by the mass driver would occur. This makes the option of mass driver bucket retrieval possible.

2.6 SHIELDING

The mix is composed of fission products whose sources of radiation are beta and alpha particles, and gamma rays. The beta and alpha particles are simple to stop. The gamma rays are difficult to stop.

With beta particles, the absorption of their energy in matter gives rise to the production of electromagnetic radiation known as Bremsstrahlung radiation. This radiation is more penetrating than the beta particles which produce it. Therefore, it is necessary to use shielding material of low atomic number.

The gamma radiation is not completely absorbed by any thickness of shielding, however great. Instead, the intensity of the transmitted radiation decreases approximately exponentially with the thickness of material traversed. The shielding must be thick enough to reduce the dose rate to an acceptable level.

The weight of the shield is important. It has been determined that a single layer of tungsten (W) followed by a layer of lithium hydride (LiH) gives the best shielding for its weight (Reference 11). The tungsten is for the shielding of the gamma rays and the lithium hydride is for the neutron shielding.

Shielding tickness as a function of fission product contamination and mass of actinides for a range of dose rates are shown in Figures 2.1 and 2.2. It has been found that the actinides within the container become self shielding (see Figure 2.2); that is, the shielding thickness becomes nearly a constant value for increased amounts of actinides.

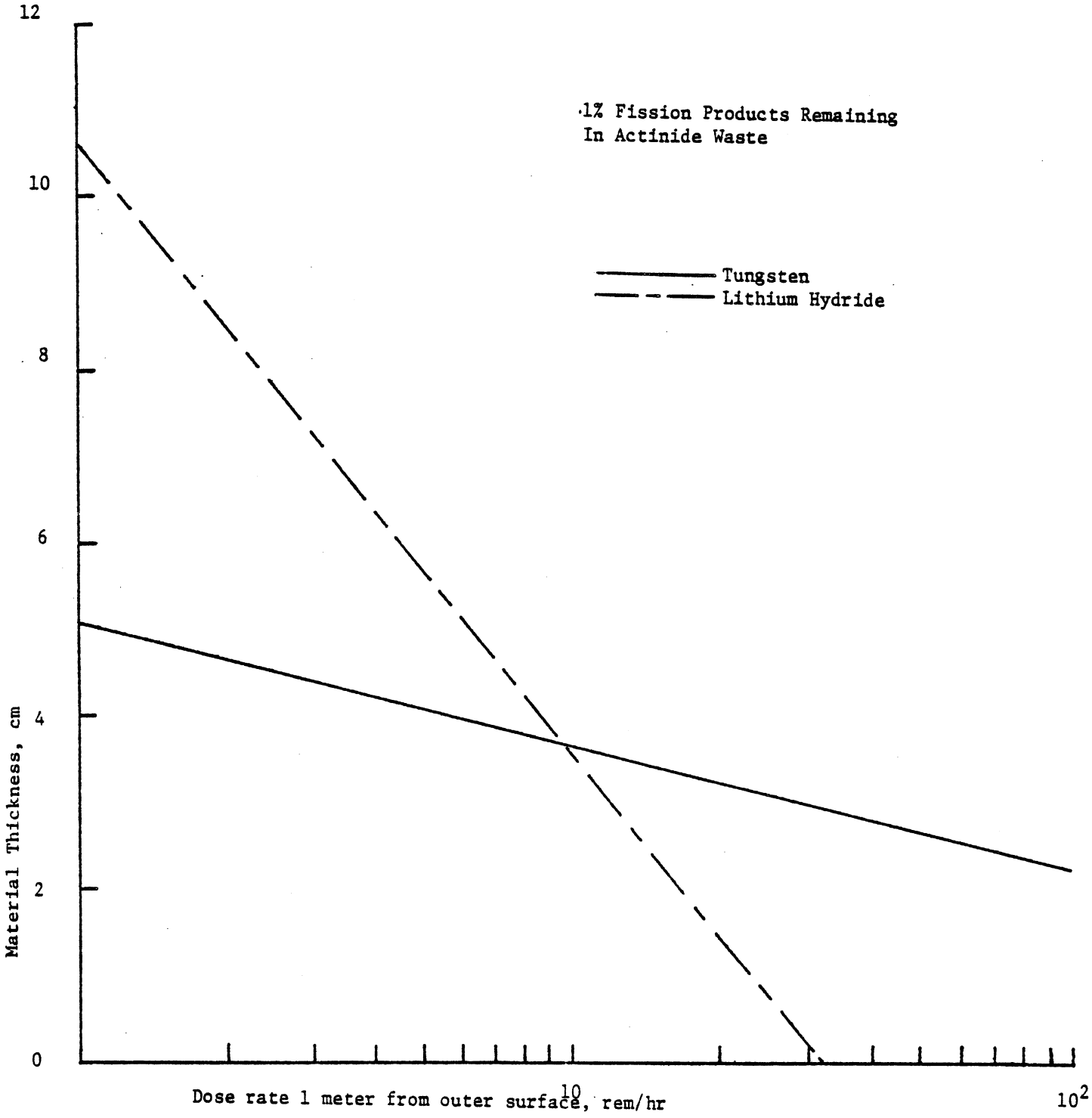

FIGURE 2.1: THICKNESS OF TUNGSTEN AND LITHIUM HYDRIDE SHIELDING MATERIAL REQUIRED TO REDUCE DOSE RATE 1 METER FROM OUTER SURFACE OF PACKAGE FOR MATRIX CONTAINING 250 KILOGRAMS OF ACTINIDE WASTE. (ref. 9)

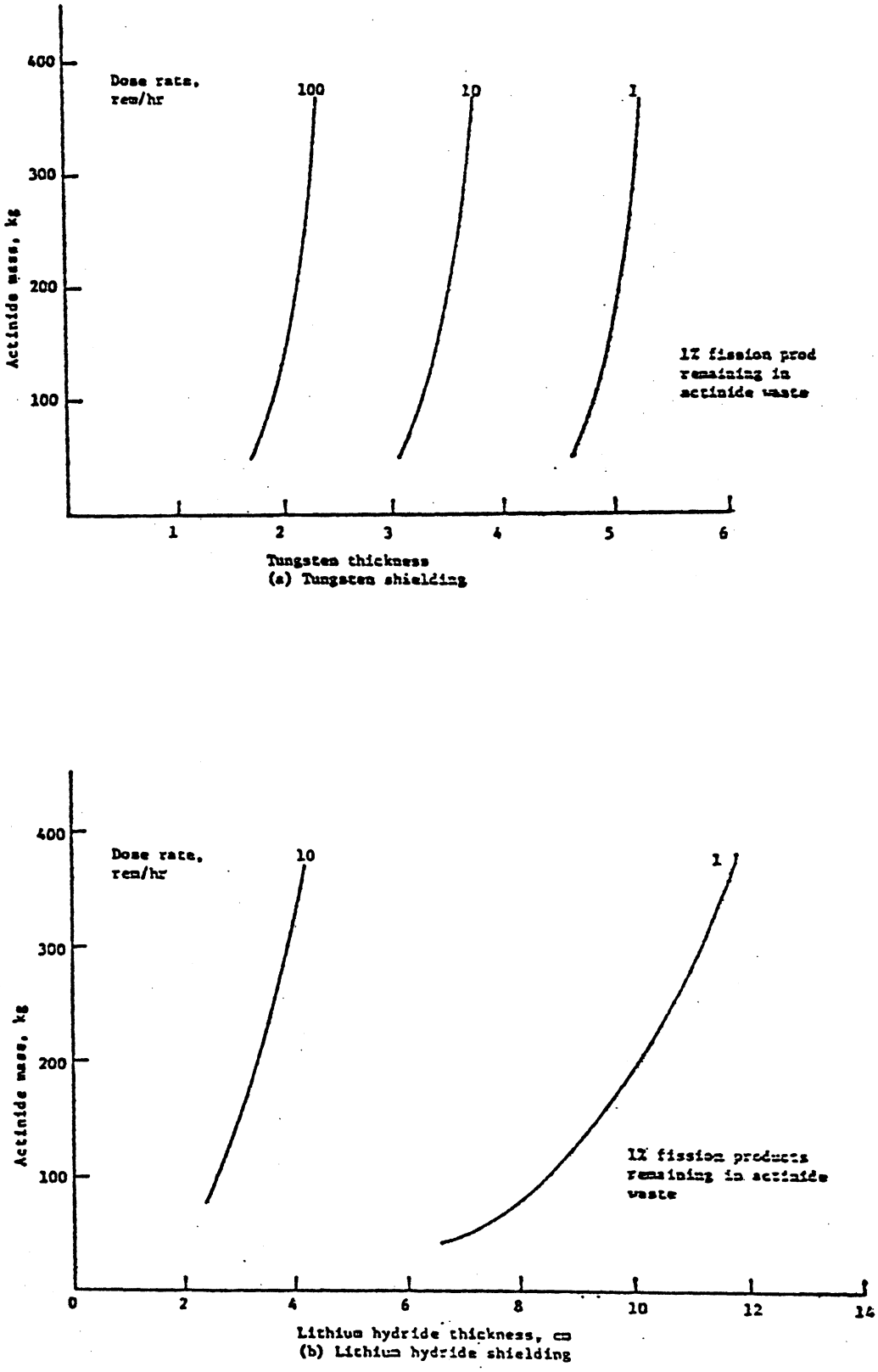

Figure 2.2 Working Curves for Shielding Thickness (Ref. 9)

Removal of the shielding package once the waste containers are deposited on board the mass driver is also considered permissable from the nuclear standpoint. Tungsten (W) 186, because of its large cross section (Reference 8), is the one isotope which is affected significantly by radioactive waste. By the absorption of a neutron, it transforms to W 187 which has a half life of approximately 24 hours and decays to rhenium (Re) 187 which is not radioactive. The amount of radiation expelled by the decay of W 187 is very small. (Comparable to the dose from having x-rays taken at the dentist's office (Reference 10).)

The optimum package ratio occurs for a dose rate of 10 rem/hour at one meter from the external surface. This gives the best weight reduction to dose increase. Further increases to higher allowable dose rates are less effective in increasing package ratios (Reference 7).

With reference to 10 CFR 71 for transporation of radioactive waste, a base point of 1 rem/hour at one meter from the external surface of the package was suggested in case of accidental exposure to the general public. Hence, this is the suggested dose value to be used for shielding requirements.

2.7 FURTHER CONSIDERATIONS

Before implementation, further studies and tests must be performed to determine the effects of radiation on the mass driver, shuttle, and waste handling equipment. This information was unavailable to this research group and is beyond the scope of this report.

2.8 REFERENCES

1. Alexander, C. W., Kee, C. W., Croff, A. G., and Blomeke, J. O., Projections of Spent Fueld to be Discharged by the U. S. Nuclear Power Industry," Tennessee, Oak Ridge National Lab (Oct. 1977).
2. Burns, R. E., Causey, W. E., Galloway, W. E., and Nelson, R. W., "Nuclear Waste Disposal in Space," Alabama, George C. Marshall Space Flight Center (1978) NASA Tech Paper 1225.
3. Chalke, H. D., Williams, K., Smith, C. L., Radiation and Health, Toronto, Longmans LTD, (1962).
4. Deutsch, R. W., "Nuclear Power", Columbia Maryland, General Physics Corporation (Oct. 1977).
5. Fisher, Arthur, "What Are We Going to do About Nuclear Waste?", Popular Science, (December 1978).
6. Heckstall, H. W., Atomic Radiation Dangers, London, T. M. Dent and Sons, LTD, (1958).
7. "High Level Radioactive Waste Management Alternatives," Richland, Washington, Battelle Pacific Northwest Laboratories, (May 1974), BNL-1900-4.

8. Hughes, D. J. and Schwartz, R. B., "Neutron Cross Sections" Upton, New York, Brookhaven National Laboratory, (July 1958).
9. Hyland, R. E., Wohl, M. L., and Finnegan, P. M., Study of Extraterrestrial Disposal of Radioactive Wastes. Part 3" NASA TMS-68216 (1973).
10. Kikuchi, C., Nuclear Engineering Professor, Nuclear Engineering Department, University of Michigan, personal communications, Jan-Feb 1979.
11. Lynche, C. T., CRC Handbook of Materials Sciences, Vol. I, General Properties.
12. "Management of Radioactive Wastes from Fuel Reprocessing," Symposium, OECD-Paris, (1973).
13. McKeon, D. C., Nuclear Engineer, University of Michigan, personal communications, (Jan-Mar 1979).
14. Meek, M. E., and Rider, B. F., "Complications of Fission Product Yields", Pleasonton, California, Vallecitos Nuclear Center (1972).
15. Pines, David, ed., "Reviews of Modern Physics", New York, American Physical Society, (Jan 1978), Vol. 50, Number 1, Part 2.
16. Summerfield, G., Notes From Nuclear Engineering Course No. 400, University of Michigan, College of Engineering, Ann Arbor.
17. "The Problem of Nuclear Waste-We've Got to Solve it Soon" Changing Times-The Kiplinger Magazine (Feb 1979).
18. Wang, Yen, CRC Handbook of Radioactive Nuclides, The Chemical Rubber Company (1969).
19. Wilson, B. J., The Radiochemical Manual: 2nd ed., Amershan, The Radiochemical Center (1966).

3
ORBITAL MECHANICS

3.1 DESTINATION REQUIREMENTS

Crucial to any discussion of space disposal of nuclear waste is the question of destination. The answer to this question hinges on many criteria, such as velocity increment (ΔV) required to achieve the destination, complexi of mission requirements, possibility of later recovery, the chances of eventu return to earth, and possible traffic problems with other vehicles and celestia bodies.

Mission complexity invites cost, as do high velocity increments. Therefore, for purposes of economy both of these parameters should be minimized. While it is possible that future generations will find uses for the waste material, (much as gasoline formerly was considered a useless by product of petroleum processing), it was decided that recoverability was to be given low priority compared to the urgency of removing the waste from humanity's immediate environment. There are relatively few places that would provide easy future accessibility; to emphasize the recoverability aspec to any extent would place undue constraints on the problem. Traffic problems were given strong consideration, particularly in those cases where the chance existed of an encounter with a manned vehicle. Finally, the most important parameter of all is long-term stability: long-term in this case meaning on the order of a million years. Obviously, if the waste returns to earth eventually, the purpose of the project is defeated. To summarize, the project requireme were low ΔV, minimal mission complexity, no traffic problems, and long-ter stability, with recoverability considered irrelevant.

The first candidate is high earth orbit (HEO). The particular orbit examined was a circular orbit with an altitude of 50,000 km; safely beyond the projected communications satellite traffic in the geosynchronous region, yet close enough to earth to remain unperturbed by lunar gravity. ΔV requiremer are not prohibitive, as can be seen from Table 3.1. Keeping an eye to the futu however, it is not unreasonable to expect traffic to the moon and Lagrange points to increase considerably in the 1980's and 1990's, particularly manned traffic. Putting the payload in a polar orbit at the same altitude would ease this problem somewhat, but only at a large ΔV cost due to the plane change required. In addition, the long-term stability is questionable in either case.

Lunar orbits suffer from the same problems as HEO; possible traffic and orbital instabilities. Placing the waste on the lunar surface was briefly considered. There are two possibilities in this case: hard landing and soft landing. The hard landing option was eliminated mainly for environmental

reasons. Each landed payload would create a radioactive crater. Soft landing was ruled out on the basis of complexity; in this case, each landed payload would require the equivalent of an Apollo mission, in terms of both ΔV and logistics.

The only orbits in near-earth space that do exhibit the long-term stability required are the "gravity wells" at the Earth-Moon Lagrange Points L-4 and L-5. Precisely because these orbits are so stable, they will likely be considered valuable "real estate" in the near future. Too valuable, in fact, to be used merely as repositories for nuclear waste materials.

It rapidly becomes apparent that the solution to the problem does not lie in near-earth space. Farther out, the options include planetary impacts, planetary orbits, heliocentric orbits, solar impact, and solar system escape. Going to Jupiter's Trojan points or any of the planets is not feasible due to severe launch window constraints. Heliocentric orbits seem to offer more promise. In particular, orbits between Earth and Mars, or between Earth and Venus, display very good stability, at a moderate ΔV. Another possibility is to place the payload in an orbit about one of the Earth-Sun equilateral points. Because this mission would constitute a rendezvous rather than an orbit change, the velocity change required is very low. The only essential requirement is earth escape, after which a very small boost is sufficient to inject into the proper orbit. So-called "horseshoe" and "tadpole" orbits have been found around these points, and they have been numerically integrated for up to 10,000 years. There is good reason to believe that they would remain stable much longer than this.

There are two problems with heliocentric orbits, one minor, the other major. The minor problem is that while chances of eventual return to earth are extremely low, they are not zero. The major problem is that control of the trajectory must be maintained at long distances from earth for long times after launch. In the case of an equilateral point mission, the injection burn might take place 10 years after launch. This is a long time to expect an unmaintained system to remain reliable, and the consequences of failure would be serious; the waste would remain in an earth-crossing orbit with no easy means of rescue to prevent the eventual return.

Bearing this fact in mind, it would clearly be desirable to find some "free" trajectory that required no control once the payload leaves low earth orbit. With such a trajectory, the payload would need only a single boost in the proper direction with the proper velocity to assure that it would eventually reach the desired destination.

The study yielded two classes of such trajectories: solar impact and solar system escape. Solar impact was ruled out as a result of the very high (> 20 km/s) velocity increments required. It is possible that such velocities can be reasonably achieved in the near future, but too little researc has been done in this area for the purposes of this project.

This leaves only solar system escape. The ΔV required is moderately high, but this is compensated by several advantages. One of them is that it is a free trajectory, as discussed previously. If a payload in low earth orbit is given a high enough velocity in the right direction at the right time, it is guaranteed to leave the solar system, assuming that it doesn't encounter the moon or planets on the way out. Also, no further propulsive maneuvers are required nor is there a need to track the material for appreciable lenghs of tir Another advantage is that launch windows occur very often; once per orbit or once every 92.5 minutes in a 400 km circular orbit. The third advantage and perhaps the most important one is that once the waste leaves the solar system it will not return. Despite the high ΔV required, this option looks more attractive than any other because of its overwhelming virtues in all other respects. Thus, despite the somewhat high velocities required, there is a strong motivation to find or design a device that will provide the requisite velocity to the payload.

3.2 MASS DRIVER ORBIT OPTIONS

3.2.1 Symmetrical Configuration

Having chosen a catapult-like device (which a mass-driver is), the first problem to be confronted is Newton's Third Law. Every payload will impart a recoil velocity to the launch vehicle, causing it to behave as a retrofiring engine if the payload is fired forward. In this condition the orbit of the vehicle will decay and the vehicle will eventually burn in the upper atmosphere. The most obvious solution is to fire a payload of mass equal to the nuclear waste payload in the opposite direction. In this manner the two reactions would cancel and no net force would be exerted upon the launchir device.

If payloads are to be launched in two directions, there must be an orbital symmetry such that both directions yield a solar system escape trajectory. The only orbit found possessing the necessary properties of symmetry is a circular orbit in the ecliptic plane with the launch vehicle aligned perpendicular to the orbit (Figure 3.1). In this configuration the mass driver would fire perpendicular to the plane of the ecliptic, launching waste above and below the plane towards system escape (Figure 3.4).

If the long axis of the vehicle lies in the orbital plane, attitude control problems are introduced as a result of the required rotation. By keeping the vehicle always perpendicular to its orbit, attitude control considerations are minimized because the vehicle's attitude remains inertially fixed. In addition, firing out of the ecliptic plane eliminates any concern about hitting planets or objects in geostationary orbit.

Unfortunately, the out-of-plane launch also entails a severe disadvantage. It turns out that firing out of the plane requires very high ΔV's; ΔV's that are unattainable using a conventional mass driver design. By not launching in the direction of orbital motion, orbital velocity is not used to full advantage. A ΔV perpendicular to the ecliptic implies a ΔV perpendicular not only to the orbital velocity about the earth but also to the velocity of the earth about the sun. Because the launch velocity is normal to these two orbital velocities, the velocity must be quite large in order to get a vector sum of solar system escape velocity. The exact amount required at any point in the orbit was calculated with a PET microcomputer. The minimum ΔV was found to be in excess of 20 km/sec. This velocity would require a mass driver operating at 1000 gravities acceleration to have an accelerating length of over 20 km.

While this disadvantage is major, it seems to be the only one, and the configuration displays a great deal of promise in other respects. Its use awaits only the development of more powerful accelerators.

3.2.2 In-Plane Configuration

The high ΔV's discussed in the previous section can be reduced considerably by launching payloads in the direction of orbital motion. In this configuration the vehicle lies in the orbital plane, oriented parallel to its orbital velocity about the earth (Figure 3.3). Unfortunately, this orientation does not possess the symmetry of the perpendicular configuration. Payloads fired forward easily achieve escape velocity, because they utilize to full advantage both the orbital velocity of the launch vehicle and the velocity of the earth about the sun. Compensating payloads must be fired backward to maintain the orbit of the launch vehicle, however, and these packages fired in retrograde will not escape the solar system; they will, in fact, fall immediately to earth. This is a disadvantage from the standpoint of lift costs, because each kilogram of nuclear waste requires another kilogram of "dummy" reaction mass. Despite this, it is a more attractive option than the perpendicular configuration because the ΔV requirements are lowered by a factor of ~ 2.5.

The exact orbit chosen was a posigrade, circular orbit with an altitude of 400 km. This orbit has a local circular velocity of 7670 m/sec with a period of 92.5 min (5550 sec). The orbital plane is coincident with

the plane of the ecliptic. 218.44° of the orbit lies in sunlight with 141.56° spent in the shadow of the earth. This gives 56.12 minutes or 3367 seconds of sunlight per orbit during which energy can be collected with solar panels (Figure 3.4).

A ΔV of 9000 m/sec gives a launch window 25° wide. The window is centered on a point 105.6° behind the earth velocity vector (Figure 3.5). The launch window encompasses a time period of 6.42 min (385 sec). The launch window time may be further restricted by the risk of intercepting the moon or objects in geosynchronous orbit. There is also a slight risk of slingshotting off a planet on the way out, causing the payload to return in an earth-crossing trajectory. Conservatively assuming a restriction of 50% due to these factors, the average time per orbit that waste can be launched is 192 seconds.

In addition to doubling payload lift costs, one other problem is introduced by launching in the orbital plane. Because the launch vehicle is always aligned parallel to its orbital velocity vector, it rotates at a rate of one revolution per orbit or 1.13×10^{-3} rad/sec. A consequence of this rotation is that, after release from its launching bucket, the payload is inside a long tube which it "sees" as moving sideways. The payload will strike the inner wall of the launch tube unless some measures are taken to prevent this. One approach is to build a slight curvature into the launch tube to compensate. Another solution is that used in the design of mass driver reaction engines (MDRE). Here, as the payload is released the bucket is snapped away from it and decelerated in a separate launch tube, leaving the payload in free space. A detailed analysis of the payload trajectory is included in the appendix.

3.3 REFERENCES

1. Friedlander, Alan J. and Feingold, Harvey, "Earth Re-encounter Probabilities for Aborted Space Disposal of Hazardous Nuclear Waste," Science Applications, Inc., Schaumberg, Ill, AAS/AIAA Astrodynamics Specialists Conference, September 7-9, 1977.
2. Davis, Donald R. and Greenberg, Richard, "Long Term Stability of Solar Storage Orbits," Planetary Science Institute, presented at the 1977 Astrodynamic Specialists Conference, September 7-9, 1977.
3. Weissman, Paul R. and Wetherill, G. W., "Periodic Trojan-type Orbits in the Earth-Sun System," The Astronomical Journal, March 1974, Vol. 79, No. 3.
4. Szebehely, Dr. Victor, Theory of Orbits, Academic Press, Inc., New York, N.Y., pp 231-266, 1967.

Table 3.1 Destination Velocity Requirement

Destination	ΔV m/s	Comments
NEAR EARTH SPACE		
HEO (50,000 km)	4042	traffic problems
HEO (polar)	6761	relieves traffic but expensive
Lunar Orbit		
Equatorial	3900	traffic, unstable
Polar	3900	unstable traffic
L-4, L-5	3900	
Lunar		
Soft Impact	6600	expensive, complexity
Hard Impact	3100	environmental
BEYOND EARTH GRAVITY FIELD		
Jupiter, Saturn Trojan Points	8000	expensive
Heliocentric (.86 AU)	4450	throw-away vehicles
Earth-Sun Equilateral Points	3400	possible instability, throw-away vehicles
Solar Impact	24,000	EXPENSIVE but free trajectory
Solar System Escape	8760	free trajectory, very stable

All ΔV's are calculated from an initial 160 nm shuttle orbit.

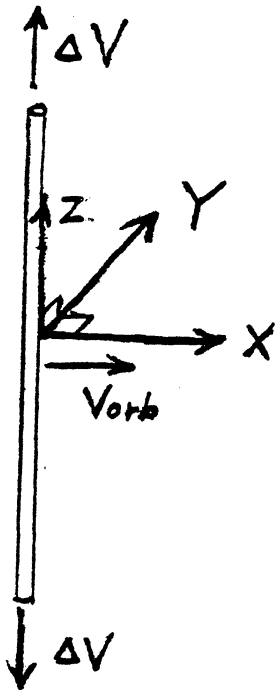

Figure 3.1 Orbital Plane is the X-Y Plane with Payloads Launched in the ± Z direction.

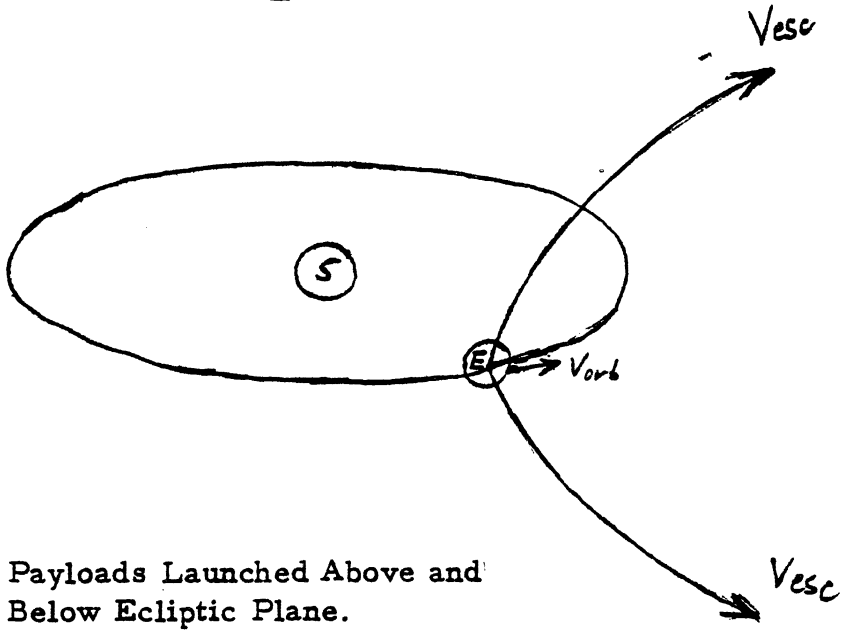

Figure 3.2 Payloads Launched Above and Below Ecliptic Plane.

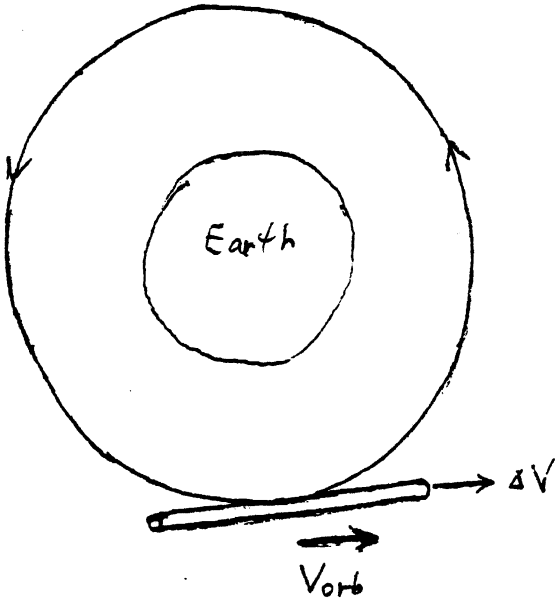

Figure 3.3 Payload Launched in the Direction of Orbital Motion.

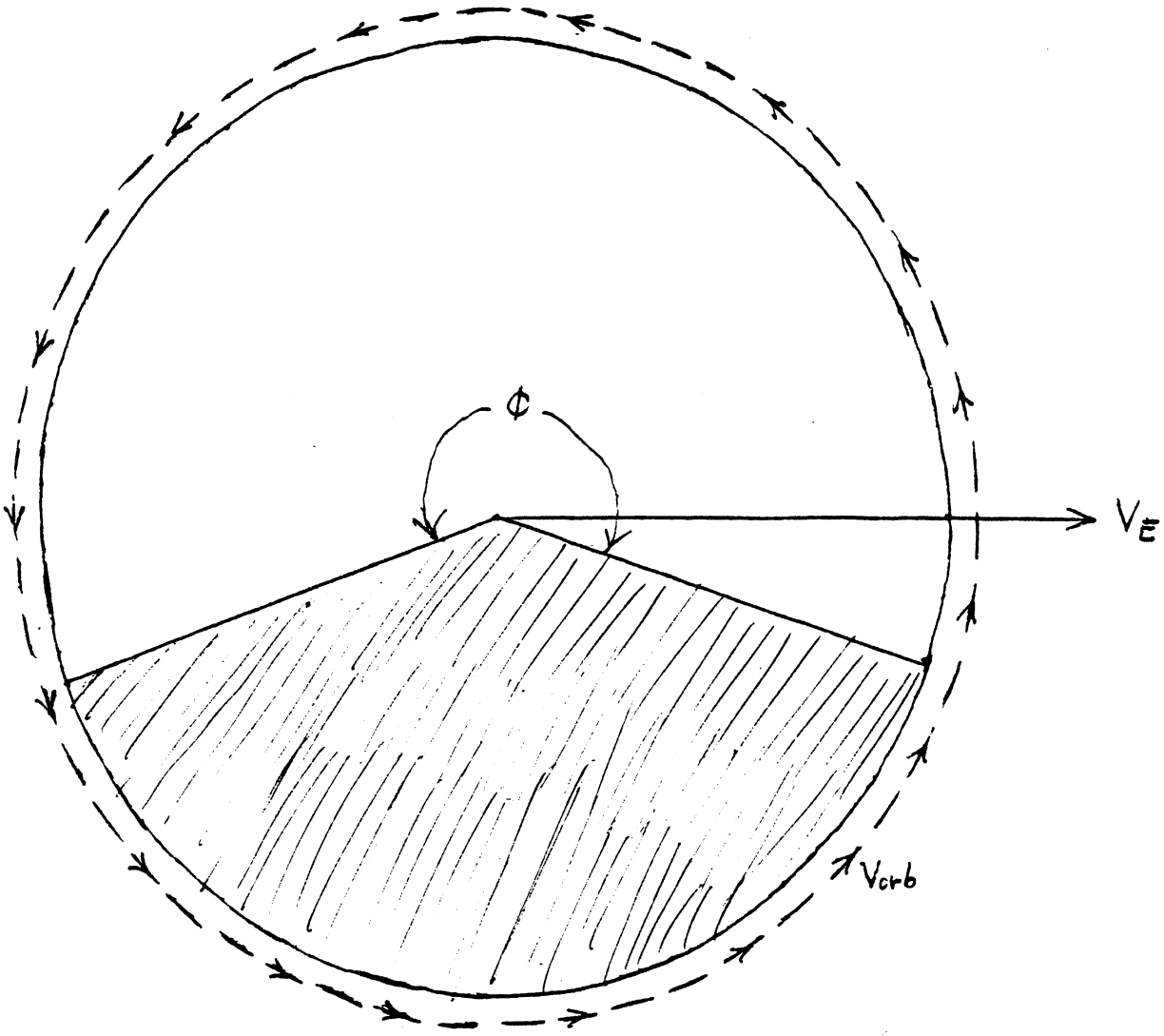

Figure 3.4 ϕ = Amount of Orbit Spent in Sunlight = 218.44°.

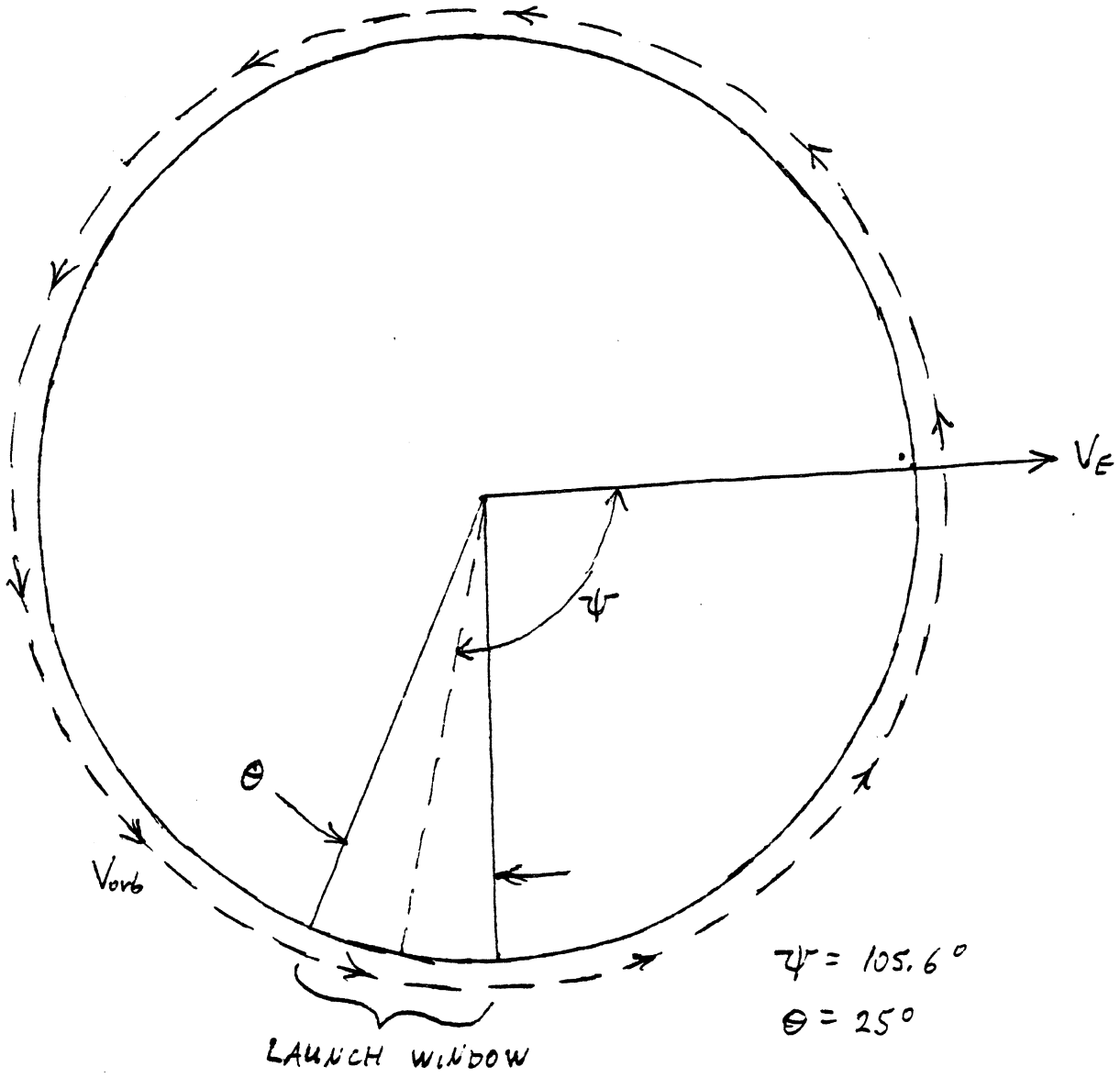

Figure 3.5 Location and Width of Launch Window for 9000 m/s ΔV.

4
MASS DRIVER: LINEAR SYNCHRONOUS MOTOR

4.1 INTRODUCTION

In the broadest terms a mass driver is any machine that accelerates a payload of material to a high velocity. This definition would include a cannon, an air rifle, an aircraft carrier catapult, or a child's slingshot. In this report, however, the term "mass driver" will refer specifically to a linear synchronous electric motor.

Basic Principles

Converting the energy of a magnetic field into mechanical motion is not a new idea; indeed, electric motors have been used in one form or another since electromagnetism was first discovered, over one hundred fifty years ago. Many people are familiar with the operating principles of the garden-variety electric motors that run elevators, start our cars and blow dry our hair.

In a conventional electric motor a rotating electromagnet is attracted by a stationary magnet. As the poles are aligned, the polarity of the electromagnet is reversed, resulting in an unstable configuration. The magnet moves around to become realigned with its new north and south poles and the polarity is switched again. The process continues, resulting in a continuously rotating magnet, or a motor.

Both in theory and in practice, such a motor can be "unwound" to impart motion to a magnet in a linear direction. This is the principle that leads to the design of linear induction and linear synchronous motors. In these motors, an electromagnet is placed in a tube lined with stationary electromagnets that are switched on and off in sequence. As the magnet moves through the tube it is pulled by an attractive force from a stationary magnet in front and pushed by another stationary magnet from behind. When the moving magnet reaches the end of the tube, the moving magnet has a high velocity. This velocity is a function of the magnitude of the magnetic forces and the length of the launch tube.

In a linear induction motor the sequence of changing magnetic fields is a predetermined function of time. In theory this is a reasonable design, but in practice it leads to inefficiencies because the magnet cannot be relied upon to be in the right place at precisely the right time.

A linear synchronous motor, as its name might imply, synchronizes its magnetic fields according to the actual measured position of the magnet. This allows the maximum force to be generated at any given

time, and allows very high accelerations, on the order of 10^2 to 10^3 g's (1 g = 9.8 m/s^2). Use of either type of linear motor (induction or synchronous gives an additional bonus; the magnetic fields provide a guide force tending to keep the vehicle in the center of the tube, so that the system is mechanically frictionless.

4.2 SYSTEM DESCRIPTION

The mass driver is essentially a long tube of aluminum. The inside of the tube contains thousands of coaxial, equally spaced aluminum coils. The payload carrier, henceforth referred to as the bucket, is a can with two superconducting coils of square cross section at either end. One coil would be sufficient to propel the device, but two are employed to give stability in pitch and yaw. The spacing between the bucket coils is six times the spacing betwee the aluminum drive coils (Figure 4.1). The payload to be launched is placed inside the bucket, the front end of which is left uncovered. In general applications, the payload can be loaded at any time previous to launch, but in this particular application, the payload generates a great amount of heat which would likely have an adverse effect on the superconducting coils. For this reason loading occurs immediately prior to launch. The loaded bucket is then placed at one end of the tube.

An electric current is pulsed through the two drive coils (stationary magnets) immediately in front of the bucket coils. The current has a direction such that an attractive force acts on the bucket. As the bucket moves forward, a negative pulse is sent through the coils behind it, setting up a repulsive force which also gives forward motion (Figure 4.2). In addition to forces in the direction of motion, there are forces perpendicular to the motion as the bucket is repelled or attracted by its magnetic image in the tube walls (Figure 4.3). The "pulling" force from the front coils tends to center the bucket, while the "push" from behind destabilizes the motion. For this reason the "pull" is made slightly greater so as to lend an overall stability to the system (Figure 4. As the bucket moves on to the next set of coils, its position is sensed by the interruption of a light beam. This triggers the next cycle. The next cycle is similar to the first one, except that the frequency of the pulses must be a little higher because the bucket now has a higher velocity and is moving past the coil more quickly. This process continues as the bucket moves down the tube, accelerating the bucket until it reaches the desired velocity.

At this point the currents are reversed, pushing from the front and pulling from behind, causing the bucket to decelerate. The payload, being relatively non-magnetic, does not decelerate. It exits the front of the bucket as the bucket is slowed and continues at a constant velocity. The decrease in mass of the bucket as the payload is released causes it to decelerate more rapidly then it was accelerated, because the magnitude of the magnetic forces is the same in both cases. This results in a shorter decelerating section.

The bucket is slowed to a stop and removed from the tube. If necessary, its coils are recooled and their current is readjusted inductively. It is then reloaded to be sent back the other way.

4.3 MASS DRIVER PARAMETERS

The mass driver launch vehicle consists of four, long parallel mass driver tubes in a square configuration. Four tubes are required to eliminate any net force or torque on the system. If there were only a single tube firing nuclear waste forward, the reaction force backward would result in a rapid orbit decay. Therefore, a "dummy" reaction mass is launched backward to compensate. Only two launch tubes would create a couple which would rotate the structure. Hence, two more tubes are added to give zero moment to the system. The entire vehicle is then kept constantly parallel to its orbital velocity about the earth.

Each mass driver tube is 6.4 km long and .156 meters in diameter. The accelerating section has a length of 4.13 km. The length of the decelerating section is 2.19 km. Inside these tubes are circular aluminum drive windings spaced every 2.89 cm.

The buckets which carry the payloads are right circular cylinders, with the forward end open to allow insertion and removal of the payloads. A superconducting coil is wrapped around each end of the bucket. Each coil carries a current of 6.08×10^4 amps. The total empty bucket mass, including coils, is 1.123 kg. With a payload of one kilogram, the loaded bucket mass is 2.123 kg. The payload, also cylindrical, has a length of 14.43 cm and a diameter of 4.68 cm. Payload density is assumed 4×10^3 kg/m^3.

To dispose of the 200,000 kg/year of nuclear waste projected for the year 2000, 40 kg must be launched per orbit. Two kilograms can be launched at once through the two forward tubes, so this works out to 20 launches per orbit. 20 launches in the 192 second launch window gives 9.63 seconds between launches.

The time required to accelerate the loaded bucket to the desired 9000 m/sec is .92 seconds at an acceleration of 1000 gravities or 9800 m/s^2 The payload will spend .24 seconds in the launch tube after release from the bucket. The empty bucket will decelerate to zero velocity at 1890 gravities in .49 seconds.

4.4 POWER SUPPLY

A formidable design problem occurs due to orbital mechanical considerations because launches must be made on the night side of the orbit. Since solar power is employed, this means that when power is most needed, it is least available. It becomes clear that some sort of energy collection and storage system is required.

4.4.1 Energy Collection

The vehicle will spend 61% of its orbit or 56 minutes of each orbit, in sunlight. The amount of energy that must be collected is the sum of the payload kinetic energy plus housekeeping requirements while in the earths shadow. The payload kinetic energy lost per orbit is given by the formula

$$E = \frac{1}{2} m V^2 \qquad (4.1)$$

To launch an average of 40 kg of nuclear waste per orbit, it may prove necessary to launch 80 kg on some orbits to make up for down-time. Thus the m in Equation (4.1) is 160 kg (80 kg of nuclear waste plus 80 kg of dummy reaction mass).

The V is the ΔV of 9000 m/s giving

$$E = 6.5 \times 10^9 \text{ Joules}$$

Assuming housekeeping requirements for cryogenics and life support of 10^6 watts x 2190 sec (time spent in the dark) gives an additional 2.2×10^9 Joules or a total energy storage requirement of 8.7×10^9 Joules. To collect this much energy in 56 minutes requires a collection capability of 8.7×10^9 Joules/ (56 min x 60 sec/min) = 2.6×10^6 watts. Adding housekeeping power of 10^6 watts gives a total power requirement of 3.6×10^6 watts.

If solar panels are evenly distributed along the length of the structure, there will be two sections of the orbit where the structure will be pointing at the sun, and will not be able to collect energy efficiently due to panels shadowing each other. Therefore, the amount of usable sunlight time was cut to 40 minutes. This yields a power collection requirement of 4×10^6 watts.

Assuming a solar cell efficiency of 17% and a solar constant of 1400 w/m^2 gives a total panel area of 1.7×10^4 m^2. If at any given time 25% of the panels are shadowed by structure, 2.3×10^4 m^2 are required for the same power capability. There are four panels placed at each of the 628 ring sections, or 2512 panels total, each with an area of 9.16 m^2 or square panels 3.03 meters on a side.

For maximum efficiency the panels should be rotatable to track the sun. This should not present any problems with slip rings, because the panels will never have to make a full revolution. The panels would rotate in the sunlight, transferring power through flexible cables, and could be "unwound" in the dark in preparation for the next orbit. The back sides of the panels, always facing away from the sun, would serve as waste heat radiators.

4.4.2 Energy Storage

Storage batteries were chosen to store the collected energy. Although this is not the most economical solution, it is the simplest. The options of homo-polar flywheels, pulsed magneto-hydrodynamics and thermal storage were briefly explored, but the use of such storage systems would require extensive research and development. Certain present state-of-the-art batteries combine the high power densities, high energy densities, and long cycle lives required.

Lithium-aluminum/iron sulfide batteries were determined to be the most suitable at this time. The batteries exhibit a power density of 145 w/kg and an energy density of 5.4×10^5 Joules/kg. Cycle life is on the order of 1000 cycles.

The power requirement at any time during the launch phase is housekeeping plus each single launch requirement. The single launch requirement power is

$$P = \frac{m V^2}{2 \Delta t}$$

where V = 9000 m/s, m = total loaded bucket mass and Δt = time between launches = 9.63 seconds.

$$P = \frac{(4)\ 2.123\ \text{kg}\ (9000\ \text{m/s})^2}{2\ (9.63\ \text{sec})} = 3.6 \times 10^7\ \text{watts}$$

with housekeeping the total power is 3.7×10^7 watts or a total battery mass of 3.7×10^7 w/ 145 w/kg = 2.55×10^5 kg. Note that this much battery mass will store 1.37×10^{11} Joules or 16 times the energy storage requirement. The fact that the batteries will never even approach full discharge should greatly enhance battery life.

4.5 ELECTRICAL MASSES

Except where noted all the equations are taken from the results of the 1977 NASA Ames summer study on space industrialization.

v = exit velocity = 9000 m/s
m_p = specific power plant mass = .005 kg/watt
m_1 = payload mass = 1 kg
a = acceleration = 9800 m/s^2
fr = launch rate = 1/9.63 sec^{-1} but taken conservatively to be 1 hz for the purposes of these calculations

Winding mass = $Mw = .122\ v^{3/2}\ mp^{1/2}\ fr^{1/2} \times 4$

= 29460 kg

Solar panel mass = mp x 4 x 10^6 watts = 2 x 10^4 kg

Radiator mass = Solar panel mass = 2 x 10^4 kg

Feeder mass = $M_F = 7.19 \times 10^{-4} v^{5/3} a^{1/3} m^{5/9} fr^{1/3} \times 4$

$= 2.4 \times 10^5$ kg

Capacitor mass = Feeder mass = 2.4 x 10^5 kg

Kinetic Power Mass = .0025 fr m V^2 x 4

$= 8.1 \times 10^5$ kg

SCR mass is $1.66 \times 10^{-10} v^3 a m^{1/3} \times 4$

$= 4.75 \times 10^6$ kg

but this equation is based on the weight specifications off-the-shelf 1977 silicon controlled rectifiers. Since that time the specific mass of SCR's has been reduced by a factor of two. Further reduction can be expected in the next decade as solid state devices are developed specifically for use in large-scale space applications. The reason that such reduction has not occurred already can be attributed primarily to a lack of research in the appropriate areas. It was assumed that these devices can be reduced in mass by an order of magnitude by the year 1990. This represents a total reduction of a factor of 20 from the optimized equation yielding an SCR mass of

2.4×10^5 kg.

By summing all of the above masses the total electrical mass is

1.6×10^6 kg.

4.6 REFERENCES

1. O'Neill, Gerard K., "The Low (Profile) Road to Space Manufacturing," Princeton University, Astronautics and Aeronautics, March 1978, Vol. 16, No. 3.
2. Billingham, Gilbreath and O'Leary, Space Resources and Space Settlements NASA Publication SP-428, August 1979
3. Graham, Robert W., Secondary Batteries: Recent Advances, Noyes Data Corporation, Park Ridge, N. J., 1978.
4. NTIS A03/MF A01, "Development of Lithium/Metal Sulfide Batteries at Argonne National Laboratory: Summary Report, 1976", March 1977.

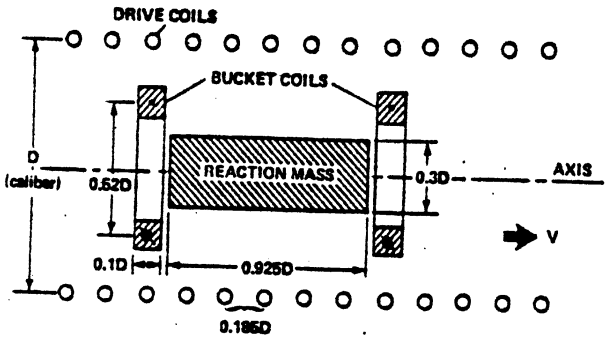

Figure 4.1 Longitudinal Cross-Section of Axial Drive Coils and Loaded Bucket

Diagrams reprinted from Ref. No. 2.

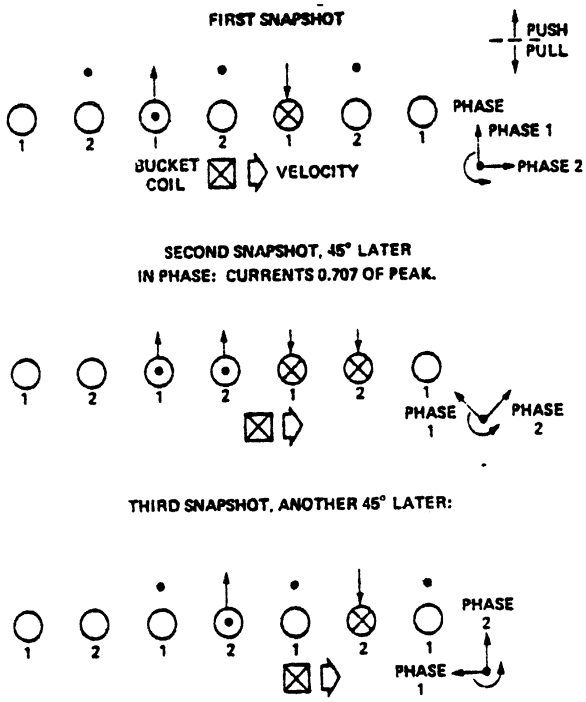

Figure 4.2 Current in Drive Coils

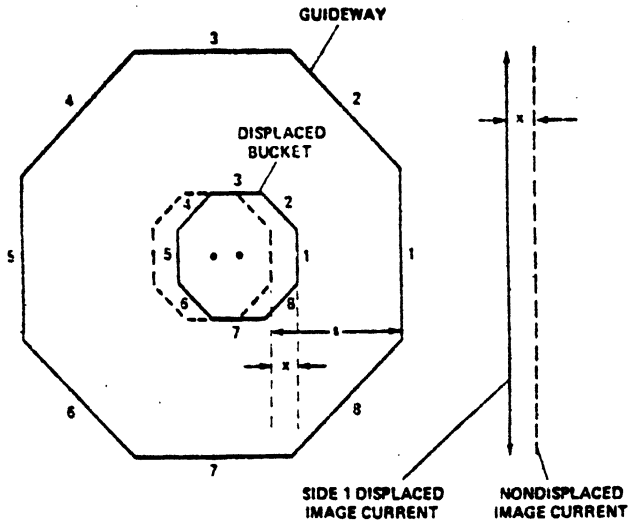

Figure 4.3 Bucket and Guideway Geometry

5
STRUCTURAL DESIGN

5.1 INTRODUCTION

The structural design is motivated by three primary considerations: First, it is necessary to insure that the mass driver remains straight while the payloads are being launched. Second, it is important to design the mass driver to be able to withstand the stresses induced by the rapidly accelerating payloads. Third, the containment package for transporting waste material from earth to the orbiting mass driver must meet specified standards for performance while minimizing overall package weight.

Due to the extreme slenderness of the mass driver structure, the difficulty of insuring structural integrity becomes great by comparison with 'conventional' spacecraft.

It is, of vital importance to maintain the 'straightness' of the launching tubes so that the payloads will not graze the tubes' inner walls. This problem is not trivial because the structure's extreme slenderness causes it to behave somewhat like a 'string'; that is, it has negligible flexural rigidity on a global scale. Thus any disturbing influences such as the earth's gravity, local perturbations in the gravitational field, thermal irregularities, etc. will have a considerable influence on the mass driver, and will manifest themselves in their tendency to cause the mass driver to deviate from the desired 'straight' configuration.

In fact, the mass driver is stable in a curved configuration while in earth orbit (Reference 4). The affects of all such disturbing influences will be counteracted by a network of tension cables attached to the mass driver.

Materials chosen for the mass driver must meet the requirements of high strength and low weight, and must also retain favorable characteristics in the harsh environment of earth orbit.

The package for transporting the nuclear waste material from earth to the orbiting mass driver was designed to make the most efficient use of materials possible. The mission objectives dictated the design of a lightweight system which can withstand the most severe in-flight loadings. No design work was done on a re-entry heat shield or other fail-safe systems. However, approximately 15,000 lbs of shuttle payload capacity has been allocated for the accommodation of such systems.

The total structural mass of the mass driver was found to be 2.527×10^6 kg (5.559×10^6 lbm).

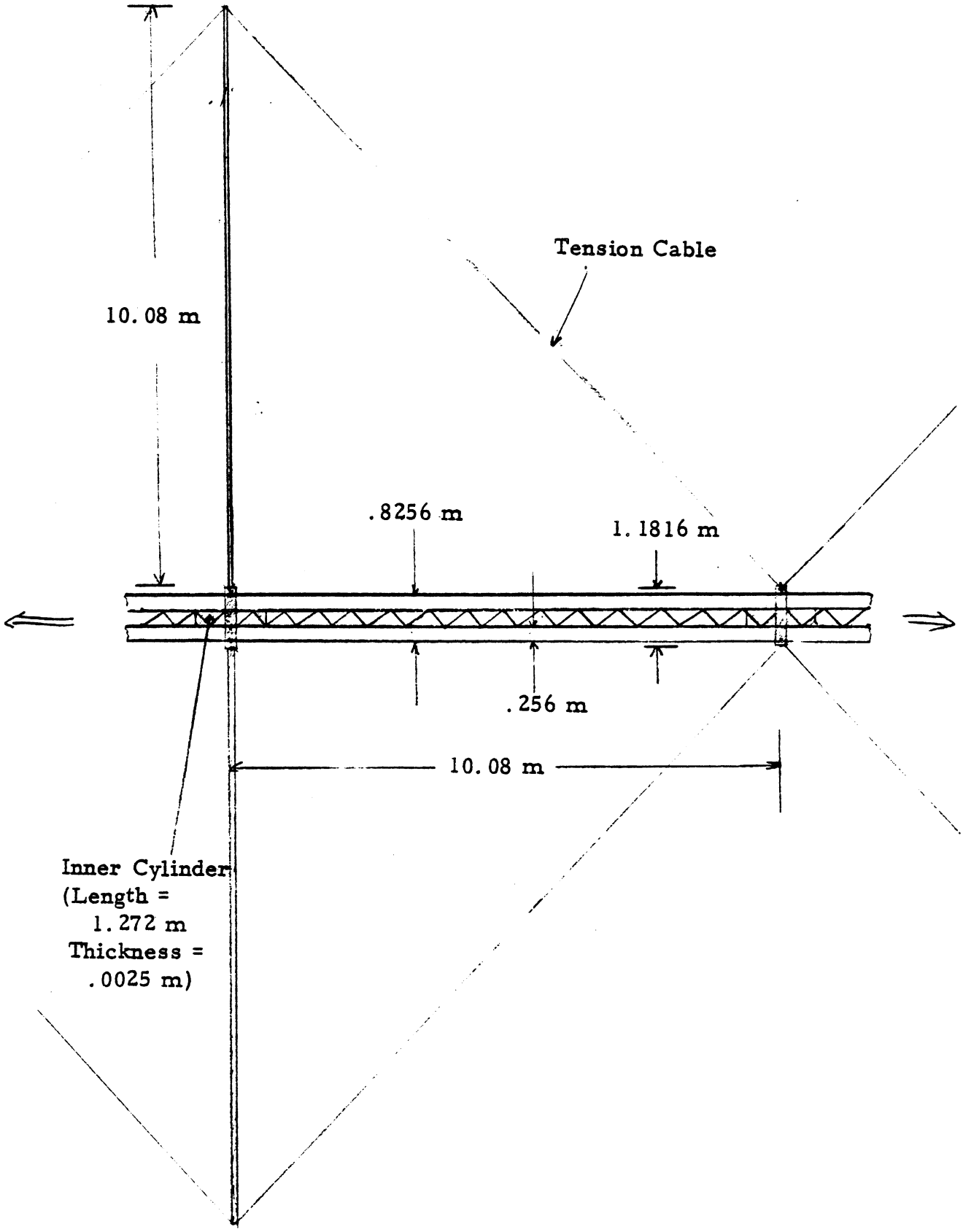

Figure 5.1 Mass Driver Segment Geometry (excluding solar cell arrays)

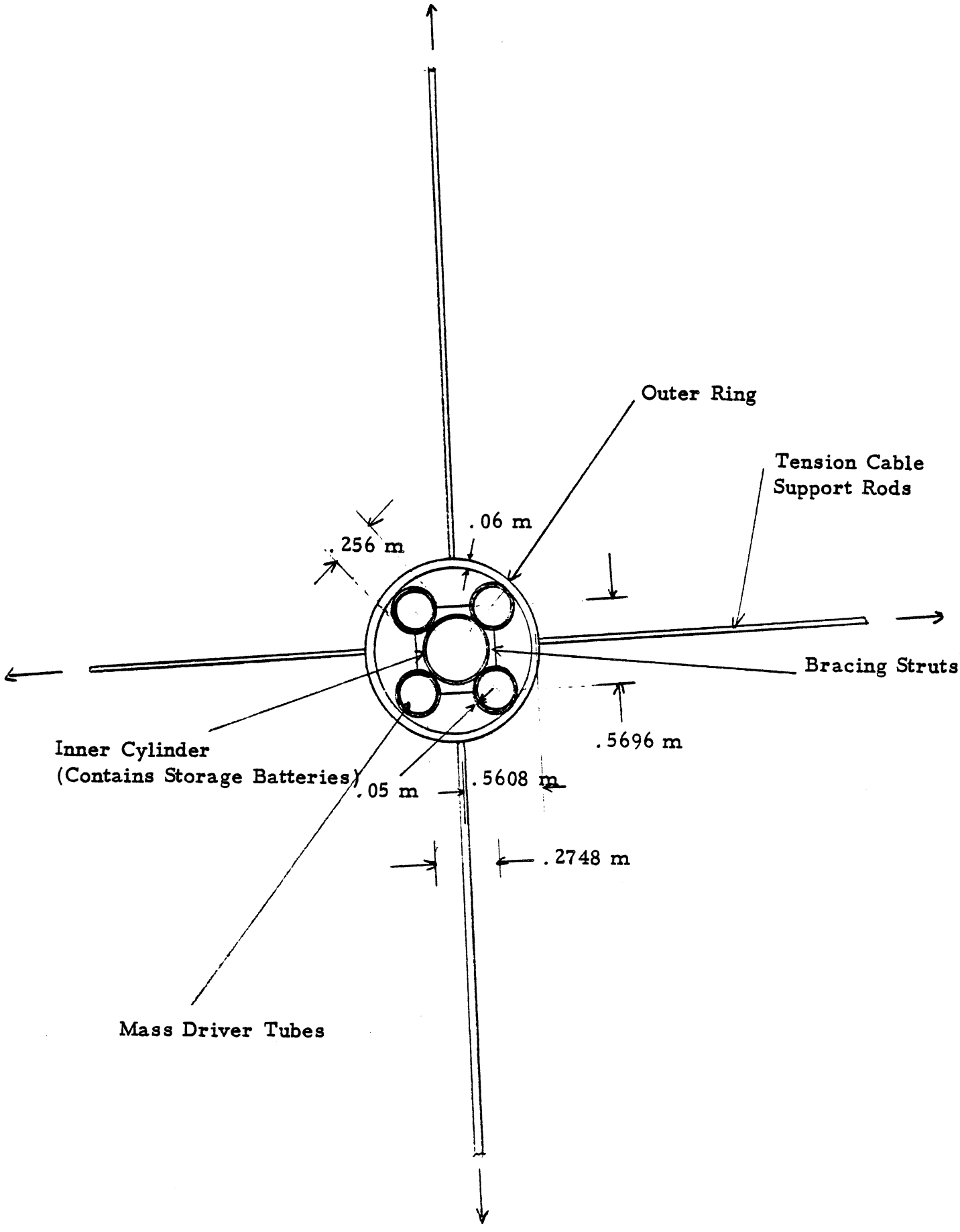

Figure 5.2 Mass Driver Geometry, Cross-Sectional View

5.2 MASS DRIVER TUBE SIZING

It so happens that the analysis of the mass driver tubes presents considerable difficulty for the following reasons:

The nuclear waste payload is accelerating from rest in the mass driver tubes. The interaction of the magnetic fields associated with the payload bucket coils and the mass driver's drive coils causes stress waves to be propagated from each drive coil as the bucket passes that drive coil. These stress waves are propagated through the tube in two directions from each drive coil. The stress waves in one direction are tensile while those in the opposite direction are compressive (Figure 5.3).

When the velocity of the bucket is substantially subsonic (i.e., less than the speed of sound in aluminum, which is approximately 5000 m/sec or 16,390 ft/sec), the waves propagated as a result of the passage of the bucket will arrive at the following drive coil considerably in advance of the traveling bucket. Thus, the instantaneous force between two drive coils will give the transient stress which the tube must tolerate. This force is found to have a maximum tensile value of 800 newtons (180 lbf) and a maximum compressive value of 500 N 9112.5 lbf) (Reference 4).

These forces are found by numerically solving a series of non-linear simultaneous equations involving drive coil current, bucket coil current, and 'gradients of mutual inductance' (Reference 4).

However, the complete description of the stresses in the mass driver tubes requires a more rigorous analysis.

When the accelerating bucket attains a velocity which is supersonic, the magnetic field interaction will cause stress waves to be propagated (again, at the speed of sound) which travel at a slower rate than the bucket. Thus, the bucket will reach the next drive coil in advance of the stress wave generated by the previous drive coil.

If our bucket were traveling at a constant velocity, the stress waves generated by each coil would be identical in amplitude and waveform. The magnitude of the transient stress which the tubes must endure would be given by the superposition of these waveforms where they undergo constructive interference. This is not a difficult problem to analyze but the result has little relevance because our payload is accelerating. Due to this acceleration, stress waveforms will be generated which have successively shorter wavelengths because the bucket is in the vicinity of a drive coil for successively shorter periods of time. The constructive and destructive interference patterns of these waves are very difficult to ascertain. Thus, the ultimate transient stress which the tubes must tolerate is very difficult to arrive at. This analysis is beyond the present capabilities of the authors and must await further research.

To further compound the problem, the effects of shock stress waves produced by the accelerating bucket must also be considered. The fact that the wave source (bucket) is accelerating complicates this problem considerably This analysis must also await further research.

Thus, for design purposes, it was decided to use the maximum tensile and compressive forces which are encountered in the subsonic region outlined previously. This analysis includes a very considerable safety margin which should account for the aforementioned effects of the accelerating payload.

A major concern in this project is to insure that no stresses occur in the mass driver as a result of attitude control maneuvers. It was decided that a linear distribution of thrust, which passes through zero at the mass driver's center of mass, provided the desired effect. Section II of the appendix includes a verification of this fact.

It is also important to prevent dynamic resonance of the mass driver during such maneuvers. Accordingly, the flexural vibrations of the mass driver which would arise from attitude control thrusting are discussed in Section III of the appendix.

5.3 SHUTTLE BAY WASTE CONTAINER SIZING

5.3.1 Design Criteria

The nuclear waste containment package was designed using the following criteria:

1. Radiation shielding sufficient to insure that a radiation level of one rem/hour at a distance of one meter (3.28 ft) from the package is not exceeded.

2. Package integrity must be maintained during launch.

3. The package must be thermally and chemically stable so that it may resist the heat and corrosive agents produced by the nuclear waste material.

4. The package weight must be minimized to permit a maximum payload (nuclear waste) carrying capacity.

5.3.2 Summary of Container Properties

I. Small, cylindrical waste containers:

Dimensions:

r (≡outer radius) = 2.34 cm (.921 in)
l (≡length) = 14.43 cm (5.68 in)
m (≡mass) = 1 kg (2.2 lbm)

These dimensions were determined from an optimization formula which is included in the Mass Driver report.

The containers are made of stainless steel for thermal and chemical stability.

II. Large cannister for containment of nuclear packages:

A. Materials
- Tungsten layer
- Lithium Hydride layer
- Stainless steel load-bearing outer shell (cylindrical)

1. Tungsten layer (closest to nuclear waste containers) is 5 cm in thickness (1.97 in). Justification for this specification is given in the materials specification Section 5.5.

2. Lithium Hydride layer (surrounding tungsten layer) is 12 cm (4.72 in) thick. Again, see Section 5.5.

3. Stainless steel load-bearing layer (surrounding Lithium Hydride Layer) is .5 cm (.197 in) thick (see Section 9 of the appendix for an explanation of the specifications).

B. Shape

Right circular cylinder with length to diameter ratio equal to one for efficient packaging and high strength.

C. Procedure for Optimization of Package Dimensions

1. The small cylindrical nuclear waste containers have the dimensions given in Part I of this section. Also, the density of the waste material is know to be 4 gms/cm^3.

In addition, the shielding and load-bearing materials in the containment cannister are as given in "A", above. Material densities are:

a) steel (8.0 gms/cm^3
b) Lithium Hydride (.7759 gms/cm^3)
c) Tungsten (19.3 gms/cm^3).

2. Procedure (as shown in Figure 5.4)

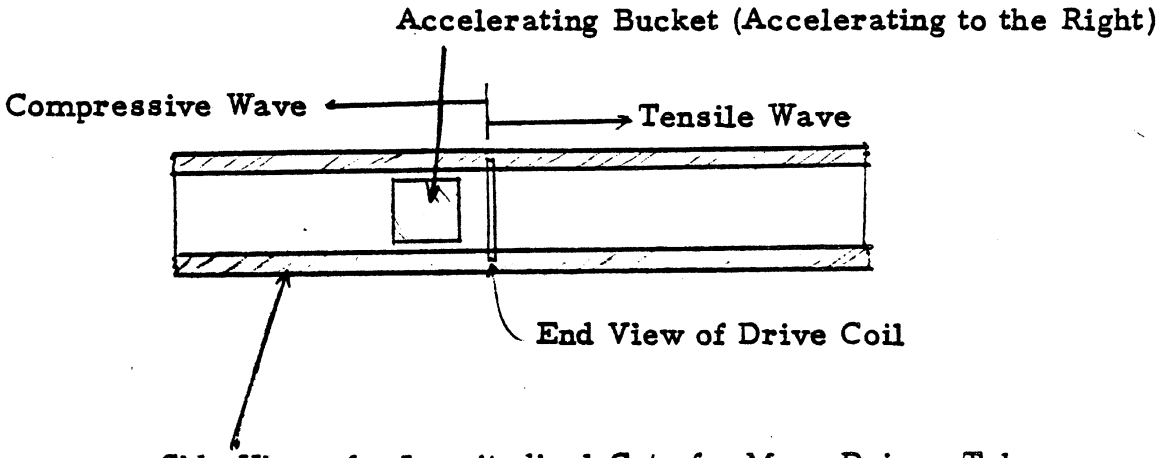

Figure 5.3 Schematic Representation of Mass Driver - Bucket Interaction.

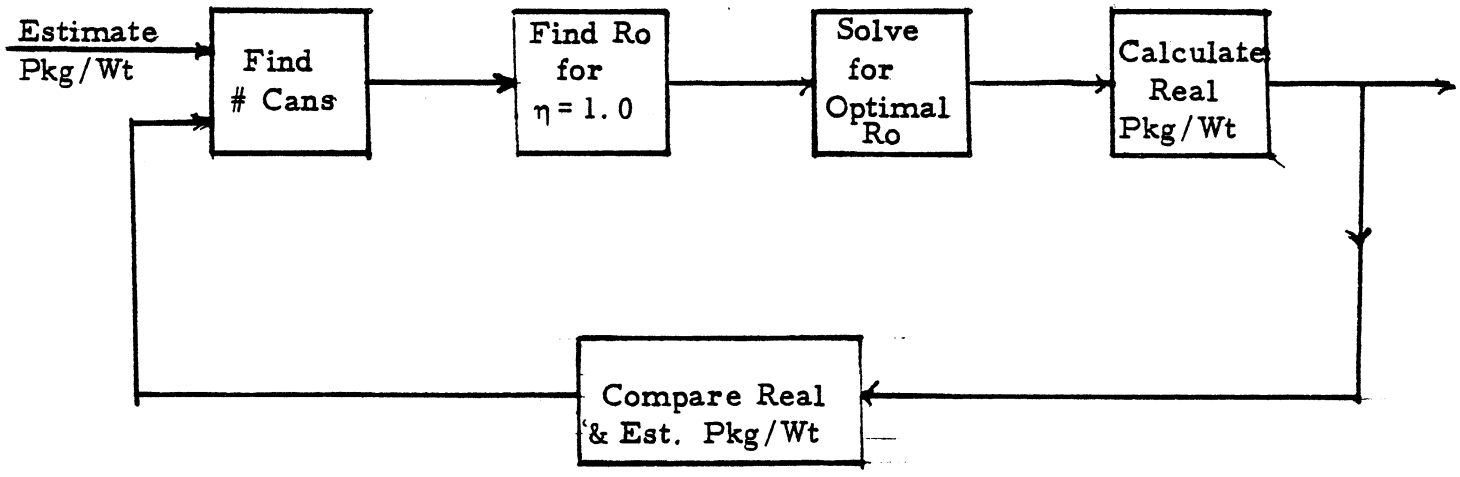

Figure 5.4 Method for Package Size Optimization

a) Estimate a ratio of package weight (loaded) to contents weight.
b) Using the maximum total weight limit, find the weight of the nuclear material for the estimated ratio. Each small container has a known mass (1 kg), so solve for the number of small containers in each large cannister.
c) Assuming 100% packaging efficiency, find the inside radius of the cannister to contain the computed amount of nuclear material. (This radius corresponds to the radius required to contain 'loose' (unpackaged) nuclear material.
d) Assume a packing efficiency for the small containers in the large cannister. Find a new cannister radius corresponding to the decreased (previously 100%) efficiency, and determine the number of cans possible for the new radius. Since the total number of small containers is known, and the number of cans per layer (shelf) has been determined (see Section 8 of the appendix), one can solve for the number of layers needed to contain all the cans. Again, the cannister has a ratio of length to diameter equal to one, so the length of the cannister for the radius computed (a function of packing efficiency) can be determined. This package length can then be compared to the internal container length (number of layers times the length of each small container). One may now calculate the thickness of each shelf (see Section 8 of the appendix). Reiterate, using a smaller packing efficiency ($\equiv\eta$) if the shelf thickness is less than that required for structural purposes (again, see Section 8).
e) Calculate the true weight of the package using the radius (a function of η) needed for the best efficiency with acceptable shelf thickness.
f) Compute 'real' ratio of package weight to contents weight for the real weight, and the number of containers for the estimated ratio of package weight to total weight. This will be greater than or equal to the actual ratio if it is less than the estimated value because the number of cans will be greater.
g) Reiterate, using an estimated value of the ratio of package weight to contents weight equal to the 'real' value found from the previous iteration. The error will decrease to zero using this method (when the estimated and 'real' ratios are equal). The result is the optimum ratio of package weight to contents weight.
h) A numerical example is given in Section 8 of the appendix.

III. Conclusion

The small cylindrical waste containers are contained in the large cylindrical cannister.

A. Small containers (see Figure 5.5)

1) Dimensions:

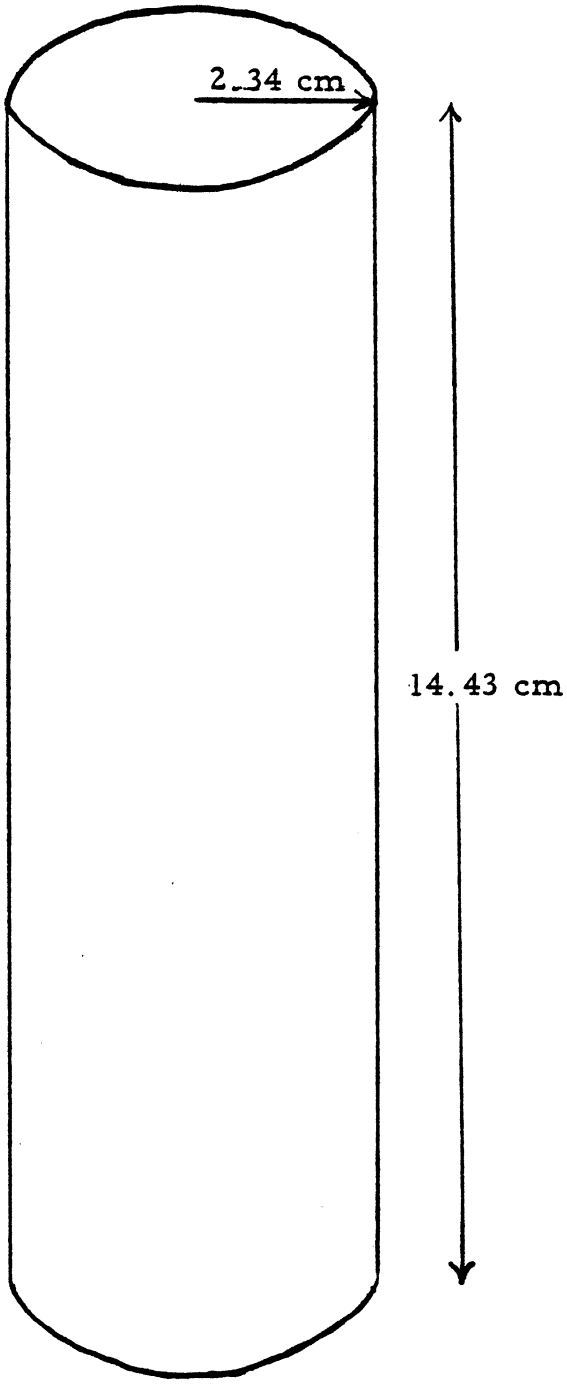

Figure 5.5 Small Nuclear Container

r = 2.34 cm
l = 14.43 cm
t (thickness) = 1.66×10^{-4} cm, from Section 8 of the appendix.

2) Mass
   a) nuclear material contained: .9997 kg (2.199 lbm)
   b) stainless steel container: 3.27×10^{-4} kg (7.19×10^{-4} lbm)
   c) total mass of each package: 1 kg (2.2 lbm).

B. Large cannister (see Figure 5.6)
   1) Dimensions:
      a) outer radius = 95.83 cm (37.73 in)
      b) inner radius = 78.33 cm (31.04 in)
      c) outer length = 191.66 cm (75.46 in)
      d) thickness = 17.5 cm
         1) tungsten layer: 5 cm
         2) Lithium Hydride layer: 12 cm
         3) stainless steel shell: .5 cm
   2) Internal shelving:
      a) number of shelves = 7
      b) thickness of each shelf = .507 cm
      c) mass of each shelf = 77.5 kg
      d) maximum shelf deflection during launch = 3.18 cm
         b) & d) were determined in Section 8 of the appendix.
   3) Packaging:
      a) packing efficiency (by shelf area) = 78.7%
      b) number of containers per shelf = 882
      c) number of concentric rings of containers per shelf = 17.
   4) Mass
      a) ratio of package weight to contents weight = 1.90
      b) mass of nuclear material = 6,174 kg (13,583 lbm)
      c) mass of package = 11,730 kg (25,807 lbm)
      d) total mass = 17,904 kg (39,389.8 lbm)

5.4 SIZING OF SUPPORT STRUTS FOR MASS DRIVER TUBES

5.4.1 Design Criteria

The support struts for the mass driver tubes were designed using the following criteria:

1. The struts should withstand a conservative model of the applied forces, with a safety factor equal to 1.2.

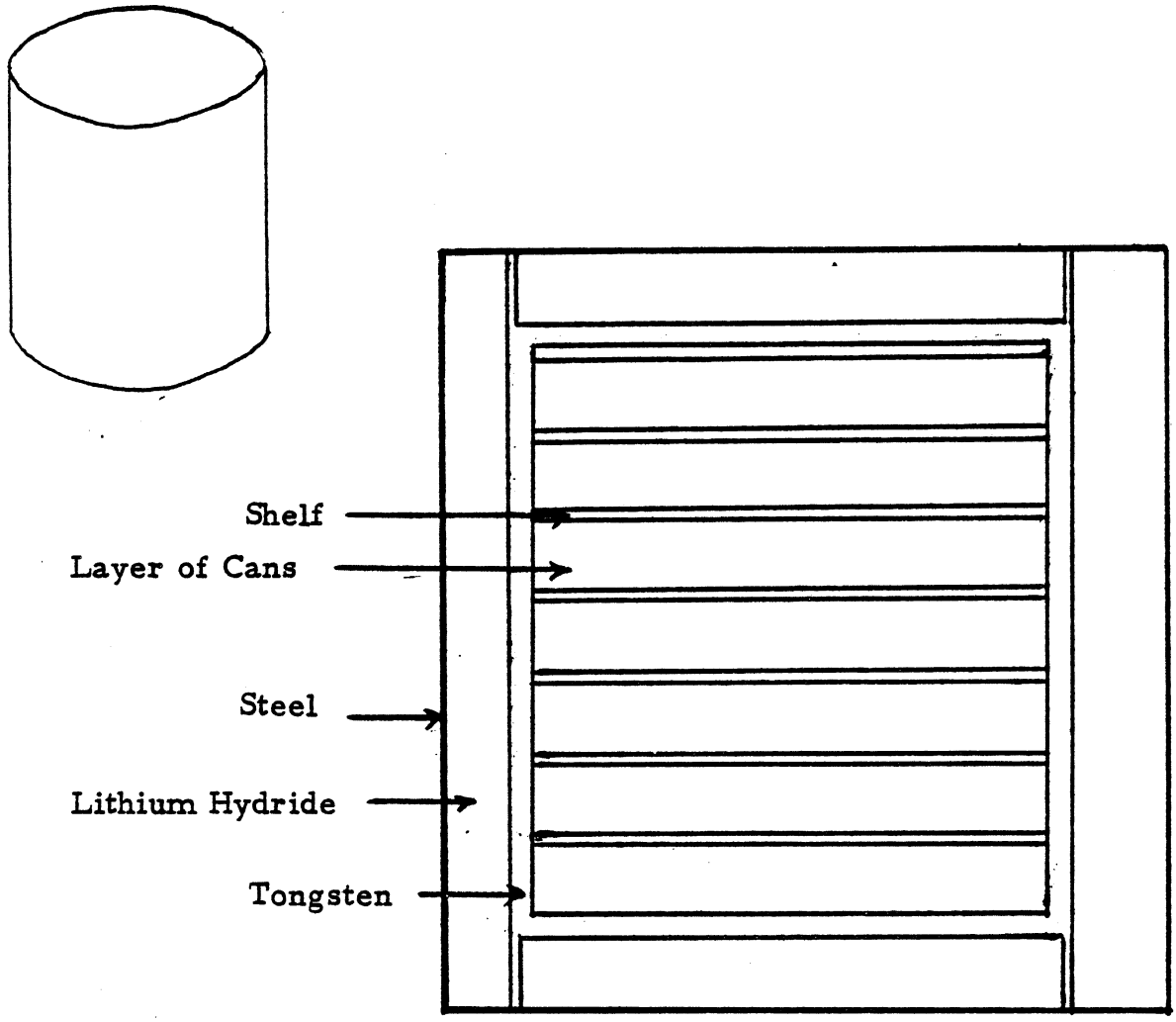

Figure 5.6 Large Cannister for Shuttle Transport

2. The mass of the struts should be minimized.
3. The struts must not interfer with the mass driver's inner structure.

The applied force may be conservatively modelled as the mass of the payload inside the mass driver multiplied by its acceleration. The largest applied force on a strut will occur when the payloads are traveling (in adjacent tubes) in opposite directions and are located at the ends of a single strut.

One might suppose that the entire mass driver would buckle when the applied forces are directed towards one another and are applied at opposite ends of the mass driver. However, due to the fact that the payloads are traveling at supersonic velocities for the majority of the launch time, the axial applied force will not be 'felt' by the entire mass driver instantaneously. Buckling is a quasi-static phenomenon and will not occur unless the applied force is 'felt' globally by the entire structure.

5.4.2 Conclusion (see Section 10 of the appendix for calculations)

The support struts are welded to the mass driver tubes at an angle of 45° to the tubes longitudinal axis (see Figure 5.7).

Dimension:

a) length of strut = .4435 meters (17.48 in)
b) height, width = 1.854×10^{-2} m (.73 in)
c) cross-section area = 3.437×10^{-4} m^2 (.533 in^2)
d) mass of each strut = 4.116×10^{-1} kg (9.055×10^{-1} lbm)
e) number of struts = 8.063×10^{4}
f) total strut mass = 3.318×10^{4} kg (7.3×10^{4} lbm)

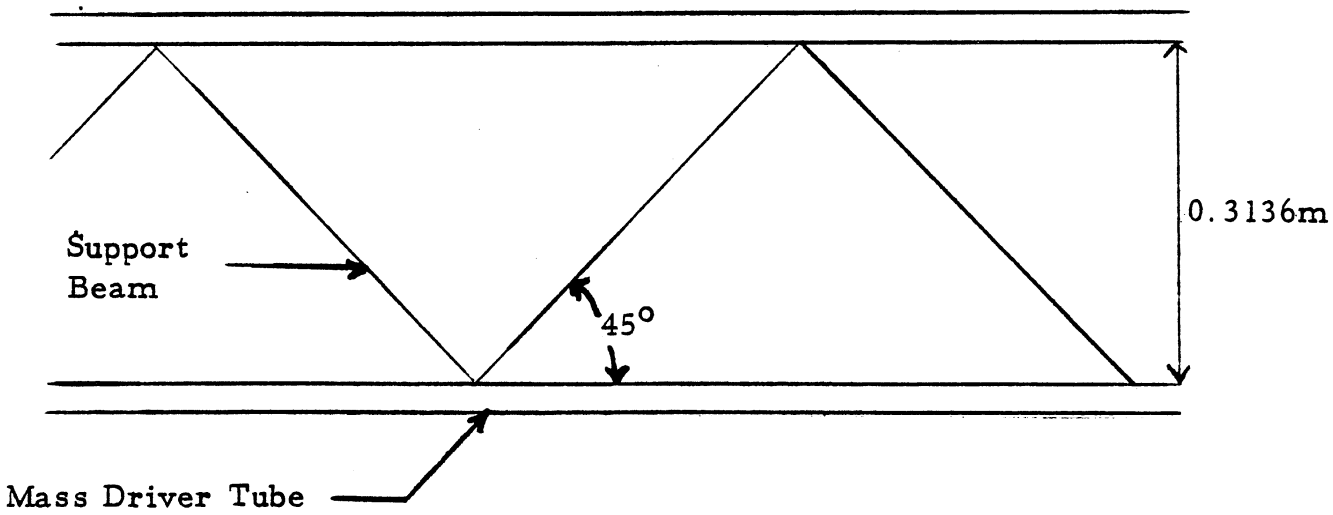

Figure 5.7 Side View of Mass Driver Support Bracing

5.5 LARGE SPACE STRUCTURE CONSTRUCTION METHODS

The 'beam-builder' is a realistic and efficient method for large scale space construction. The space shuttle serves as an ideal launch vehicle and construction base for the unit. Following the boost to orbit, the unit is deployed from the stowed configuration in the shuttle bay. Beam builders are now capable of fabricating an interconnected skeleton of four triangular beams 200 meters long. The unit can turn out a triangularly shaped cap structure of thin aluminum or other desirable material at a rate of 5 ft/min. This is the equivalent of fabricating a one mile long structure in a period of 24 hours.

Longitudinal members and cross-beams are made up of elements referre to as caps. The cross-beams serve to interconnect the four longitudinal members, and are otherwise identical to the longitudinal structure. Pre-formed cross-members are located at intervals along the caps and provide rigidity. Continuous cord is installed diagonally across opposite corners of each cap section.

The two principal parts of the unit are the beam-builder and the assembly jig. The beam building process occurs in the following sequence: Pre-consolidated flat strip material is rolled out of a storage cannister by a drive mechanism. Next, the material is heated, fabricated into the desired shape, and rapidly cooled. As the cyclic process continues, cross-members are discharged from their storage clips and are ultrasonically spot welded to the caps. At the same time, constant-force tension mechanisms are installing the diagonal cord, which is being unwound from the storage spool.

The assembly jig serves to retain and transport the completed structure across the face of the unit so that the following section can be fabricated. Once the longitudinal structure has been constructed, caps are fabricated into nine (9) cross beams which connect the four (4) longitudinal beams. The completed assembly takes on the appearance of a ladder.

The process just described is best utilized in the manufacturing of long, continuous structures. For instance, the process would be well-suited to the construction of solar power satellites. The beam-builder concept, with certain modifications, can be employed in two ways for the construction of the mass driver. First, the diagonal bracing struts (discussed in the previous section) could be fabricated using this system. Second, thousands of rods are necessary in the tension cable system mentioned previously. Beam builder concepts provide a means of extruding these structures in space. Thus, the employment of a beam-builder(s) would accelerate the construction of the mass driver and its related structure.

5.6 SUSPENSION CABLE SYSTEM

The center of the mass driver is orbiting the earth at an altitude of 400 km (216 nautical miles). Assuming that the mass driver is in a straight configuration, the radius of the orbit will increase as the mass driver is traversed from the midpoint to the ends. In other words, individual elements of the mass driver travel at different orbital altitudes. Each elemental part tends to seek an orbit at a certain altitude with respect to the center of the earth. The result is a moment distribution along the mass driver structure which tends to displace the ends of the mass driver towards the center of the earth (see Section 11 of the appendix).

In order to counteract this moment, a system of supporting rods and tension cables has been developed (see Figure 5.1). The principle behind this system is as follows: when the mass driver begins to bend, forces would be applied to the cables in order to restore the mass driver to the aligned configuration.

The first consideration was to determine the spacing between individual supporting rods. In an effort to achieve maximum effectiveness and maximum weight, it was decided that the supporting rods would be installed on alternating outer rings of the mass driver (see Section 4 of the appendix for details).

Since the moment on the mass driver due to gravity is continuous with respect to the longitudinal axis (see Section 11 of the appendix), it is desirable to counteract this moment by a continuous applied moment. Spacing the supporting rods on alternating rings gives a good approximation.

To minimize thermal stresses, it is desirable to rotate the mass driver about its longitudinal axis. In this event, it would be necessary to install supporting rods symmetrically around the cross-section. Accordingly, four supporting rods are installed at equidistant points on the outer rings to compensate for the gravitational bending moment regardless of the mass driver's orientation.

The distance between supporting rods is 20.16 m (66.14 ft). The angle between the cables and the mass driver's longitudinal axis is 45°. Thus, the length of each rod is 10.08 meters (the distance between adjacent outer rings).

Deciding on the rod's cross-sectional shape was the next consideration. It was determined that a square section was superior to a circular section because the former has a greater moment of inertia for a given cross-sectional area. The 'I'-section proved to be yet more attractive due to a 40% savings in mass for a given strength.

Aluminum (7075-T6) was chosen for use in I-beam construction due to its high strength and low density. The material chosen for the cable is stainless steel (347) due to its high yield strength. Due to cyclic loadings, the tension cables will experience metal fatigue over a period of time. As a result, cables will require periodic replacement.

A series of equations were used to relate cable and beam cross-sectional areas to cable tension (see Section 7 of the Appendix). The cables and beams were designed to sustain a load of 4448 N (1000 lbf), which, it is believed, will be sufficient to generate a bending moment to counteract that which is produced by gravity.

Conclusions: a) The rods will have an "I"-shaped cross-section with an area of $3.7 \times 10^{-3}\ m^2$.
b) Mass of each rod = 106.01 kg
c) The cables have a cross-sectional area of $1.84 \times 10^{-5}\ m^2$ and each has a mass of 2.09 kg.

The complete system will consist of 12.62 km of I-beam support rods having a total mass of 132,725 kg. The cables will have a total length of 35.7 km and a total mass of 5.233 kg. The total system therefore has a mass of 137,958 kg.

Rotating the mass driver requires that the tensions in the cables be varied continually so that the gravitational bending moment will be counteracted. This gives rise to the metal fatigue discussed previously.

This continuous adjustment necessitates the use of a computer.

The cables are threaded through teflon-coated holes at the tops of the support rods to minimize friction.

Tension in the cables is controlled by electromechanical actuators (linked to the computer by a feedback control system) which are installed on alternate outer rings.

Laser-beam sights will be used as an auxiliary system for detecting deviations in the mass driver's alignment.

5.7 MATERIALS

5.7.1 Space Environment Considerations

The mass driver will experience varying temperatures once the 400 km altitude is attained. These temperatures are determined by direct solar radiation, reflected solar radiation (albedo), and planetary radiation (Figure 5.8).

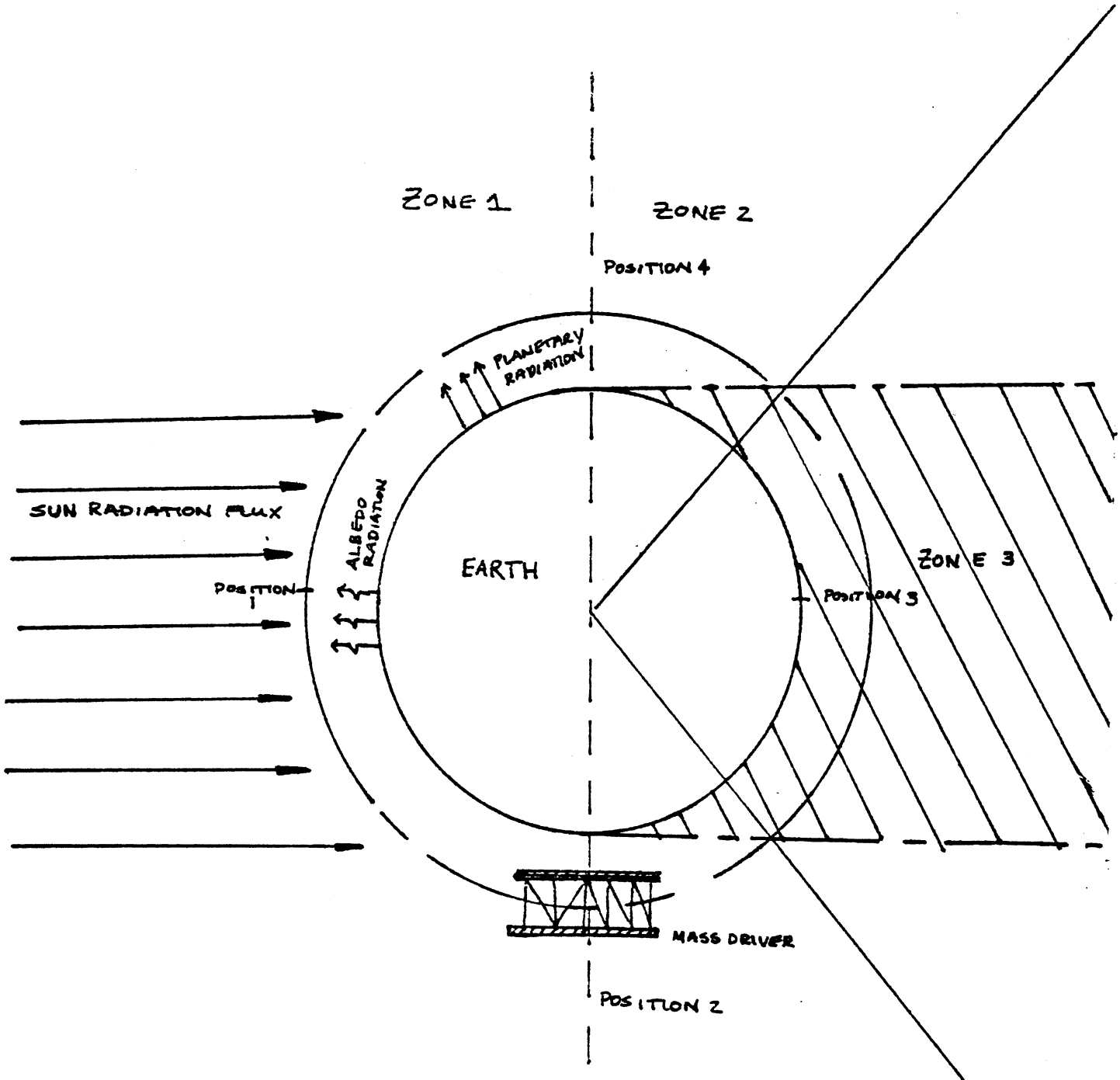

Figure 5.8 Radiation Zones
Zone 1. Solar, Albedo, Planetary
Zone 2. Solar, Planetary
Zone. Planetary

The solar radiation received depends upon the distance from the sun. The greater the distance, the smaller the radiation flux. This value is assumed approximately constant since the earth's orbit varies by only 3.4% during the year.

The reflected radiation, or albedo, is dependent upon the fraction of solar radiation which is reflected and backscattered from the clouds, atmosphere, earth's surface, and the moon. Since albedo varies continually according to the position of the moon and atmospheric conditions, an average albedo of .36 was used in the calculations (see Section 8 of the Appendix).

Planetary radiation depends upon the mass driver's altitude. The high the orbit, the lower the heat transfer to the mass driver caused by planetary radiation. If the orbital altitude remains nearly constant, the planetary radiation may be considered to be approximately constant also.

The combination of these three types of radiation determines the surface temperature of the mass driver. These surface temperatures were calculated for various points in the mass driver's orbit.

Stainless steel and aluminum were chosen for the construction of the mass driver because of their excellent strength, weight, and thermal characteristics.

5.7.2 Waste Containment Materials

Since transportation of the nuclear waste from processing plants to orbit consumes a significant amount of time, waste containment packages must resist corrosion to avoid radioactive contamination. The container must also have good strength and heat transfer properties. Accordingly, stainless steel 347 was selected as the material for the small cylindrical containers.

It may be necessary to incorporate an active cooling system to ensure package integrity during launch, though stainless steel's extremely high milting temperature is an advantage here.

5.7.3 Radiation Shielding

The thickness of the tungsten layer (which shields gamma radiation) and lithium hydride (neutron radiation) was determined from the graph in Figure 5.10 (which may be found in Reference 2). Accordingly, thicknesses of 12 cm and 5 cm for lithium hydride and tungsten respectively were chosen to ensure that a radiation level of 1 rem/hour at one meter from the package is not exceeded (see Figure 5.9).

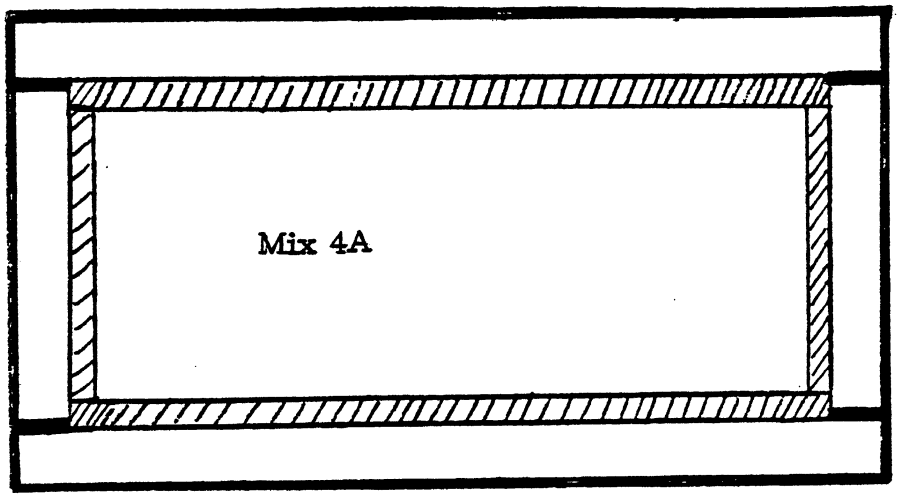

Figure 5.9 Nuclear Waste Containment Package

Stainless steel .5 cm (.2")

Tungstun .5 cm (2")

Lithium Hydride 12 cm (4.73")

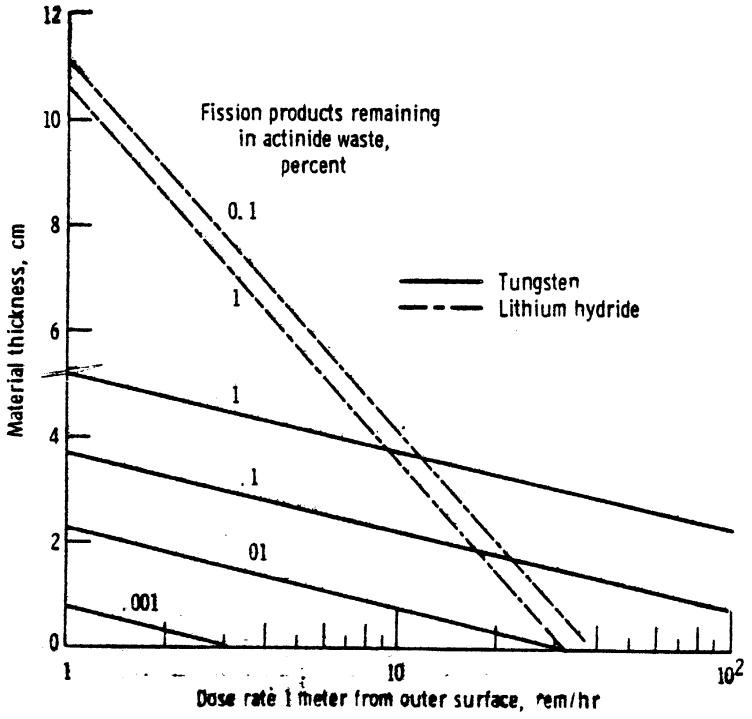

Figure 5.10 Thickness of Tungstun and Lithium Hydride Shielding Material Required to Reduce Radiation Dose Rate 1 Meter from Outer Surface.

5.8 STRUCTURAL EFFECTS OF FIRING FAILURES

Launch failures were investigated to determine the magnitudes of the resulting torques on the mass driver. There are two fundamental cases to consider:

1. one- or three-tube failure
2. adjacent-tube failure

Case 1:

When there is a one or three tube failure, a torque is developed about the y' or z' axes (Figure 5.12).

Case 2:

When adjacent tubes fail, torques are developed about the y' and z' axes (Figure 5.12).

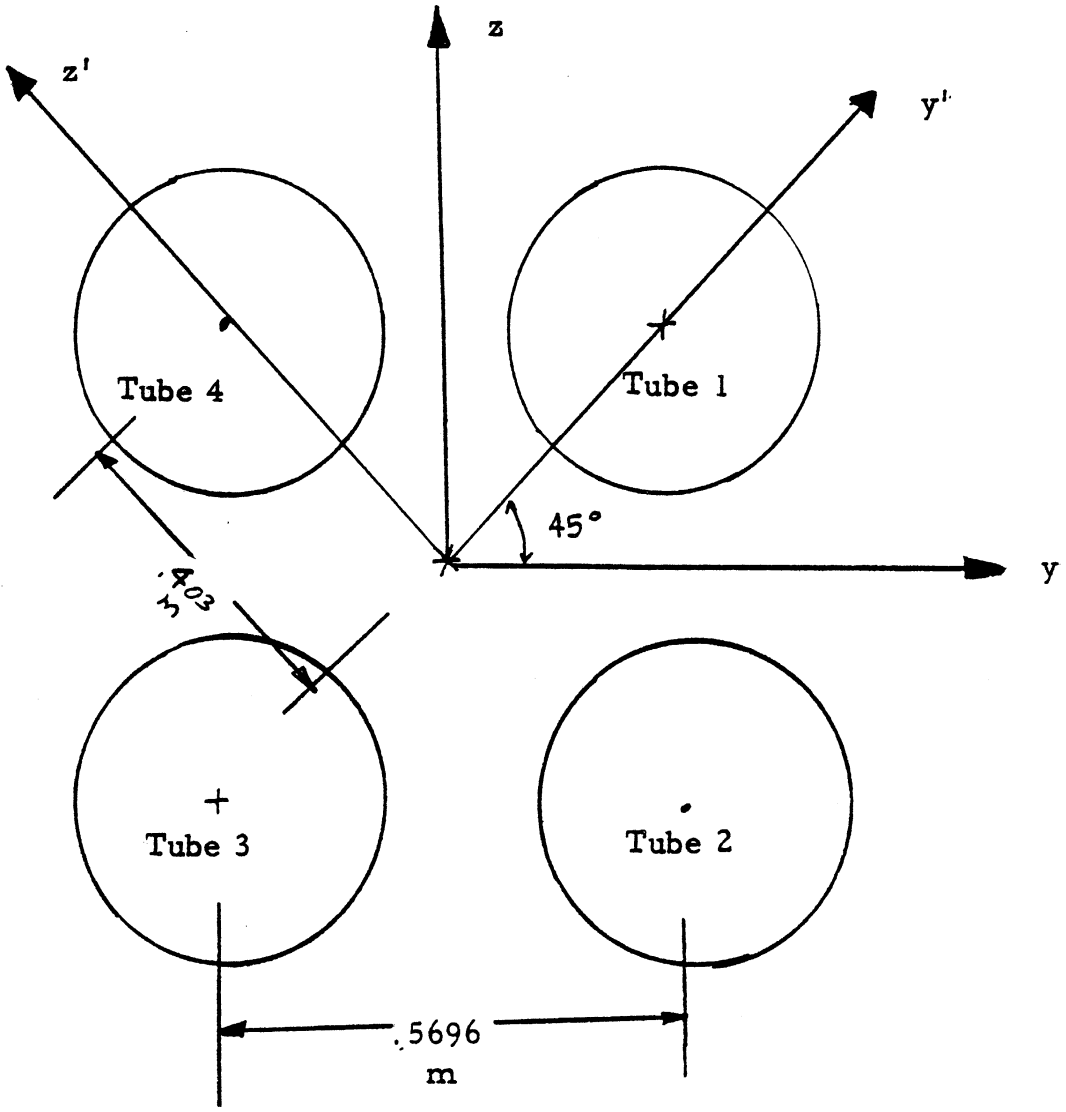

Figure 5.11 Mass Driver Cross Section

+ Force in

• Force out

✳ Mass Driver Cross Section

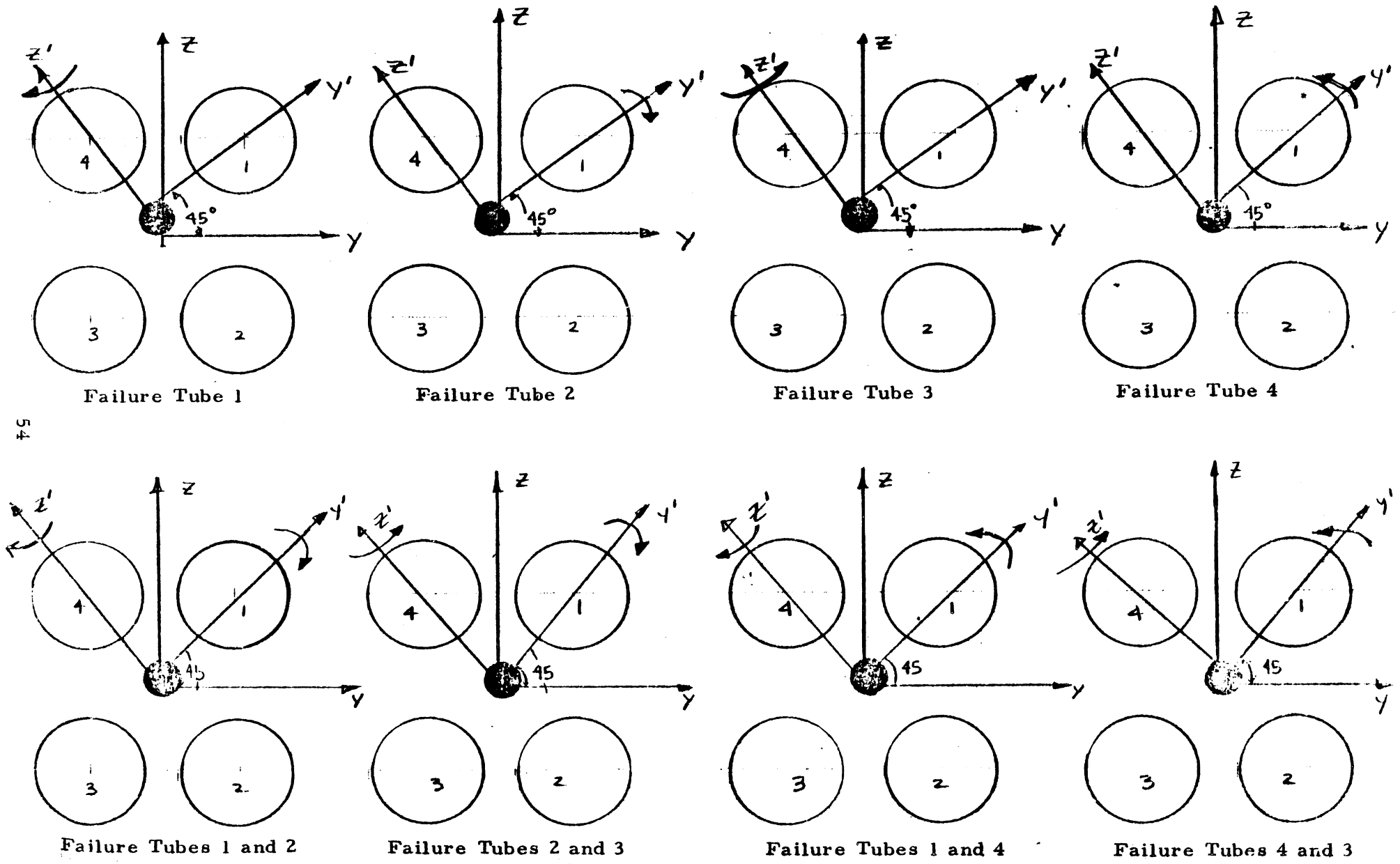

Figure 5.12 Torques Acting on Mass Driver Due to Launch Failure.

6
ATTITUDE CONTROL

6.1 INTRODUCTION

The primary objective of the attitude control system (ACS) is to maintain a suitable orientation in space for operation of the overall system. It is essential to closely monitor and actively control the mass driver due to instability in pitch due to the gravity gradient. It was figured that the mass driver would realign itself to vertical attitude from 0.1^{o} of the horizontal in 6 hrs. The proposed attitude control system incorporates a series of thrusters, evenly spaced along the length of the mass-driver. Attitude sensing is accomplished by a system of horizon sensors and rate gyros. Control is accomplished by a high-throughput digital control system. Pitch control laws were developed for maintaining longitudinal stability in the presence of the gravity gradient. Guidance laws were also developed for rotation of the mass driver from an initial vertical attitude (assumed by the mass-driver during construction operations) to the horizontal attitude for firing without exceeding structural limits.

6.2 DEFINITION OF AXES

It is useful to define three sets of reference coordinates to describe the motion of the mass-driver.

One coordinate system is an earth-centered system used to describe the orbital motion of the mass-driver in formulating the reboost problem.

Another system is a right-handed stability axis system with the +x-direction corresponding to the direction of motion in the circular orbit, and the +z-direction toward the center of the earth. This stability axis system was used to develop guidance and control laws.

A third system is a right-handed body-fixed system with the x-axis as the long axis of the mass driver. The pitch angle is defined as the angle between the stability x-axis and the body-fixed x-axis.

6.3 REQUIREMENTS

The ACS/guidance system requirements in pitch were based on the following considerations

1. Must be highly accurate,
2. Must take into account instability in pitch due to gravity gradient,

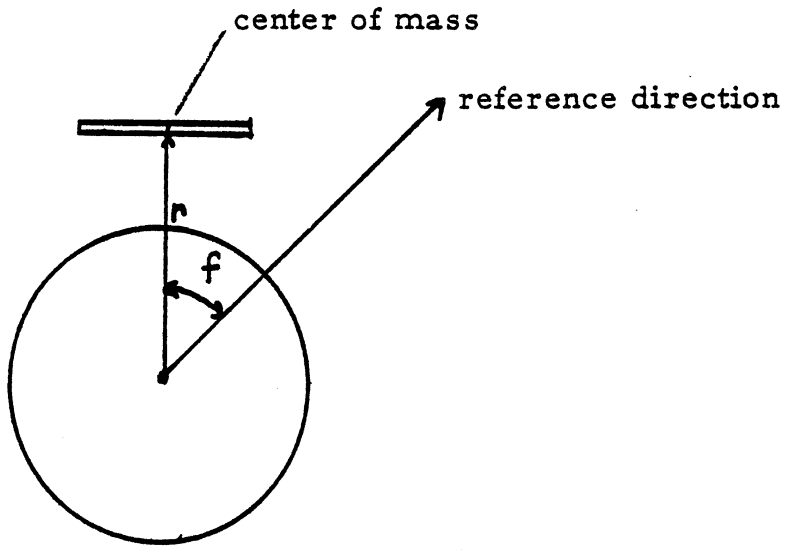

Earth Centered Axis System

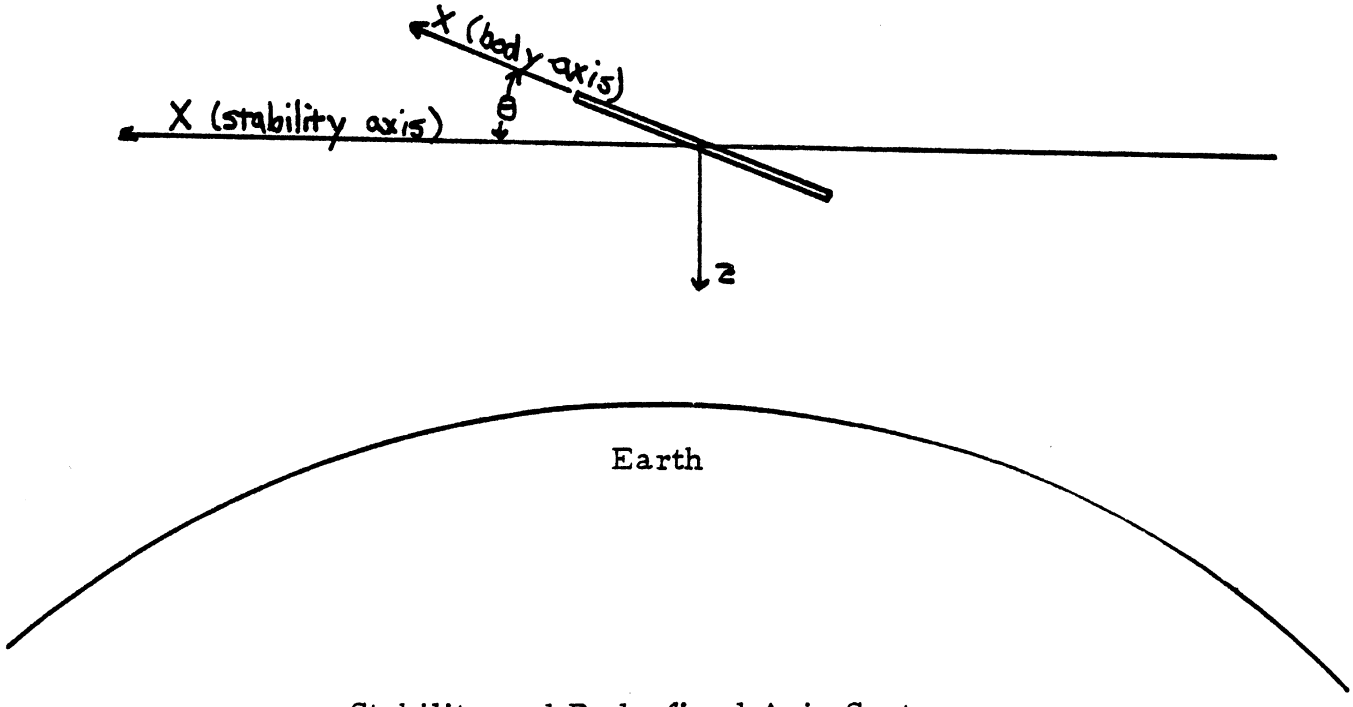

Stability and Body-fixed Axis Systems

Figure 6.1 Axis Systems

3. Must dampen to a tolerably small pitch displacement in a minimum amount of time,
4. Must not exceed structural limits,
5. Must possess a high degree of system reliability for maintaining steady operation and minimum of repair,
6. Must be capable of remaining on station in the desired orbit.

The following specifications were developed in accordance with the above guidelines:

1. Accuracy of alignment:

   $\theta = .1^{\circ}$ (pitch)
   $\psi = .1^{\circ}$ (yaw)

2. Dampens from a $\pm 10^{\circ}$ perturbation in θ to within $.1^{\circ}$ within 250 seconds.

3. Structural limits:

   $\dot{\theta}_{max} = .668^{\circ}/sec$
   $\ddot{\theta}_{max} = .25^{\circ}/sec^2$ similar requirements in yaw

4. Meantime between failures (MTBF) per thruster assumed to be 10 years in accordance with present reliability capability.

6.4 REBOOST PROBLEM FORMULATION

The Project NEWDUMP vehicle is subject to orbit decay due primarily to aerodynamic drag. This drag results in a change of altitude for orbit given by:

$$\Delta h = -2\pi\left(\frac{C_D A}{w}\right) g_o \rho r^2$$

where

C_D = drag coefficient = 2 for
A = frontal area = n/m^2
w = vehicle weight = $\sim 2 \times 10^6$ kg
ρ = density = 4.67×10^{-15} kg/m^3
r = orbit radius = 6775 km

The result is an altitude loss on the order of .07 meters per day, or a 1 km drop in 37 years, approximately.

The most convenient way to counteract this force is to occasionally re-boost the satellite by accelerating more reaction mass from the aft-facing mass-driver than waste payload from the foreward-facing mass-drivers, resulting in a net positive thrust. The ΔV produced in this manner is found from the mass driver group report.

Even though the atmospheric density is a function of solar activity. The orbit decay problem is not especially critical. The orbit altitude can simply be monitored so that when it falls to a certain level a ΔV will be applied to raise the vehicle to a higher orbit. To avoid transferring the vehicle into an elliptical orbit, if part of the required ΔV is applied when the mass-drivers fire payload, then a similar ΔV must be applied 180^{o} past this point to re-circularize the orbit.

As an example, if the orbit is allowed to decay 1 km a re-boost ΔV of .6 m/sec will be required (Hohman transfer). This can be accomplished by accelerating an additional 40 kg of reaction mass from the aft-facing mass drivers every orbit for 7 orbits.

6.5 PITCH DYNAMICS AND CONTROL SYSTEM

6.5.1 Assumptions

Since the attitude displacement θ was defined with respect to the local horizontal (Figure 6.1) the frame of reference will be noninertial and must reflect the constant angular rate due to the motion in the circular orbit (Figure 6.2). The mass driver will rotate with a steady-state pitch rate Q_o, where

$$Q_o = \frac{2\pi}{T_o} \quad , \quad T_o \equiv \text{orbital period (92 min)} = .065\ ^{o}/\text{sec.} \qquad (6.1)$$

For the attitude control design, this angular rate is assumed negligible. The ACS provides for maintenance of $\theta = 0$ along the flight path due to the use of horizon sensors, providing a direct measure of θ locally.

There are four kinds of forces acting on the satellite: magnetic, radiation, aerodynamic, and gravitational.

Magnetic effect are assumed to be negligible over 'long' time periods ($\gtrsim$ 1 min). Magnetic disturbances will arise due to the local, but powerful magnetic field generated by the mass-driver coils. Since these magnetic disturbances are of short duration ($\sim$ 3 sec) they can be neglected as a biasing torque and treated stochastically.

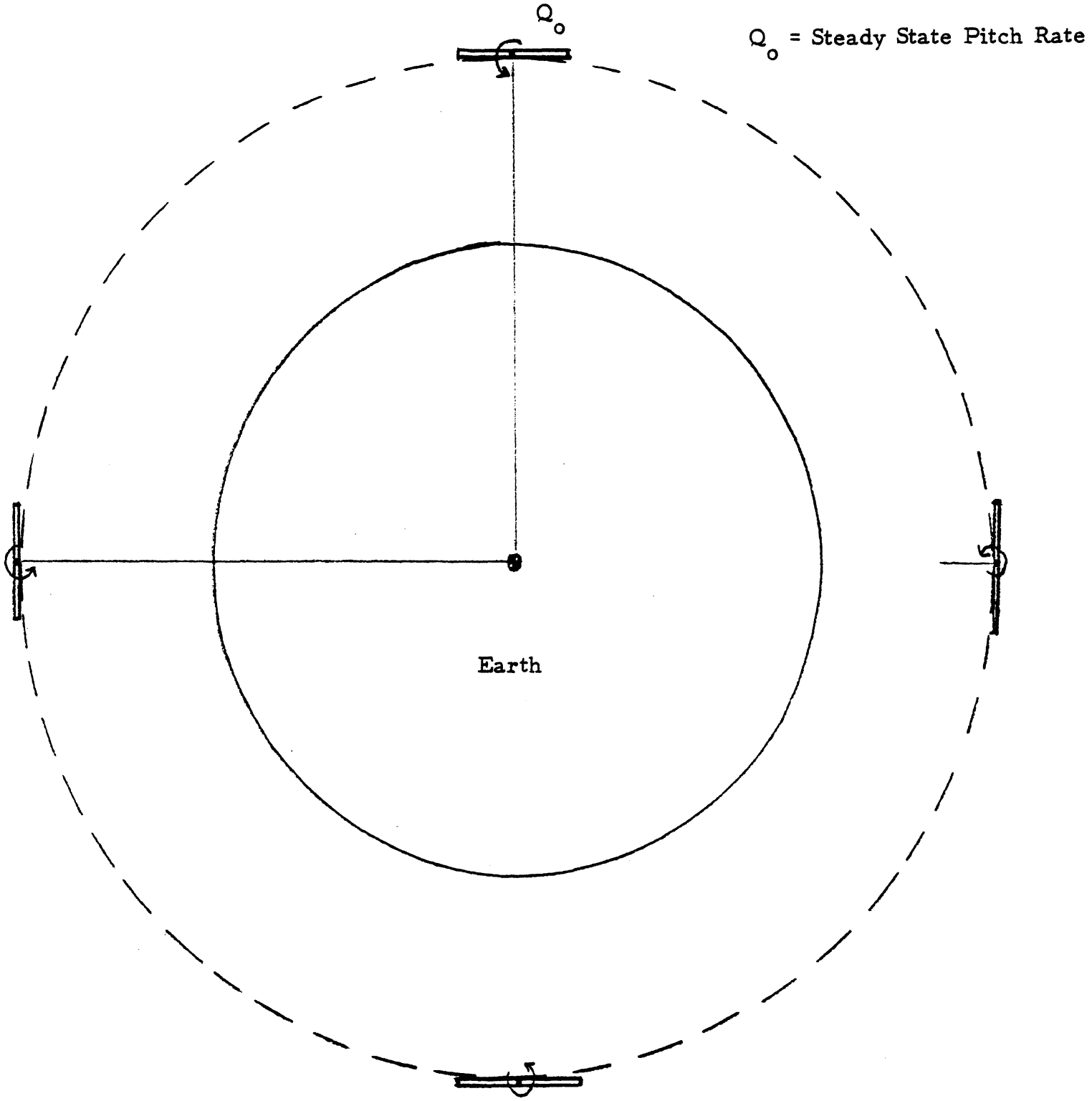

Figure 6.2 Steady-State Mass-Driver Motion.

Due to the small frontal area and high altitude (400 km) aerodynamic forces can be neglected relative to the gravity gradient moment.

Solar radiation pressure on the solar panels can be neglected since the panels are distributed symmetrically with respect to the center of mass of the mass driver, giving a center of radiation pressure coincident with the center of mass (i. e. no moment arm).

The fourth force, gravity gradient is modeled as a perturbing torque due to its large magnitude (19,200,000 nm at 45^{o} pitch attitude).

The mass driver is assumed sufficiently straight allowing the products of inertia to be considered negligible, with respect to the principal moments of inertia. This follows from the structures requirement that the mass driver be maintained straight for acceptable bucket clearances during firing. This also allows the longitudinal mode to be uncoupled from the lateral and directional modes, resulting in a simple, rigid-body model.

6.5.2 Equation of Motion

The rigid-body assumption allows the pitch dynamics to be modeled as in Equation 6.2:

$$I_{yy} \ddot{\theta} = M_c + M_{gg} + M_d \qquad (6.2$$

where

I_{yy} = y-principal moment of inertia
M_c = moment commanded by thruster firing (control moment)
M_{gg} = gravity gradient moment
M_d = disturbing torques.

The gravity gradient moment, assuming a high structural fineness ratio and constant longitudinal mass distribution is:

$$M_{gg} = \frac{1}{8} \frac{\mu}{r_c} m \left(\frac{\ell}{r_c}\right)^2 \sin 2\theta = k \sin 2\theta. \qquad (6.3$$

where

$\mu \equiv$ gravitational constant for earth
$r_c \equiv$ orbital radius
$m \equiv$ mass of mass-driver
$\ell \equiv$ mass driver length

$\therefore$ Equation (6.2) becomes.

$$I_{yy} \ddot{\theta} = M_c + k \sin 2\theta + M_d \qquad (6.4)$$

6.5.3 Maximum Required Control Moment

The control moment must be large enough so that the maximum gravity gradient moment can be overcome. This requirement follows from the need to attain a horizontal attitude when initially aligned vertically. The max moment will occur at $\theta = \pm 45^{o}$ and is found to be:

$$M_{c_{max}} = k = 19,200,000 \text{ N. M.} \tag{6.5}$$

6.5.4 Perturbation Equations of Motion

Lower case of θ was used in the above since the trim value of pitch attitude is 0^{o}. Since θ is taken to be sufficiently small ($|\theta| \leq 10^{o}$), the sine term is approximately proportional to the argument, yielding the equation:

$$I_{yy}\ddot{\theta} - 2k\theta = M_{cs} + M_{cmd} = M_{c} \tag{6.6}$$

where

M_{cs} = contribution to moment due to control system
M_{cmd} = contribution to control moment due to attitude command.

The equation may be written in state-matrix form as (letting $q \equiv \theta$):

$$\dot{q} = \frac{2k}{I_{yy}}\theta + \frac{1}{I_{yy}}M_{cs} + \frac{1}{I_{yy}}M_{cmd} + \frac{1}{I_{yy}}M_{d}$$

$$\dot{\theta} = q$$

This allows the dynamics to be stated in the following state form:

$$\dot{\bar{x}} = A\bar{x} + B\bar{u} + B\bar{u}_{cmd} + C\bar{w} \tag{6.8}$$

where

$$A = \begin{bmatrix} 0 & \frac{2k}{I_{yy}} \\ 1 & 0 \end{bmatrix} \quad ; \quad B = \begin{bmatrix} \frac{1}{I_{yy}} \\ 0 \end{bmatrix} \tag{6.9}$$

$$C = \begin{bmatrix} \frac{1}{I_{yy}} \\ 0 \end{bmatrix} \qquad \bar{x} = \begin{bmatrix} \dot{\theta} \\ \theta \end{bmatrix} \qquad \bar{u} = M_{cs}$$

$$\bar{u}_{cmd} = M_{cmd} \qquad \bar{w} = M_{d}.$$

It can easily be ascertained that the dynamic system (6.7) is completely controllable via the control moment M_{cs}.

6.5.5 Natural Dynamic Characteristics

To obtain the roots of the natural motion, the characteristic equation of the perturbation equation must be solved. This involves finding the eigenvalues for the matrix

$$A = \begin{bmatrix} 0 & a^2 \\ 1 & 0 \end{bmatrix} \tag{6.10}$$

This gives the characteristic equation,

$$s^2 - a^2 = 0 \tag{6.11}$$

with natural roots

$$s = \pm a$$

This represents an exponential growth of time constant

$$\tau = \frac{T_o}{2\pi\sqrt{3}} \tag{6.12}$$

For an orbital period of 92 min, this gives a time constant (time to increase amplitude by a factor of e) of 8.45 min. From the time constant, it can be estimated that from a $.-1^o$ misalignment from the horizontal, it will take approximately 2 hr to achieve vertical attitude orientation.

6.5.6 Control Law Synthesis

An optimal control law was developed for attaining a damping to a minimal attitude perturbation in a minimal amount of time. The controller gains follow from the solution K of the algebraic matrix Riccati equation:

$$2 + KA + A^T K - KBR^{-1} B^T K = 0 \tag{6.13}$$

where

$$K = \begin{bmatrix} K_1 & K_2 \\ K_2 & K_3 \end{bmatrix}$$

and A, B are the state and control matrices defined previously. R is a $|x|$ control weighting matrix set equal to 1. Q is a diagonal weighting matrix penalizing large excursions in q^2, θ^2.

Solution of the Riccati equation gives a control law minimizing the ≠cost≠ functional:

$$J = \int_0^\infty \bar{x}^T 2\bar{x} + \bar{u}^T R\bar{u}\ dt \qquad (6.14)$$

$$2 = \begin{bmatrix} 2_1 & 0 \\ 0 & 2_2 \end{bmatrix} \qquad R = 1$$

The controller gains are computed from the Riccati matrix K by:

$$G = R^{-1} B^T K. \qquad (6.15)$$

$$G = [g_1\ g_2]$$

where, g_1 ≡ pitch rate feedback to moment command (rate gyro)
g_2 = pitch attitude feedback to moment command (horizon sensors)
(Figure 6.3).

Solution of the optimal regulator problem gives the following relations.

$$w_n = \sqrt{b^2 K_2 - a^2} \qquad K_2 = \frac{a^2}{b^2} + \sqrt{\left(\frac{a^2}{b^2}\right)^2 + \frac{2_2}{b}} \qquad (6.16)$$

$$\zeta = \frac{1}{2} b \frac{\sqrt{2_1 + 2K_2}}{\sqrt{b^2 K_2 - a^2}} \qquad K_2 > \frac{a^2}{b^2} \quad w_n > 0$$

$$K_1 = \frac{1}{b}\sqrt{2_1 + 2K_2} \qquad K_1 > \frac{a}{b^2} > 0$$

$$g_1 = -bK_1 = -\sqrt{2_1 + 2K_2}$$

$$g_2 = -bK_2$$

where w_n, ζ are the desired natural frequency and damping ratio, respectively, of the attitude controlled mass driver.

Critical damping ($\zeta = 1$) is desired since it allows for faster damping compared with overdamped modes and allows no overshoot (maintaining small $\dot{2}$ at all times).

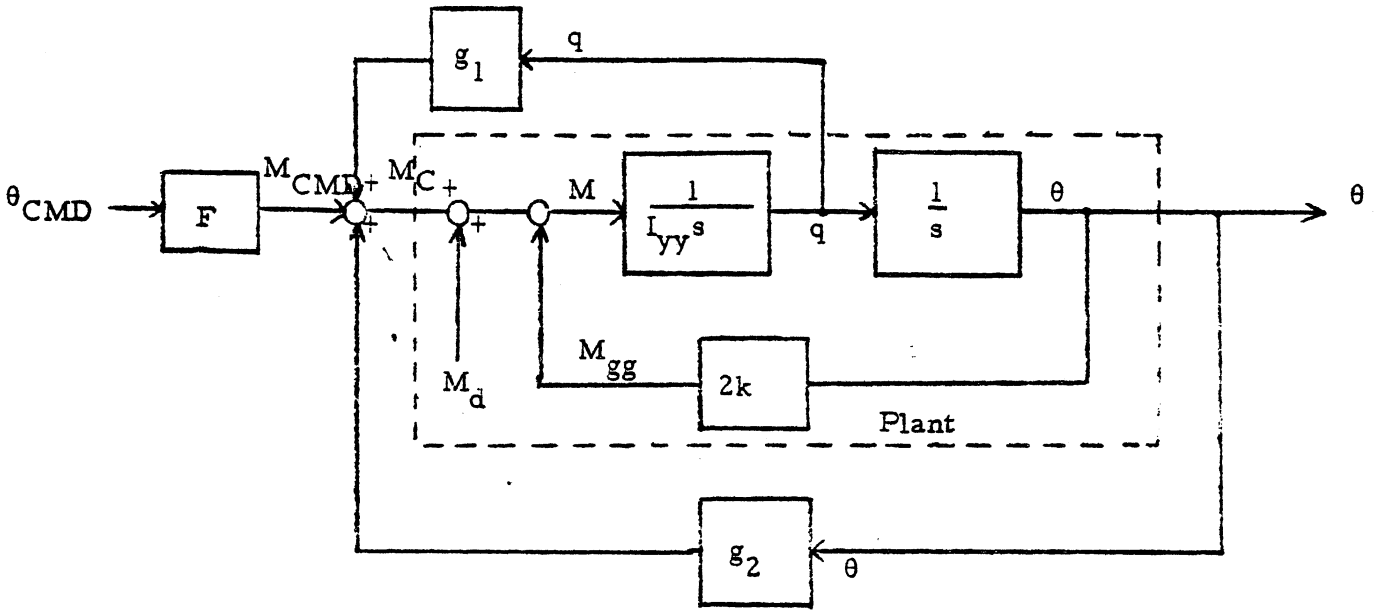

k = 19,200,000 N. M.
I_{yy} = 1.60 x 10^9 kg. m^2
g_1 = -5.17 x 10^9 N. M. / $\frac{deg}{min}$
g_2 = -4.199 x 10^9 N. M/deg
F = 2.23 x 10^7 kg. m^2/rad min^2

Figure 6.3 Control System Block Diagram

By specifying the time to damp from $\theta = 10^{o}$ to $\theta = .10$ as initially 0, w_n can be found. This time was chosen to be 250 sec where

$$M_{cmd} = F\,\theta_{cmd} \tag{6.21}$$

where F can be found by expanding the matrix A + BG:

$$F = \frac{a^2 + b\,g_2}{b} \tag{6.22}$$

F was computed to be 108.0 nm/deg.

This gives the following state/controller description of the system

$$\begin{bmatrix} q' \\ \theta' \end{bmatrix} = \begin{bmatrix} b\,g_1 & a^2 + b\,g_2 \\ 1 & 0 \end{bmatrix} \begin{bmatrix} 9 \\ 0 \end{bmatrix} + \begin{bmatrix} F \\ 0 \end{bmatrix} \theta_{cmd}$$

This description is realized in Figure 6.3.

6.6 GUIDANCE

6.6.1 Introduction

During construction the mass driver is oriented vertically with respect to the horizon. The stability of this orientation is maintained by the gravity gradient effect. The mass driver must be oriented to a horizontal attitude after construction is completed.

The mass driver must be aligned without exceeding allowable pitch rates and accelerations specified by the structural limits. The maximum allowable pitch rate was given as $.668^{o}$/sec. The maximum angular acceleration was harder to discern with the conservative figure of $.1^{o}/sec^2$ decided upon.

In order to maneuver the mass driver within these constraints, feedback guidance laws were developed. Implementing guidance laws requires a separate guidance computer, operating in conjunction with the back-up attitude control processor. The guidance computer/back-up ACS is responsible for acquiring horizontal attitude and maintaining dynamic stability until the mass driver is within 10^{o} of horizontal attitude where the primary ACS horizon sensors acquire the horizon. Control is then transferred to the primary ACS, which trims the mass driver to horizontal attitude.

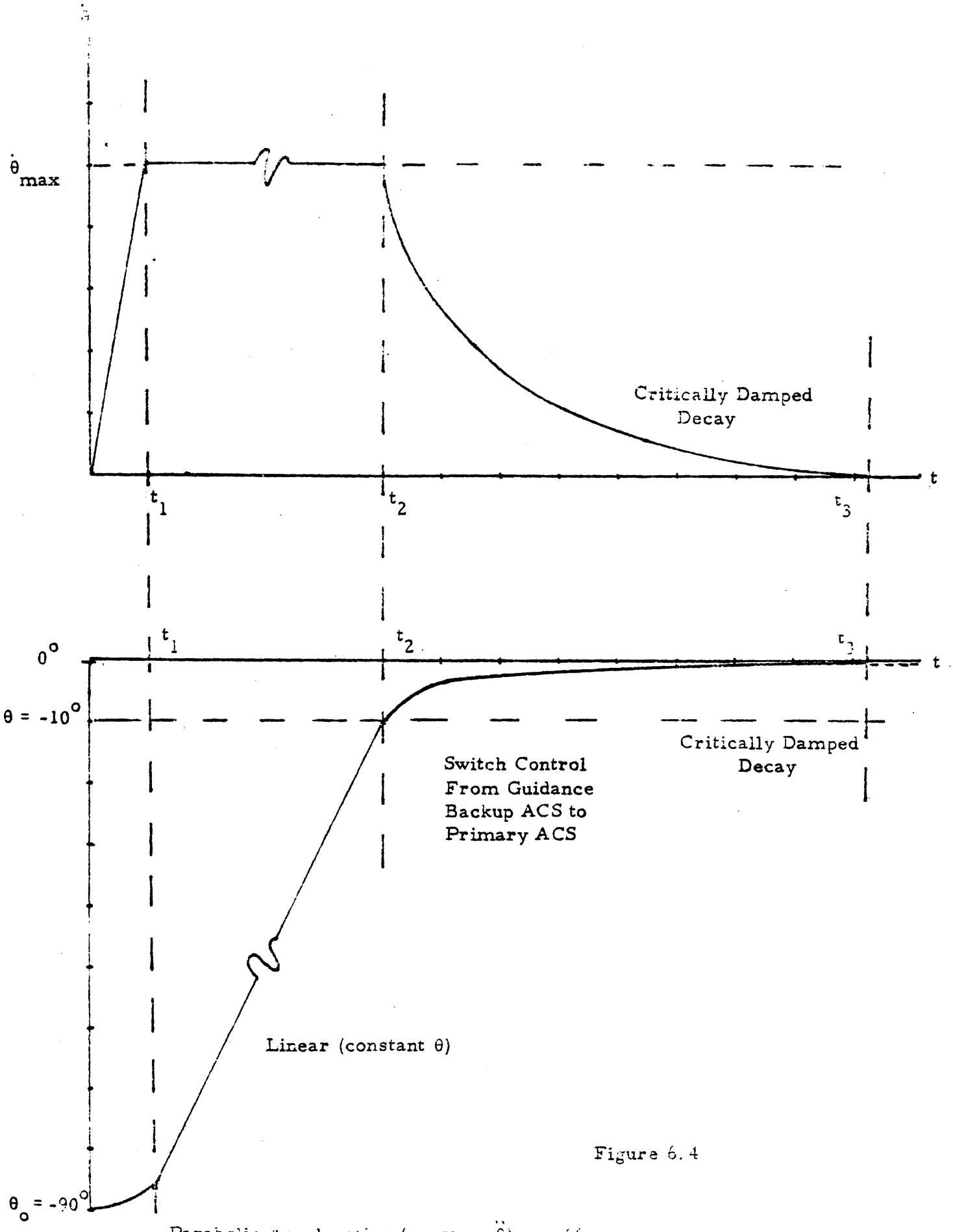

Figure 6.4

Parabolic Acceleration (constant $\ddot{\theta}$)

	t (SEC)	θ (°)	$\dot{\theta}$ (°/SEC)	$\ddot{\theta}$ (°/SEC²)	t_{TOTAL} (SEC)
t_0	0	90°	.5	.1	0
t_1	5	88.75°	.5	0	5
t_2	162.5	10°	.5	0	167.5
t_3	42.1	.1°	.001	$\leq$ .01	209.6

Table 6.5

6.6.2 Feedback Guidance Laws for Initial Orientation Maneuver

The guidance mode chosen was to implement a constant angular acceleration guidance until a pitch rate of .5°/sec was attained. The guidance computer then switches to a constant pitch rate guidance mode to limit the pitch rate to below the structural limit. When the attitude reaches the interval $-10^{\circ} < \theta < 10^{\circ}$, attitude control is transferred from the guidance/backup ACS to the primary ACS.

Referring to Figure 6.4, the guidance is initially scheduled for a constant pitch acceleration of $.1^{\circ}/sec^2$. At time t_1 when a pitch rate of $.5^{\circ}$/sec is realized the guidance switches to a constant pitch rate control of $.5^{\circ}$/sec and maintained until the pitch attitude is 10° at t_2 where control is transferred from the guidance/backup ACS system to the primary ACS. The mass driver is then critically damped to an attitude of $.1^{\circ}$, the resolution limit of the horizon sensors.

The feedback guidance laws, corresponding to the appropriate time intervals are:

$$[t_o, t_1) \text{ ; constant } \ddot{\Theta}: \quad M_{cmd} = -k \sin 2\Theta + I_{yy}\ddot{\Theta}_o$$

where $\ddot{\Theta}_o = .1^{\circ}/sec^2$ and

$$[t_1, t_2) \text{; constant } \dot{\Theta}: \quad M_{cmd} = -k \sin 2\Theta.$$

From the feedback guidance laws, the vehicle states at the critical times t_o, t_1, etc are given in Table 5.

6.7 ATTITUDE SENSING

The attitude sensing system is a highly accurate system that incorporates two Horizon Edge Trackers (HET) and six rate gyros. The HET's generate pitch data in the range of pitch angles from $\theta = \pm 10^{\circ}$. This is the range wherein the output remains linear. Each HET has three heads to have a three-edge tracking field of view. The HET's are mounted on the ends of the mass driver. Roll, pitch, and yaw rates and displacement data are generated from a system of six rate gyros mounted on the crew station at the center of the mass driver. The sensor specifications can be assumed to be as accurate or more accurate than those listed below.

Horizon Edge Trackers

Accuracy: with $.1^{\circ}$ Full scale: $\pm 10^{\circ}$
Output: pulse amplitude modulated (PAM)
Converter: pulse amplitude modulated (digital)
Number: 2 sensors (3 head per sensor)

Rate Gyros

Accuracy:	within .01°/sec	Full scale:	6°/sec - 1200°/sec
Output:	analog		
Converter:	analog/digital		
Number:	six		

6.8 FLIGHT COMPUTER

6.8.1 Processor Requirements

Hardware architecture requirements are difficult to quantity, requiring knowledge of the number of sensors and control devices, stability margins of the flight control system, control processes to be implemented, and the complexity of the guidance and control laws. From these considerations, a set of specifications were developed:

1) The processor arrangement must allow for a high throughput in a minimum amount of time. This requirement follows from the need to control a large number of thrusters and from the large volume of data from the structural mode control (SMC) sensors.

2) The architecture must reflect the different control functions to be realized and the associated complexity of the models implmented in the software. This architecture must not affect substantially the high throughput and minimum time specification above.

6.8.2 Hardware Architecture

The requirements above were realized in the diagram in Figure 6.6. Data for attitude control is converted into digital form from the horizon sensors and the rate gyros. For the horizon sensors, since the output is in the form of a pulse-amplitude modulated (PAM) signal, PAM/digital converters are required. The output from the rate gyros is in analog form and requires appropriate A/D converters.

Two computers are used for attitude control. First is the primary ACS processor, which utilizes horizon sensor and rate gyro information for state estimation. The ACS, from the control laws program residing in the read-only-memory (ROM) computer the required roll, yaw, and pitching moment commands. Due to the complexity of such computations, a random access ('scratchpad') memory (RAM) is used to store intermediate results of calculations. The RAM is also used to store input data before processing.

The backup ACS is used to provide stability during the initial rotational maneuver from vertical attitude to horizontal attitude, and is driven by the guidance processor. It also serves as the backup to the primary ACS during normal operation. Since the horizon sensors become ineffective at large pitch attitudes and since their linearity range in pitch is $\pm 10^{o}$, the backup ACS estimates θ from the rate gyros. Associated RAM's and ROM's are implicit in Figure 6.6 for the backup ACS, guidance, SMC and input/output processors.

Since the rate gyros are skewed for high reliability, the ACS processors decode the measured angular rates into the appropriate roll, yaw and pitch components.

Data busing is used to provide a pipeline for data from the sensors to the processors, from processor to processor, and to the output device drivers. Data busing is necessary due to the large number of sensors and actuators and from the need for high reliability.

Since large numbers of thrusters need to be controlled and due to the need for reducing computational time delays, separate output processors are used to drive the roll, yaw and pitch thrusters. Individual thruster thrusts are gain-scheduled as shown in Figure 6.8. The thrustor valve drivers are disabled for unused backup thrusters or for inoperational thrusters. This function may be performed by either a self-test monitoring processor or by the flight crew. The gain schedules are stored in the ROM's with thruster enable/disable commands stored in the associated RAM's. Since speed is desired, most output processor functions are hardwired.

6.8.3 Structural Mode Control Processor

Since the mass driver is subject to thermal loads and has a low elasticity associated with a high slenderness ratio ($\ell / d \geq 1000$), active stabilization is used to maintain structural rigidity and to dampen structural vibration.

The control laws may be formulated as a regulator problem, using deflections and slopes of segments along the mass-driver as state variables. Due to the complexity of the problem, including the large number of states and the dynamics of each segment, these control laws were not formulated and are treated as a key item for further development.

Displacements are measured via accelerometers and slopes by rate integrating gyroscopes placed at equal lengths along the mass-driver. Due to the large number of sensors required, an input processor is necessary for computing the slopes and deflections from sensor data. The input processor receives structural sensor data and attitude data for computing the difference in deflection and slope perturbations from the desired rigid-body slopes and deflections.

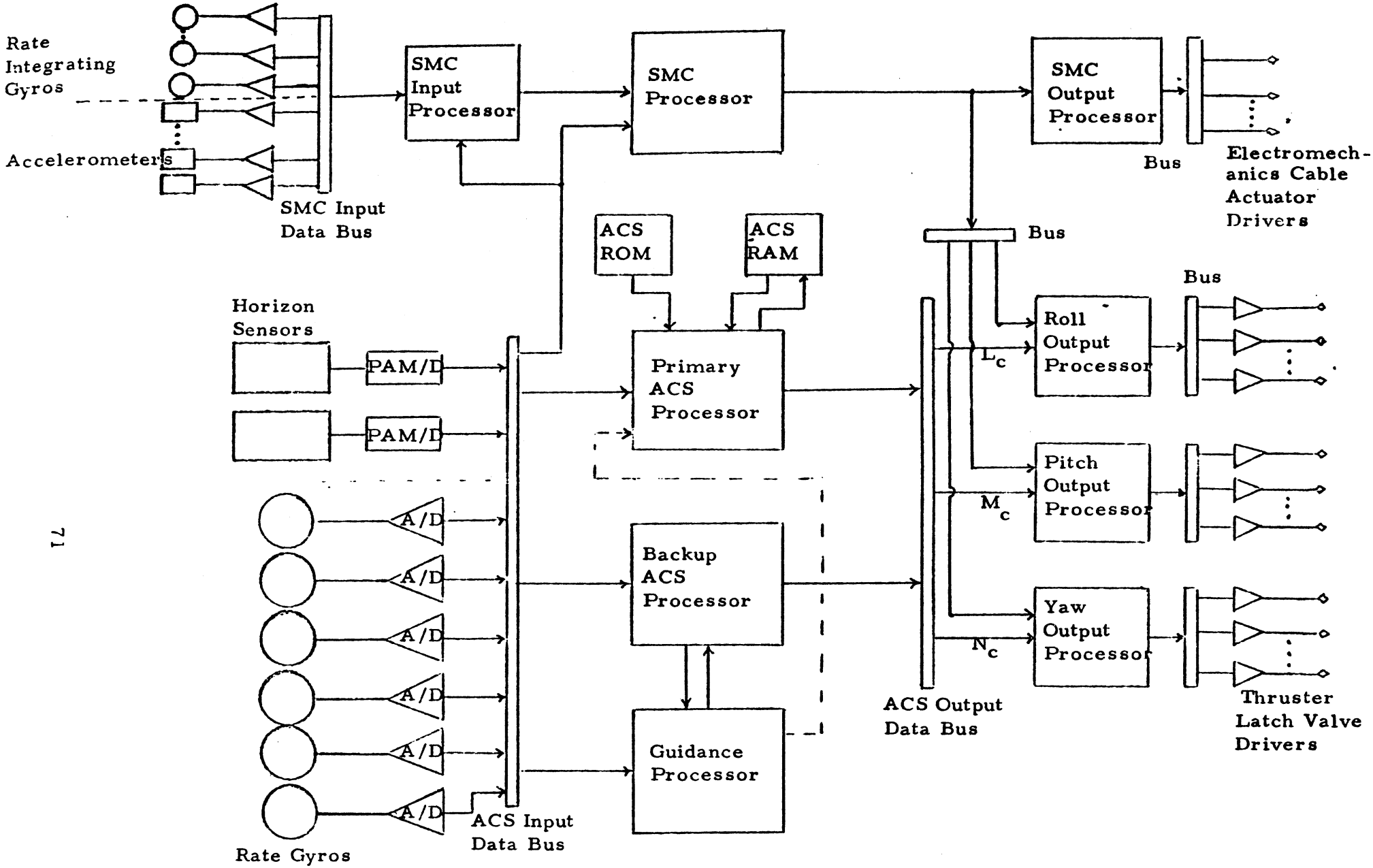

Figure 6.6 ACS/SMC Hardware Architecture

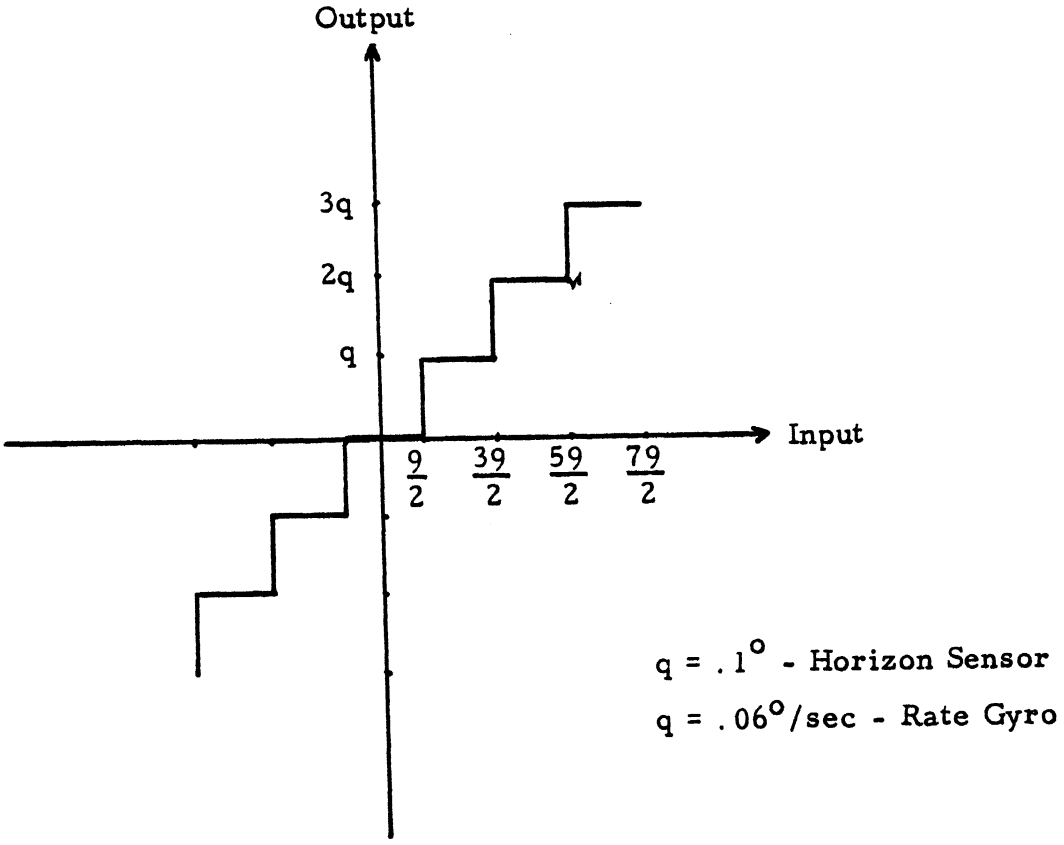

A/D Converter - Quantizer

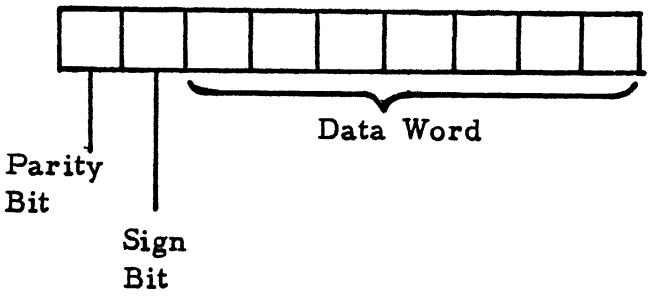

ACP Computer Word

Figure 6.7 Attitude Control Processor (ACP) Word Length

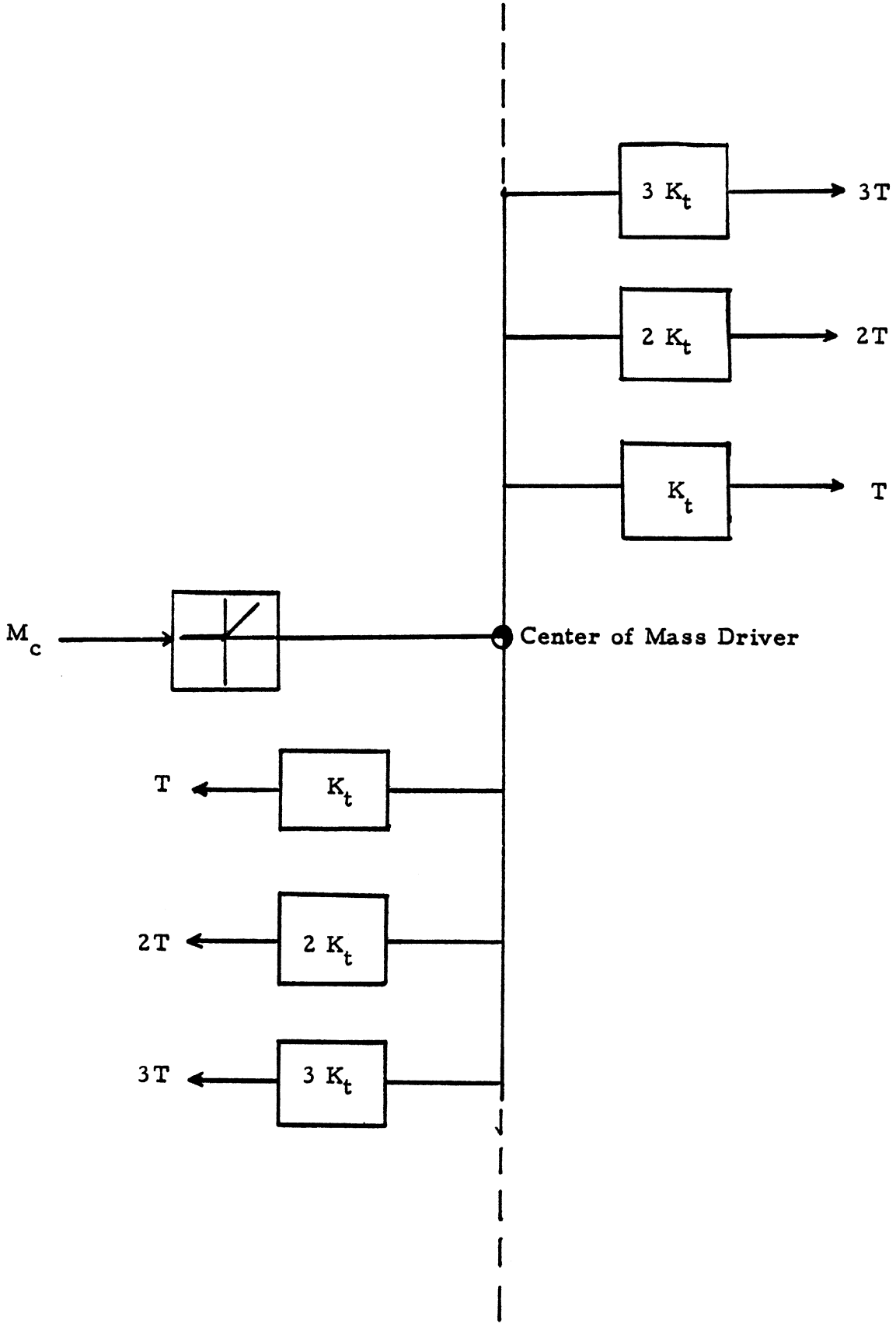

Figure 6.8 Pitch Thruster Scheduling + θ Thruster Control

The structural mode control processor then computes the static commands which are transmitted to the SMC output processor and the dynamic commands, transmitted to the ACS output processors.

To maintain alignment in the presence of thermal stresses, a network of cables, controlled by electromechanical actuators is used to maintain static alignment.

For damping structural vibrations, the ACS thrusters are used since they allow greater control power and give a faster response.

Structural static commands are converted into the appropriate electromechanical actuator commands by the SMC output processor. Structural dynamic commands are thrust commands which are added to the appropriate rigid-body thrust commands to permit rigid body maneuvers and structural damping to be initiated simultaneously.

6.9 THRUSTER SIZING

6.9.1 Design Approach

Given the thruster layout shown in Figure 6.11, the individual thrust supplied by each thruster is then obtained.

Ideally, it is desirable to have a linear distribution of thrust along the length of the mass driver (Figure 6.9) when rotating the mass driver. The linear distribution results in a zero shear force distribution along the mass-driver. In practice, since there are a finite number of thrusters with finite thrust, the actual distribution can better be modeled with a linear distribution of impulse thrusts along the mass-driver (Figure 6.10).

6.9.2 Thruster Placement

Thruster placement, ΔX, was found from the following considerations.

1. Placement on the outer collars connecting the mass-driver tubes for good structural support.

2. Providing a sufficiently wide spacing between thruster quads in order to reduce the number of thrusters required for acceptable reliability.

3. Maintaining sufficiently close separation between thruster quads for prevention of structural mode excitation during attitude maneuvers.

From these considerations, a thruster separation of $\Delta X = 30.24$ m was chosen from the approach that ΔX should be minimized as much as reliability will permit. Thruster quads would actually be placed every 10.08 m, giving triple modular redundancy to the attitude control system. Assuming a mean time between failures (MTBF) per individual thruster of 10 yrs, an MTBF for the entire system was computed to be 108 days. System reliability can be improved further by modular construction of the ACS thruster assemblies for case of replacement and active repair practices by the flight crew.

The thruster arrangement per collar was developed with the purpose of surviving two failures in + pitch, - pitch, + yaw, etc and still being operative, yet maintaining a minimum of thrusters. The thruster arrangement is given in Figure 6.11).

6.9.3 Thruster Sizing

The thrusters are sized for having idential thrusts for translational maneuvers. Thus, since the end thrust is the maximum thrust, the thrust of the end thrusters at maximum pitching moment $M_{c_{max}}$, gives the required thrust of each thruster.

There are two possibilities for sizing the thrust at maximum moment. First is the use of four thrusters at maximum gravity gradient moment ($\theta = \pm 45^{o}$) for basing thrust calculations. Second is the use of the primary pitch ACS thruster at maximum θ for the primary ACS ($\theta = \pm 10^{o}$). The second criterion proved the more conservative, requiring a higher moment per thruster.

The moment supplied by the thrust distribution p(x) is given by

$$M_c(P) = \int_{-\frac{1}{2}}^{\frac{1}{2}} x\, p(x)\, dx$$

where $p(x) = P\frac{x}{\ell}$.

Evaluating the integral ( ) gives M_c to be

$$M_c(P) = \frac{P\ell^2}{12} .$$

The thrust of the end thruster, T_e is related to the moment M_c and the spacing between thruster, ΔX, by

$$M_c(T) \cong \frac{T_e}{\Delta X} \quad \frac{\ell^2}{12}$$

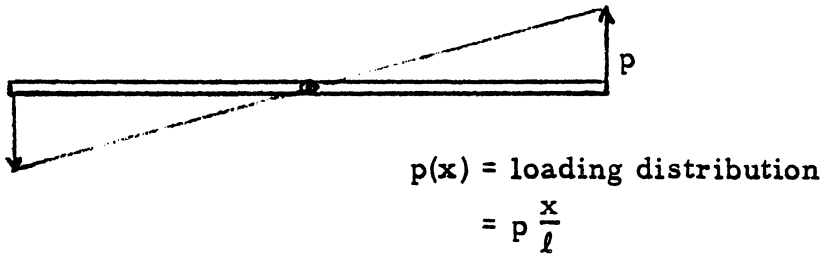

Figure 6.9 Linear Loading Distribution

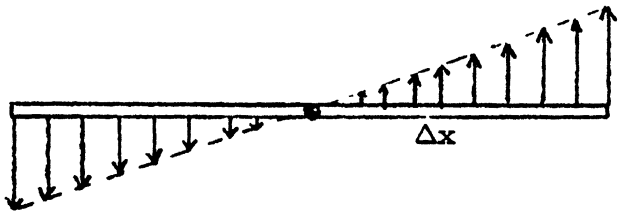

Figure 6.10 Impulse Loading Distribution

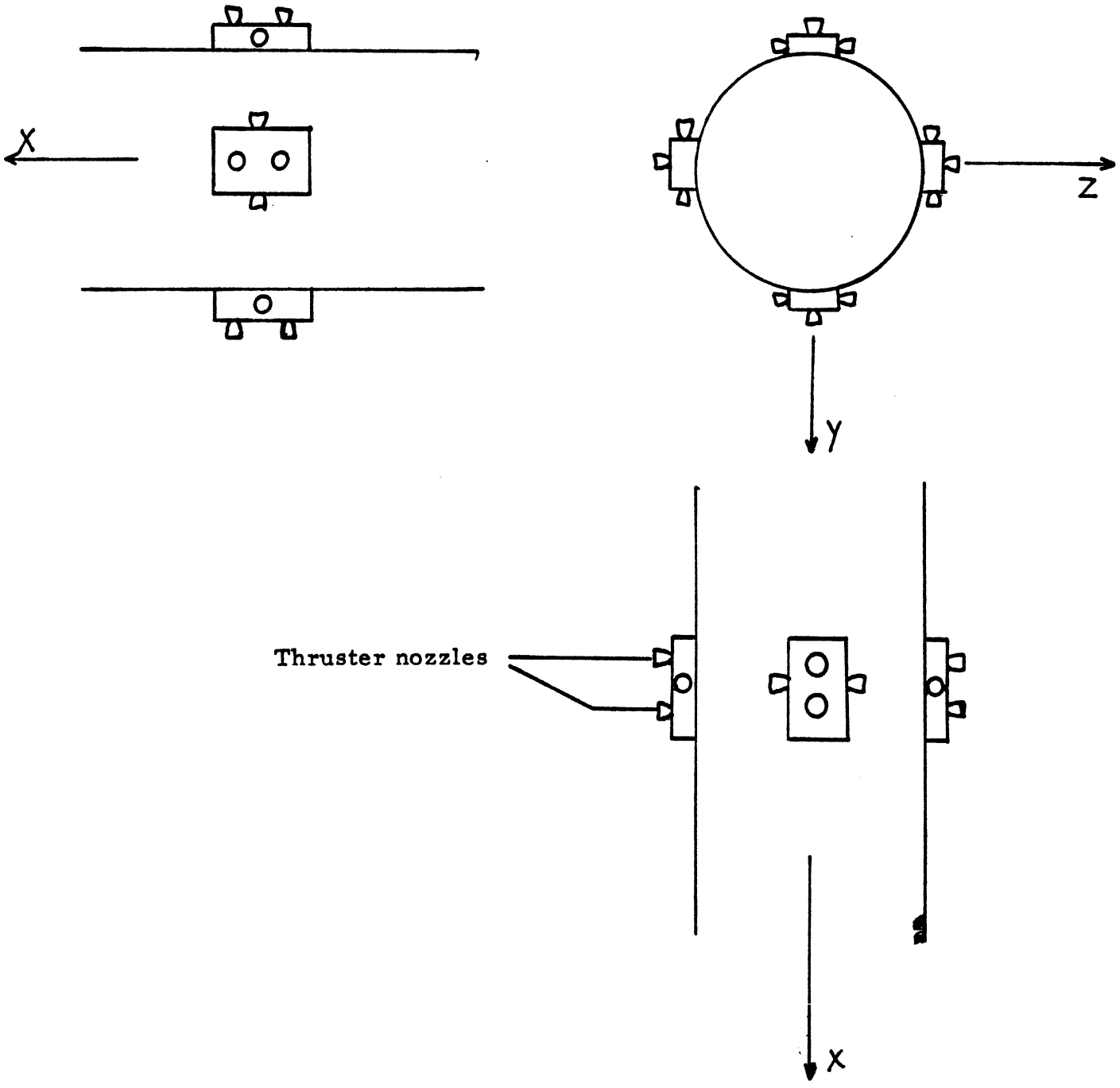

Figure 6.11 Thruster Configuration at a Thruster Station

Since M_c must be great enough to counteract the gravity gradient moment at $\theta_m = 10^o$, the above equation can give a thrust requirement for T_e

$$M_c(T) = M_{gg}(\theta_m) = k \sin 2\theta_m$$

$$T_e = \frac{12\ \Delta X}{l^2}\ k \sin 2\theta_m.$$

Substituting the appropriate values in the above, yields a thrust $T_e = 58.3$ n.

The best type of RCM (Reaction Control Motor) with the thrust capability required by this application is the hydrazine monopropellant RCM. Although no motors of this type are presently available which can be throttle in the range (0-60 n) required by this particular application, it should be practical to assign motors with this capability as this type of motor is throttleable in other force ranges, and thrust is a function of inlet pressure.

Thrust is a function of inlet pressure. This dictates that the primary fuel supply be located at the ends of the vehicle so that where the supply pressure has dropped off due to friction in the supply line less thrust and therefore inlet pressure will be required. Progressively smaller fuel supplies can be stationed closer to the vehicle's center.

Hydrazine RCM's have a specific impulse on the order of 225 seconds. Fuel consumption is a function of the perturbations on the orbit and how quickly deviations in pitch attitude can be detected and corrected before the gravity gradient force becomes large. The number of perturbations encountered and their affect on fuel consumption is an area requiring further study.

6.10 REFERENCES

1. Athans, Michael and Falb, Peter L. Optimal Control, McGraw-Hill, New York, 1966.
2. AFFDL TR-66-68 Section IX, "Quantization Errors of Numerical Integrations," Air Force Flight Dynamics Laboratory, Wright-Patterson AFB, Ohio 1968.
3. Bhat, U. Narayan, Elements of Applied Stochastic Processes, John Wiley and Sons, N. Y. 1972.
4. Greenwood, Donald T., Principles of Dynamics, Prentice Hall, Englewood Cliffs, New Jersey, 1965.
5. Hayes, John P., Computer Architecture and Organization, McGraw Hill, N. Y., 1978.
6. Seltzer, S. M. and Shelton, H. "Specification of Spacecraft Flexible Appendage Rigidity," AIAA Journal of Guidance and Control, Nov-Dec 1978.
7. Slafer, L. and Oberly, P., "Hughes Satellites: Control Systems and Their Electronics," presentation at The University of Michigan, Feb 1979.

7
GROUND SUPPORT

7.1 INTRODUCTION

The idea of disposing nuclear waste in space is exotic by nature. It requires many new ideas and technologies. The other side of the project is to use existing technology as much as possible. The main concern has been the use of existing technology to solve many of the ground operations problems.

The main portion of the work was with ground operations and in life support systems in space. The areas of investigation are:

1. Launch site selection
2. Location of power and reprocessing plants
3. Transportation and handling
    a. Power plants to reprocessing plants
    b. Reprocessing plants to the launch facility
    c. Handling interior to the launch site
4. Environmental impact study
5. Communications
6. Space station design concept

7.2 LAUNCH SITE SELECTION

In selecting a possible launch site to use in transporting the nuclear waste containers into space, three alternatives were considered: use of facilities at the Kennedy Space Center (KSC) in Florida, use of planned facilities at Vandenburg Air Force Base (AFB) in California, and the construction of a new launch facility dedicated exclusively to the disposal of nuclear waste. For the reasons outlined below, it was decided that the facilities at Cape Kennedy would be the best to use for this purpose.

For several reasons, the construction of a new facility dedicated solely to nuclear waste disposal is a very attractive option. The building of a dedicated launch facility in an isolated area greatly reduces the danger presented to the general public by an accident that would release nuclear waste into the biosphere. A dedicated facility also offers greater safety in the handling of waste. Handling and transportation equipment used should be designed exclusively for the handling of radioactive materials. Problems that could occur in handling could easily be taken into consideration in the design of the launch and handling facilities.

As attractive as these factors are, they are outweighed by two other considerations. The first of these is cost. To construction from the ground up the facilities required for the launch, control, recovery, and maintenance

of the Space Shuttles that are to be used to haul the waste into orbit would require the expenditure of several hundred million dollars. Add to this the cost incurred in the designing of the new facility and the procurement of the necessary land, which for maximum isolation from the general public would be a virtually uninhabited island. This would require several billion dollars to be spent constructing a new facility. Its isolation also means that the site's operating expenses would be higher than those at KSC since supplies and fuel necessary would have to be transported farther. In short, the construction of a new, dedicated facility is not cost-effective when compared to the cost of operating from launch sites already in existence. The second factor which argues against the construction of a new isolated facility is the additional risk that is involved in transporting the waste through a greater distance. This factor is most important when considering the transportation of waste across several thousand miles of ocean to an island facility. This journey would be subject to the possibility of a storm or maritime disaster, each of which could result in contamination by released nuclear waste. Although this risk is lessened if the facility is located somewhere in the North American continent, there is still an additional risk that is created by the transportation of waste through additional miles that would not be present if facilities at KSC are used.

The second launch site considered was the Shuttle launch facilities currently under construction at Vandenburg AFB near Lompoc, California. Although the facilities, when completed in 1982 will not be as extensive as those at Cape Kennedy, they would be adequate for the required operations. However, due to its location on the West Coast, the launching site at Vandenburg AFB is less desirable than at Kennedy for two reasons. First, Vandenburg is located on the West Coast, while the majority of the nuclear power plants and all of the existing and proposed processing facilities are located east of the Mississippi River. The additional cost that would be incurred by shipping the waste to the West Coast makes Vandenburg AFB an unfavorable choice when compared to Kennedy. The other reason is that because of its location with respect to the continental United States, all launches from there must be directed either to the west or the south away from populated areas so that a rocket which does not launch properly will not come down in any densely populated areas. To place a payload in an equatorial orbit by a Shuttle launched from Vandenburg AFB would require the expenditure of more fuel in order to cancel out the adverse effects of the Earth's rotational velocity. The extra cost and difficulty that would be entailed by conducting such operations from Vandenburg AFB make it less desirable than the Kennedy Space Center.

As a result of the above analyiss, it was decided that the facilities at Kennedy were the logical ones to be used to handle the launching of nuclear

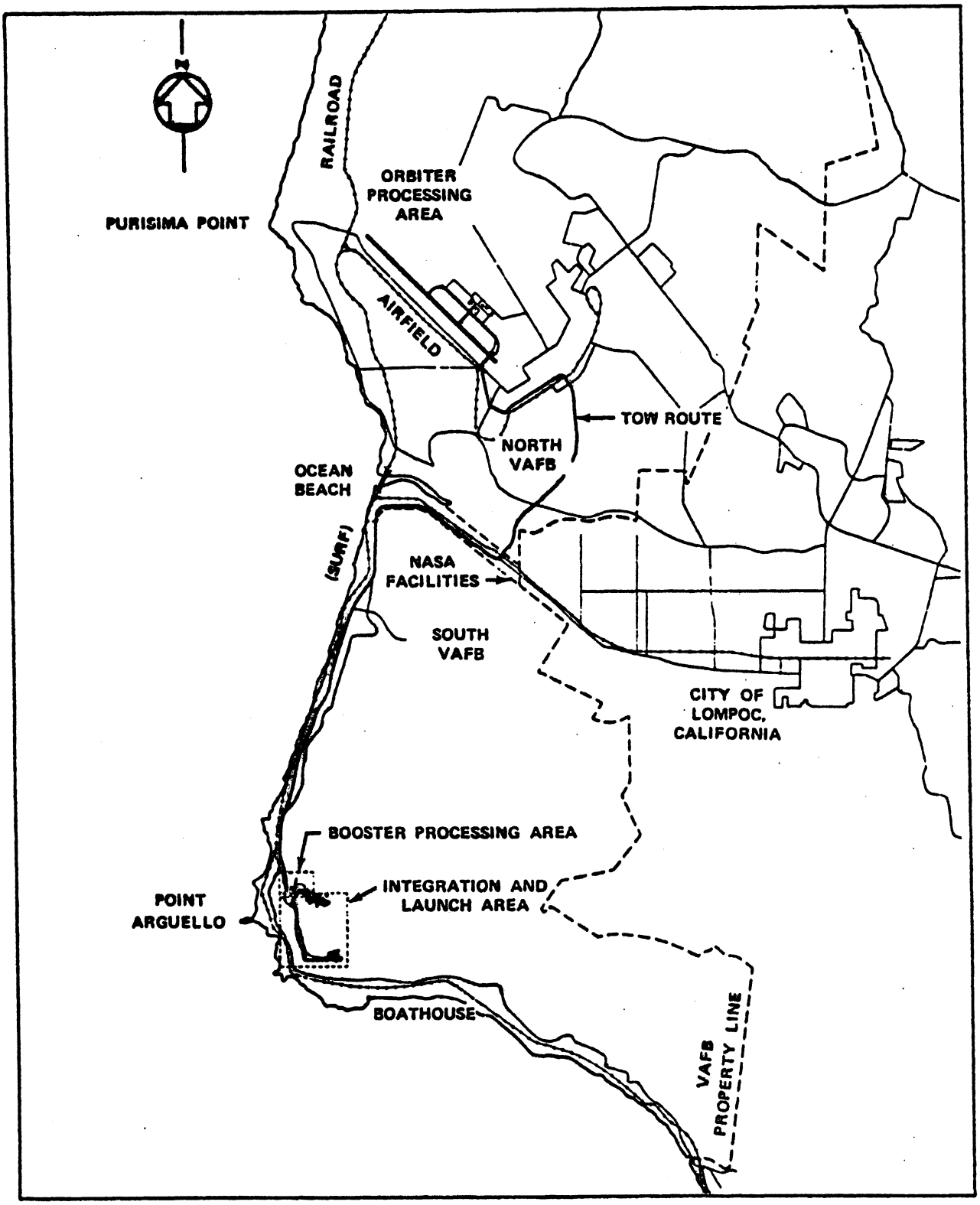

Figure 7.1 Map of Vandenburg Air Force Base.
(Facilities are projected for completion in 1982)

waste containers into orbit. Kennedy provides the best location with respect to the reprocessing centers. The facilities there are extensive with large amounts of available land suitable for the construction of the handling facilities that would be needed to unload, service, and store the waste containers prior to loading them into a Space Shuttle for launch. Kennedy is located close to several large population centers, but the danger presented to these areas can easily be minimized by proper design and planning.

7.3 LOCATIONS OF POWER AND REPROCESSING PLANTS

Irradiated fuel must be transported from the nuclear power plants to the launch site by way of reprocessing plants. Because of limited knowledge of existing facilities, a study of locations of power plant and reprocessing plant locations was necessary.

It was found that at the present time there are approximately 70 nuclear power plants operating in the United States. There are about 120 plants projected for operation within the next ten years (Reference 1). The majority of the plants are located in the eastern half of the United States, with a few locations on the west coast. A complete listing as of June 30, 1978, is included in the appendix (Reference 2).

In the United States today there are three plants which were constructed for reprocessing nuclear waste. None of the three are presently in operation due to government restrictions and only one of the plants has ever been in operation (Reference 3).

The Nuclear Fuel Service Reprocessing plant is located in West Valley, New York. Of the three reprocessing plants, this plant was the only operating plant. When it was shut down in 1971 its facilities had the capacity to reprocess 1000 kg per day and were being expanded to handle 3000 kg per day. It is located on 3300 acres of land owned by the State of New York, approximately 26 miles south of the city of Buffalo. Dairy farms are located relatively near this plant so it is constantly being monitored.

In Morris, Illinois, another reprocessing plant is located. This plant is known as the Morris Operation but was formerly known as the Midwest Fuel Recovery Plant. It is located on private land and is on the same site as a nuclear power plant owned by the General Electric Company. This plant could handle 1000 kg waste per day but was never operational due to cold checkout operation problems. The closest city to this plant is Joliet, which is 14 miles away, and is a suburb of Chicago. The plant site is located near a population center and has facilities for holding fuel along with three reactors.

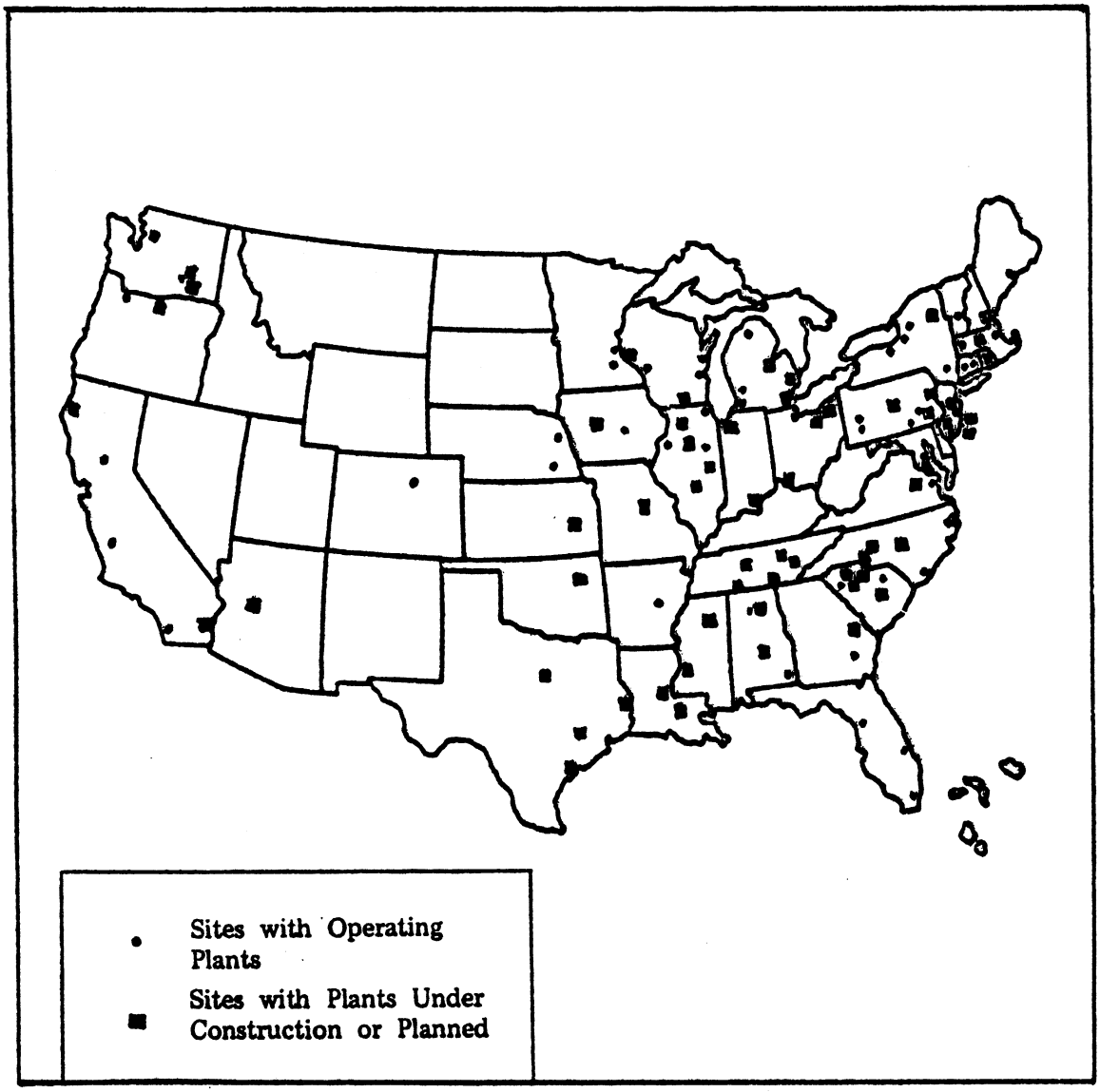

Figure 7.2 Nuclear Power Sites in the United States

In Barnwell County, South Carolina, the Barnwell Nuclear Fuel Plant is under construction. It is located on private property next to the Savannah River Laboratories. It was designed to handle approximately 500 kg of waste per day. The closest city is Augusta, Georgia, which is 31 miles away. It is not in a large population area like the Morris Operation.

Plans are underway for another reprocessing plant. The Exxon Corporation has applied to construct another facility in Oak Ridge, Tennessee.

There are several good reasons why so few plants have been constructed. To reprocess this waste requires a complex chemical process. Add on to the complex process, the effects that everything which is being worked on is radioactive. Also, licensing of a reprocessing facility takes several years and is very restrictive. These complexities make the costs and standards very high. Because of these factors, reprocessing plants are not often constructed.

The present capacity of the three reprocessing plants is about 9000 kg per day. This works out to a total of approximately 3.3 million kg per year. The capacity needed by the year 2000 will be 12.7 million kg per year. This means that by the year 2000, reprocessing plant capacity will have to be four times the present capacity to prevent backlogs. This must be achieved either by building more plants or increasing capacity of the existing plants.

7.4 TRANSPORTATION AND HANDLING: FROM POWER PLANT TO LAUNCH SITE

This analysis was made to assess the best means of transporting the waste from the nuclear power plants to the reprocessing facilities and then on to the Nuclear Payload Preparation Facilities at the Kennedy Space Center in Florida. Presently, it is estimated that 1.6 million packages per year carry a quantity of radioactive material whose shipping, packaging, and labeling are regulated by the Department of Transportation (Reference 9).

The railway system is the best mode of transportation chosen to transport the waste, since,

1. Most nuclear power plants have a rail system at the reactor site,
2. Railways can transport larger volumes per shipment. It would take 455 truckloads at an average of 22 tons per truck to carry 10,010 tons of waste, where as it takes a typical unit train of 100 tons per 100 cars to equal 10,000 tons.
3. Safety of handling and transportation. Irradiated shipping fuel casks are already in existence, have been tested for severe accidents, and used in operation (Reference 8), and
4. Low environmental risk. If a major accident were to occur the clean up operations would be more confined and isolated on a rail system in the country, than for a truck on a congested highway.

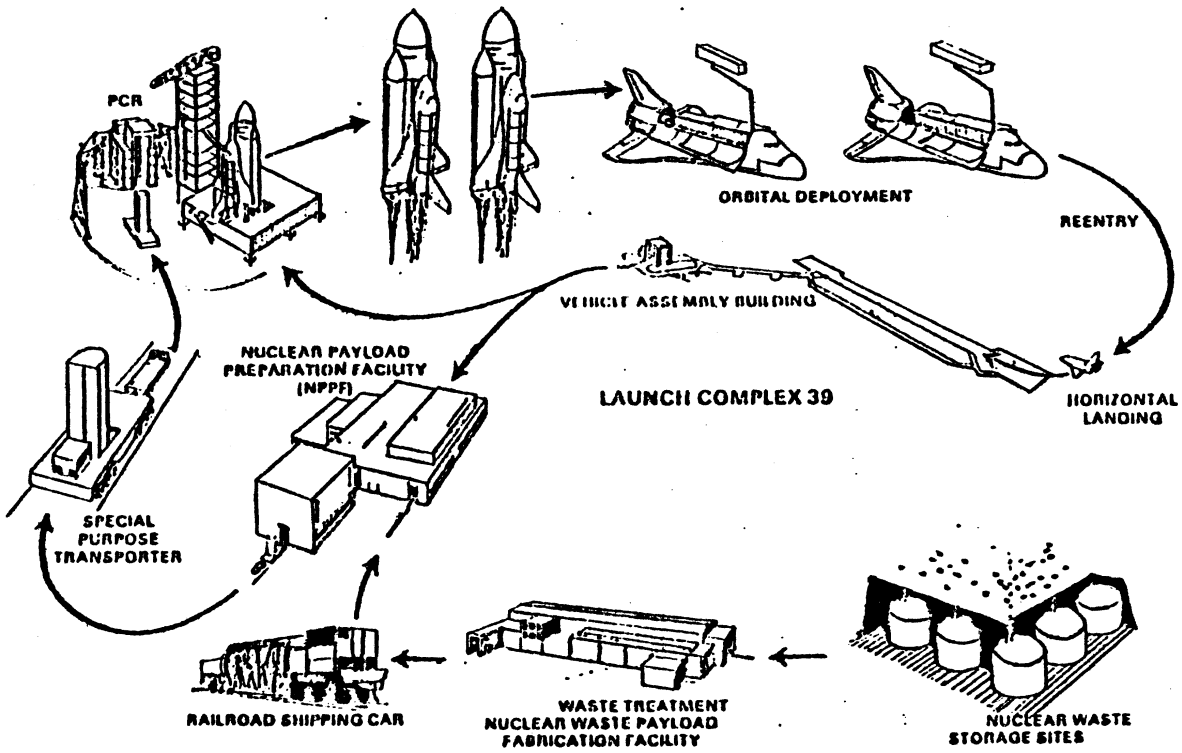

Figure 7.3 Ground Operations

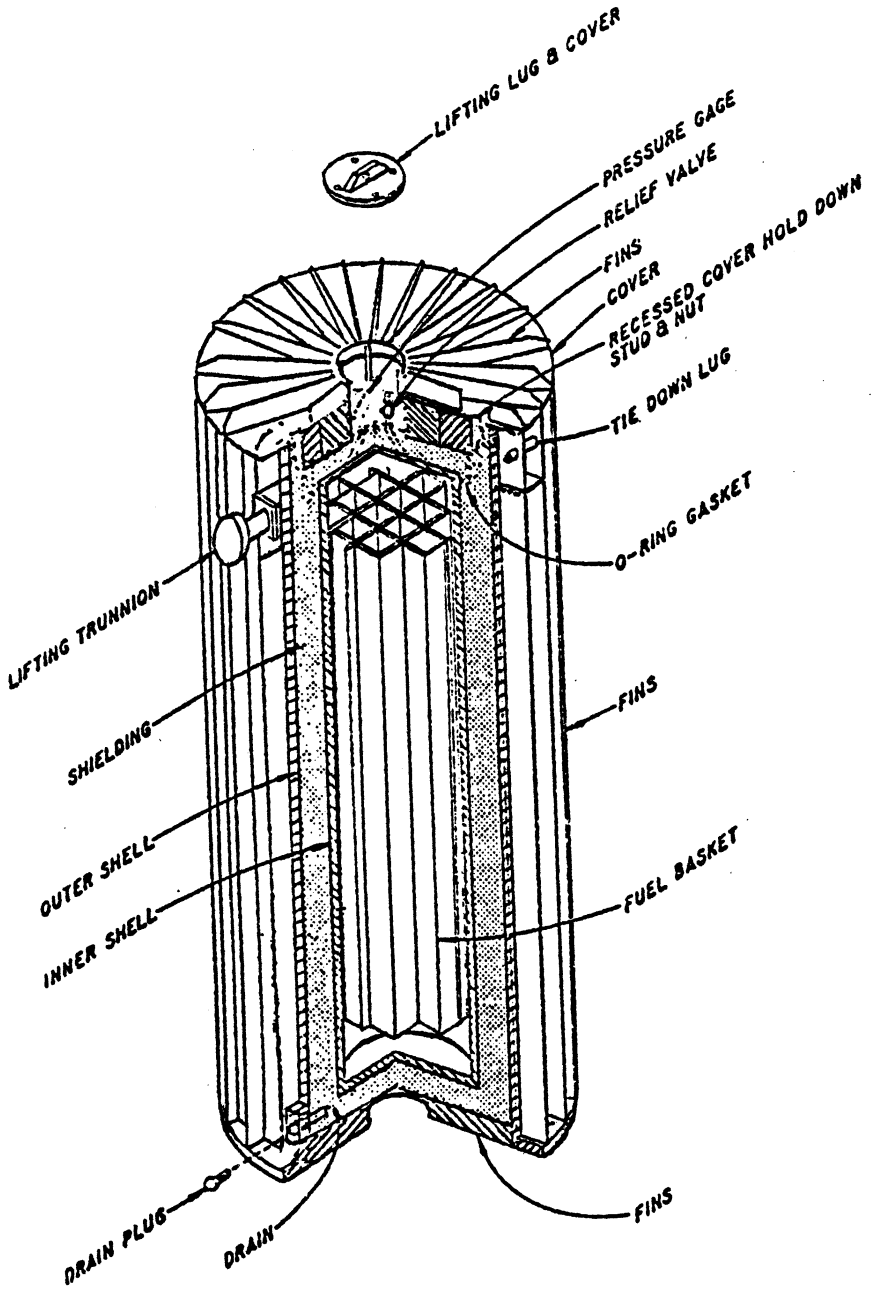

Figure 7.4 Cutaway Diagram of a Shipping Cask Showing the Principal Components

Approximate:

Length	5.3 meters
Diameter	1.6 meter
Weight	
empty	55 tons
loaded	67 tons

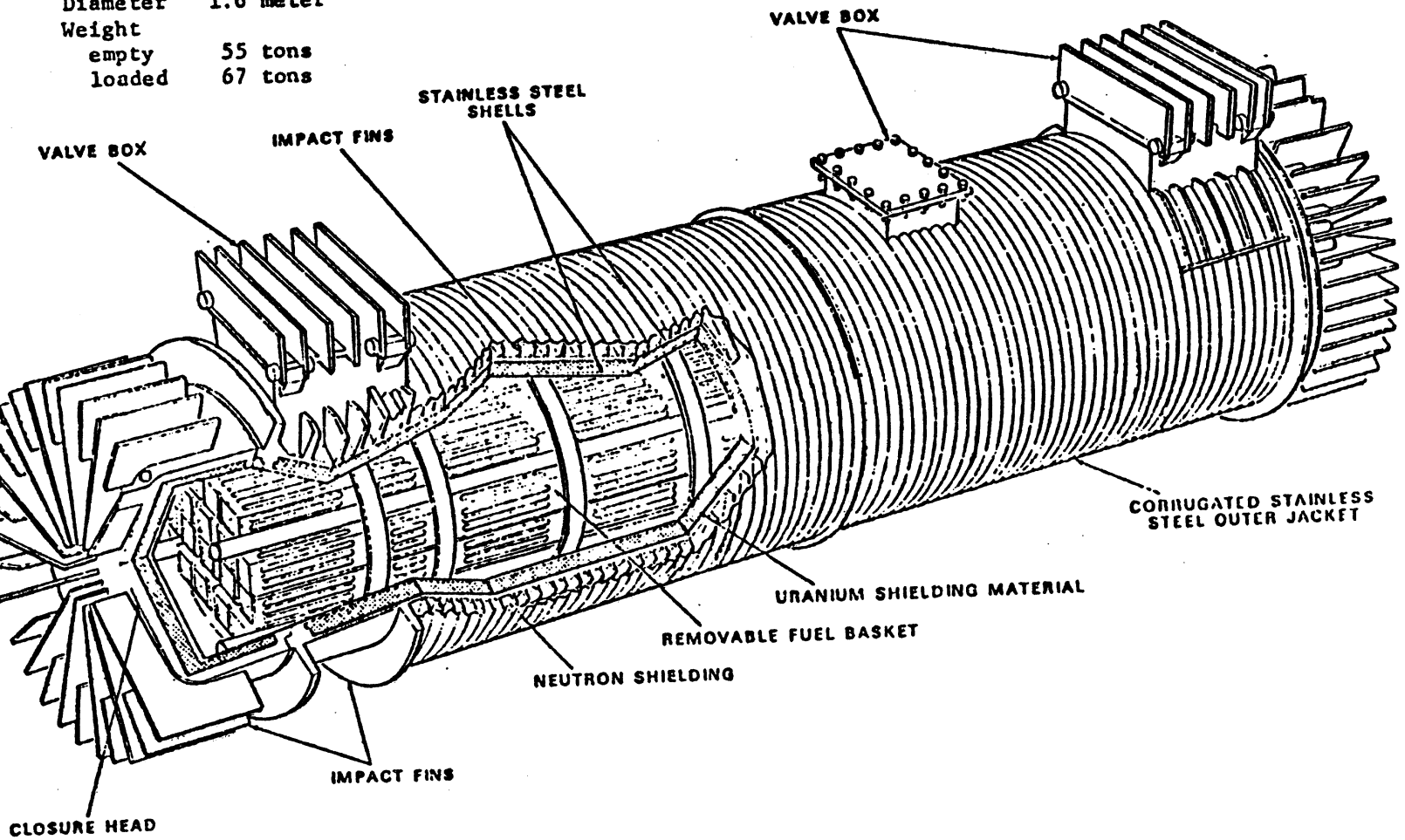

Figure 7.5 Irradiated Fuel Cask

Approximate weight of cask
and shipping assembly:

empty 70 tons
loaded 82 tons

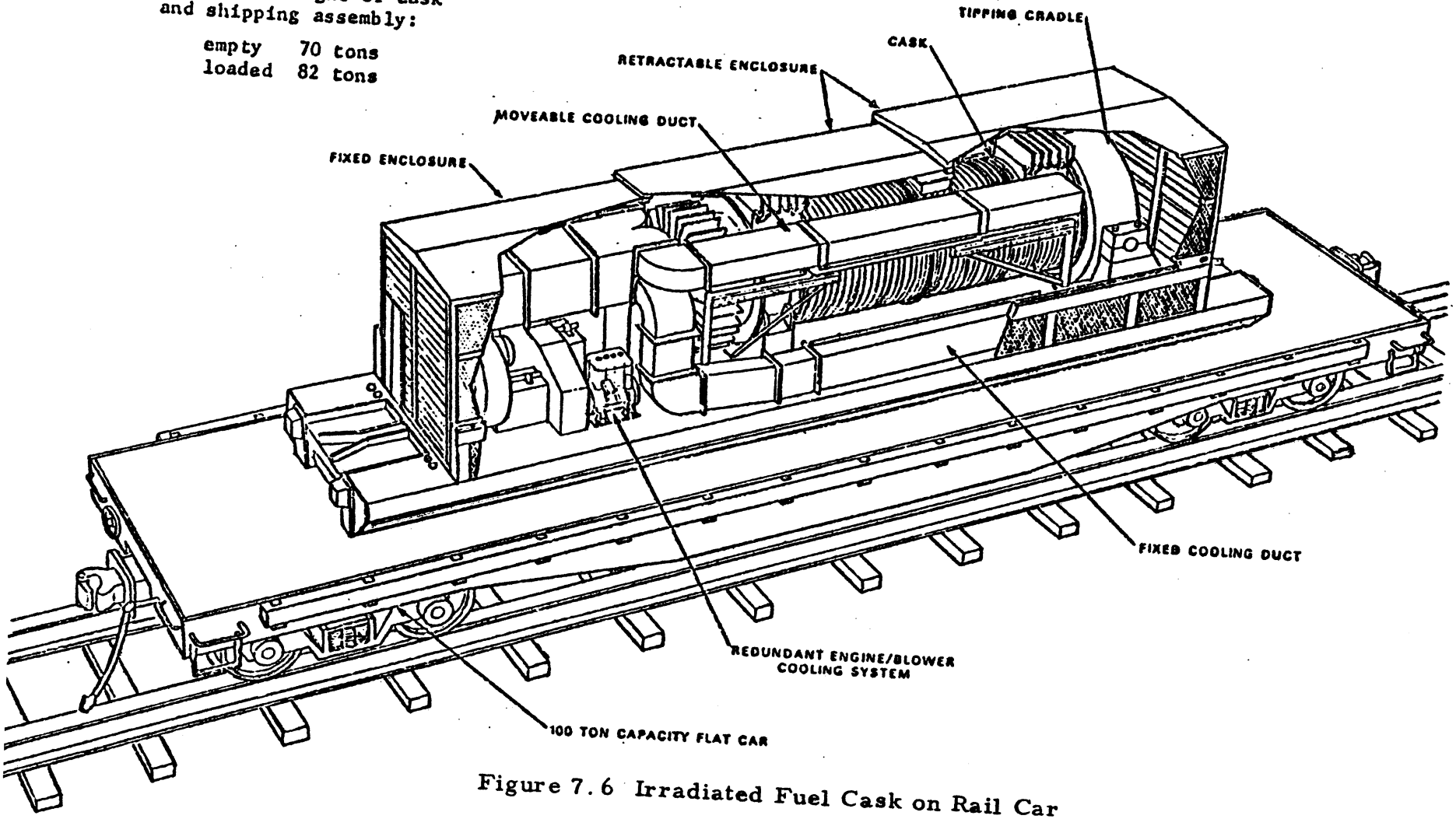

Figure 7.6 Irradiated Fuel Cask on Rail Car

The cask used to transport the irradiated fuel is housed in a thermal cooling unit in transit to deal with the continued large heat generation. Also, the containers are provided with radiation shielding and are able to withstand the impact of any transportation accident (Reference 14).

Safety in transportation does not require special routing, although special routing is used at some bridges and tunnels to avoid possible interference with the flow of traffic, should an accident occur. These shipments are therefore subject to the same transportation environment and rules as already stated. Protection of the public and transport workers from radiation during the shipment of radioactive materials is achieved by a combination of limitations on the contents according to the quantities and types of radioactivity, standards, and criteria for package design and control (Reference 10).

At the reprocessing plants the fuel is converted into an oxide powder for long-term storage and also to extract specific elements from the fuel. An extension of the reprocessing facility should be constructed to handle the oxide powder and its packaging into 1 kg modules. These modules are then placed inside the containment vessel which will be shipped by rail to the Nuclear Payload Preparation Facilities at Kennedy Space Center.

7.5 HANDLING OF THE WASTE CONTAINERS AT J. F. KENNEDY SPACE CENTER

Upon arrival at the Nuclear Payload Preparation Facility (NPPF), the cask containing the waste canister is unloaded from the railroad car. The canister is removed from the shipping cask, checked carefully for any faults, and is then transported to the holding section of the facility where it is placed in a shielded and cooled room. It will remain there, under constant surveillance, until the time comes to prepare it for loading into the Shuttle.

Approximately 80 hours before scheduled launch, the canister is removed from the holding area and moved to the preparation portion of the NPPF. Here the canister is again checked for any package faults or failures. After passing this check-out, the canister is then mated with a monitoring module which will monitor the surface temperature of the canister to insure that any irregular behavior within the canister does not go unnoticed. The information gathered will be relayed both to the ground and to the crew of the Shuttle. After installation and check-out of the temperature monitoring system, the waste container is hooked up to a cooling system which will keep the waste canister cooled to simplify handling and protect the surroundings from the heat given off by the waste. This cooling system will be used during the handling of the handling container and canister on the ground. The handling container, with the canister

inside, will be attached to the Shuttle's interior cooling system at the time of loading. After completing check-out of this portion of the package assembly operation, a parachute recovery system is attached to the package. With this system, the canister can be brought safely back to earth in the event that the canister is jettisoned by the Shuttle orbiter in an in-flight emergency. With the completion of the final check-out of this installation, the waste canister package is now ready for loading onto a special transporter for transportation to the launch pad where it will be installed in the Shuttle orbiter.

To transport the waste canister package to the launch pad, a special transporter will be required. The waste canister package weighs in excess of 20 tons. The transporter will require a primary and secondary cooling system to insure that the package will be continually cooled, as failure to do so could cause the canister to overheat and endanger the transporter and crew due to the heat generated by the nuclear waste. The assembly will also be transported in a vertical position to assist in loading the package into the orbiter bay. By carrying the load vertically, it also removes the necessity of using equipment at the launch pad to move the package from a horizontal to a vertical position. By minimizing the amount of handling of the package at the pad, it is possible to minimize the risk of an accident occuring at the launch pad and contaminating the immediate area with released waste. These requirements necessitate the use of a special transporter dedicated entirely to the transporting of waste canister packages. This will make the monitoring, detection, and containment of any radioactive contamination much easier.

The nuclear waste package will arrive at the launch pad approximately 53 hours before scheduled launch time. At this point, the package will be loaded in the payload Changeout Room (PCR), the facility at the pad used to load payloads into the Shuttle orbiter when the orbiter is in the vertical position. This operation takes 13 hours. At the end of this time the Shuttle is moved to the pad and the PCR is moved into position next to the orbiter. Starting at approximately 21 hours before launch, the waste package is transferred from the PCR into the Shuttle cargo bay. This process takes 9 hours and involves transferring the cooling of the waste package to the orbiter's internal cooling system, connecting the temperature monitoring system to the Shuttle, and securing the package in the Shuttle. A careful check-out of all systems is completed, and when all requirements are satisfied, the Shuttle bay doors are closed and the waste is ready for launch into orbit.

In the total process of handling the nuclear waste at the Kennedy Space Center, the most important link in the chain is the NPPF. This facility will need to be constructed, and there are several factors which need to be considered in its design and construction. The facility will need to have a holding area where several nuclear waste canisters could be stored for short

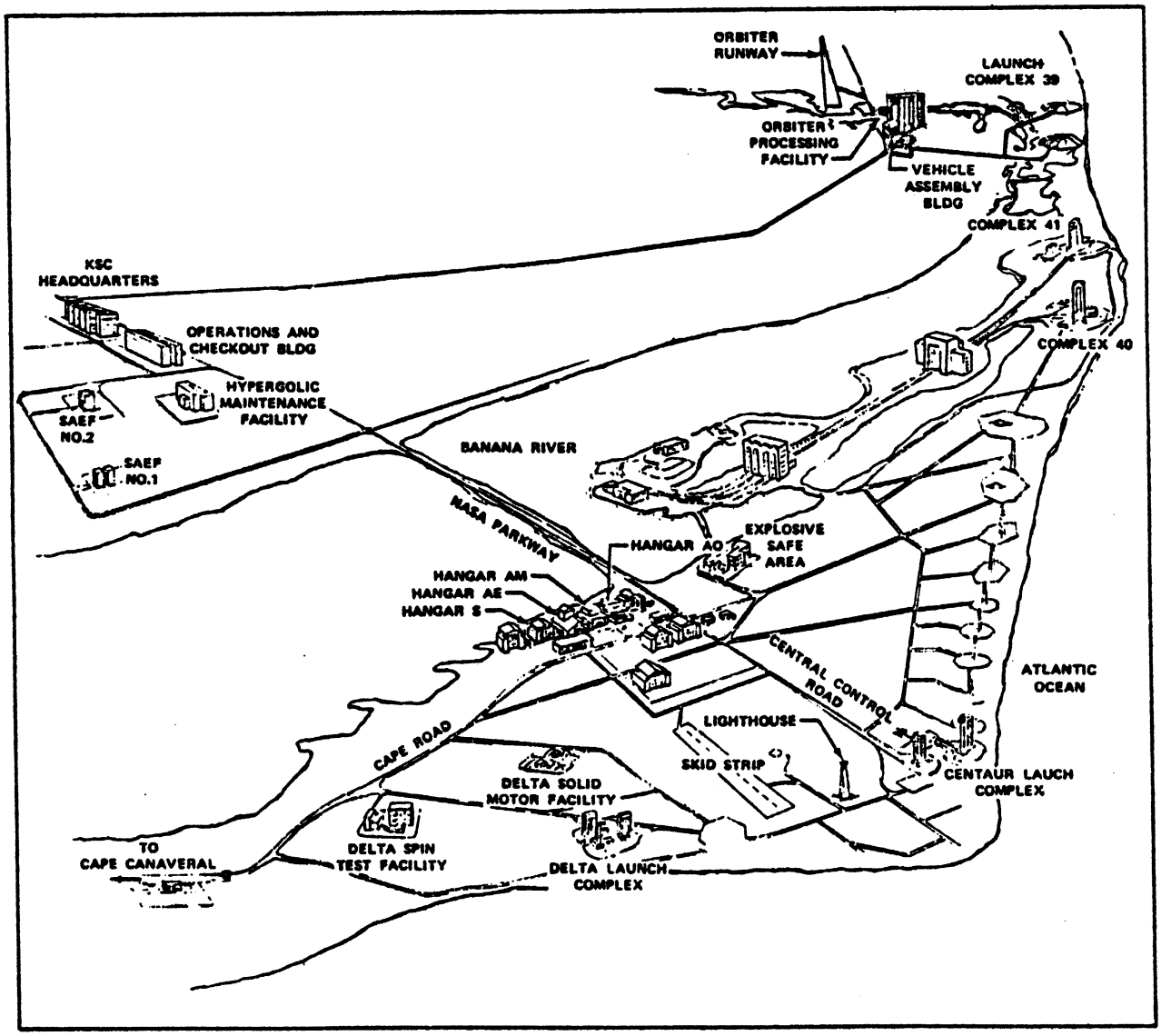

Figure 7.7 Map of J. F. Kennedy Space Center

(showing major buildings that are used by the Shuttle Transport System)

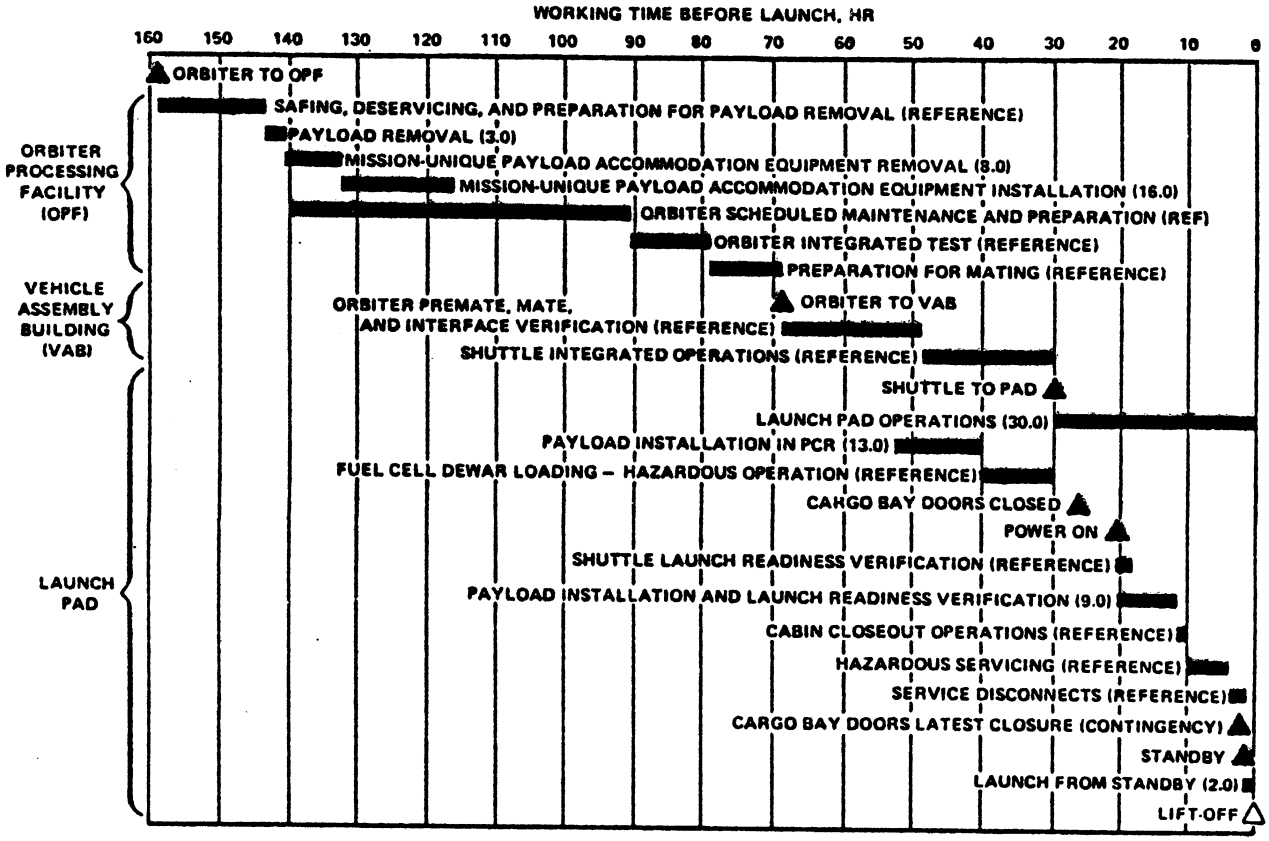

Figure 7.8 Payload Processing Schedule and Shuttle Operation Ground Flow

periods of time. This area would need to be shielded so that in the event of a canister rupture, the waste will not contaminate the surrounding area. This shielding would also protect the surroundings against the radiation given off by the waste canisters. This holding area would also need to provide individual cooling units for each waste canister and a backup system capable of switching on automatically and running continuously. Both of these would have to be capable of operating independent of outside power sources. The building should be equipped to handle a wide variety of possible accidents and circumstances. The cargo handling areas should be constructed to minimize the amount of direct human contact with the waste canisters by maximum use of remote handling equipment. The facility should also be built sturdily enough to withstand a wide range of possible weather situations. This facility should also have a wide range of mobile equipment for handling spills outside of the facility.

The handling of waste within the confines of Kennedy Space Center would also require the establishment of certain new operating procedures. Procedure for dealing with several different types of accidents should be established and the necessary personnel trained to handle them. Surveys of the transportation routes to the launch pad from the NPPF should be performed regularly to guard against the spillage of small amounts of radioactive waste. All operations involving the handling of the waste canisters should be carried out with maximum emphasis on safety and system redundancy. The canisters should be handled as little as possible and during this handling the area should be cleared of as many sharp objects and unnecessary personnel as to minimize the danger of accident and contamination. With proper planning and training of personnel, the danger to the general public will be minimized and the effect of a spillage of waste localized quickly and effectively.

7.6 ENVIRONMENTAL IMPACT

Throughout the transportation route from nuclear power plants to space, it is possible for the containment vessel to break and thus effect the environment. Several key areas of environmental impact are, transportation from the power plant to the launch pad, on or near launch pad explosions, and the possible encounter of a waste package with other space objects. All these environmental problems must be considered in the design.

In the rail link between the power plant and launch site, the possibility of a severe accident occuring is very small. In the past 25 years in the U. S., there have only been 300 reportable accidents and only 30% of these have had released radiation. None of these accidents have had related deaths. A

container would be involved in a transportation accident only once in 10 years and only one accident out of 100 will be severe. These statistics show that a rail accident is very unlikely (Reference 8).

Studies have been made about on or near launch pad explosions and have shown that the possibility of an accident occuring which would release nuclear waste is almost nonexistent. Several types of accidents were studied and showed that with a 1% release of a 5500 waste package there would be no health hazard within 100 km. This study concluded that there were no problems but much more work must be done for more conclusive results (Reference 13).

To show how devastating a waste spillage would be some examples of the previously mentioned problems are included. They readily show how important it is to make every effort to put safeguards on transportation, as already exists with the rail system.

If a severe accident were to happen (possible but not probable) enroute to the reprocessing centers, it would have devastating effects upon the surrounding areas. The water system could be affected if the waste were not cleaned up within a time limit of 10 hours. Also in this time frame (using seven irradiated fuel elements) the radiation level at 100 feet could be as much as 10^4 rem/hr (industrial limits are 5 rem/year). Approximately 30,000 persons within a mile radius (based on 10^4 persons/square mile) might receive a cumulative dose of about 1000 rem. If a person remained unshielded at an average distance of 100 feet from the fuel elements for 6 minutes, he might receive a dose of as much as 1000 rem. The land around the spillage would be uninhabitable for approximately 150 years. Even then, a cautious approach to the land is warranted, since a steady dose of radiation would be emitted from the ground level every hour (References 9, 14).

Another major concern is the assessment of the environmental impact of on or near-pad shuttle failure with the release of the nuclear waste payload, either before or after liftoff. Taking the most severe case is where the Shuttle orbiter explodes fully loaded (fuel, waste package) on the launch pad. Taking into account the meteorological circumstances (spring, fall and sea breezes) the waste dispersion would reach a radius of 100 km (62.5 miles). Assuming there are 55 kg of waste that would be released, the population would be exposed to 1000 rem.

Although these are the most severe cases, when the probability of these mishaps occuring and the extent of the consequences are taken into account, the risk to the environment due to the radiological effects of transportation accidents is small. Accidents to packages more severe than design accidents (see Figure 6) can occur but the probability is very low (Reference 13).

One final environmental consideration is the possibility of contaminating either the other heavenly bodies in the solar system or the planets in some other solar system. In the latter case, the possibility of contaiminating another solar system is non-existent. The nearest star is 4 light-years away and it would take a waste package about 60 million years to reach it. After this time, the package would simply be 1 kg of dust and would not present a danger to anyone. The other consideration, the contamination of our own solar system, is more important. The amount of waste in any one load is very small and would be incinerated in the upper atmosphere of any of the outer planets. The smaller moons have no such protective shield, but the extent of the contamination from an inpact would be localized due to the small amount of waste involved and the absence of an atmosphere which would spread the waste across the face of the body. Therefore, the contaimination of the outer planets with nuclear waste is not a serious worry. However, it is also a problem that can easily be avoided. It is possible to launch the waste packages into orbits that will avoid all the outer planets. This is a complicated problem in celestial mechanics but it is one that can be solved today. Therefore, there is no real danger of contaminating the rest of the universe with nuclear waste.

7.7 COMMUNICATIONS

The present tracking system used by the United States is the Space-flight and Tracking Data Network (STDN). The system consists of 14 ground based stations in the United States and throughout the world.

This system has become too costly to operate for several reasons. The present system has several stations in foreign countries and the land which the stations are located on must be leased from each country. These costs have increased significantly. Also, many of these stations have data storage and handling facilities which are very expensive. These reasons have boosted the cost of operation significantly (Reference 4).

The communication network projected for the 1980's is the Tracking and Data Relay Satellite Systems (TDRSS). This system incorporates the use of two satellites placed in geosynchronous orbit. These satellites will relay messages from spacecrafts to earth based stations in the United States in real time. There will still be some foreign stations for highly eliptical, lunar, and interplanetary space flight missions. Also, this system's data handling equipment is operated and paid for by the particular user. This reduces the cost of communications.

This system has a wider bandwidth for communication, and one channel could be routed via a domestic satellite. This tracking network is also planned on being used on Space Shuttle flights and for Spacelab experiments.

7.8 SPACE STATION - LIFE SUPPORT

In the existing space shuttle program, the European Space Agency has developed a program of Spacelabs. There are several configurations of module and pallet configurations which allow many scientific experiments to be conducted from the Space Shuttle. A possible life support system could be constructed of certain elements of these existing Spacelabs.

There are several reasons for using the Spacelab configuration for a life support system. Most of the experimental work has already been done resulting in low cost. The communication system used on these experiments is the TDRSS which is compatible to the tracking system for NEWDUMP. Only a slight amount of modification is necessary for application to the project. Because these space labs were designed for experimental purposes, it would be possible to add on extra modules for experiments.

The configuration chosen is shown in Figure 11. This system is approximately 18 m (59 ft) long on a side and approximately 4 m (13.3 ft) in diameter. The total system is 20 canisters with 5 per side. Each side 'bottle-necks' because airlocks will be placed in each narrow section in case a separation occurs. The facility contains the following:

1) power storage,
2) control room,
3) life support section (air conditioning, water, and food storage),
4) repair center,
5) sleeping area for 12 people,
6) latrines, and
7) galley, sick bay, recreation area.

The total interior volume is 444 m^3 (15,680 ft^3), excluding the connecting tunnels. The total weight is approximately 70,000 kg (150,000 lbs).

The life support system would be connected in some manner, exterior of the tension cables. The total weight of the life support structure is several orders of magnitude lower than the total mass driver weight, and because it is located at the half way point of the mass driver, it will not contribute significantly to moments or inertial effects.

7.9 CONCLUSIONS AND RECOMMENDATIONS

The following conclusions and recommendations were arrived at by the Ground Support investigations.

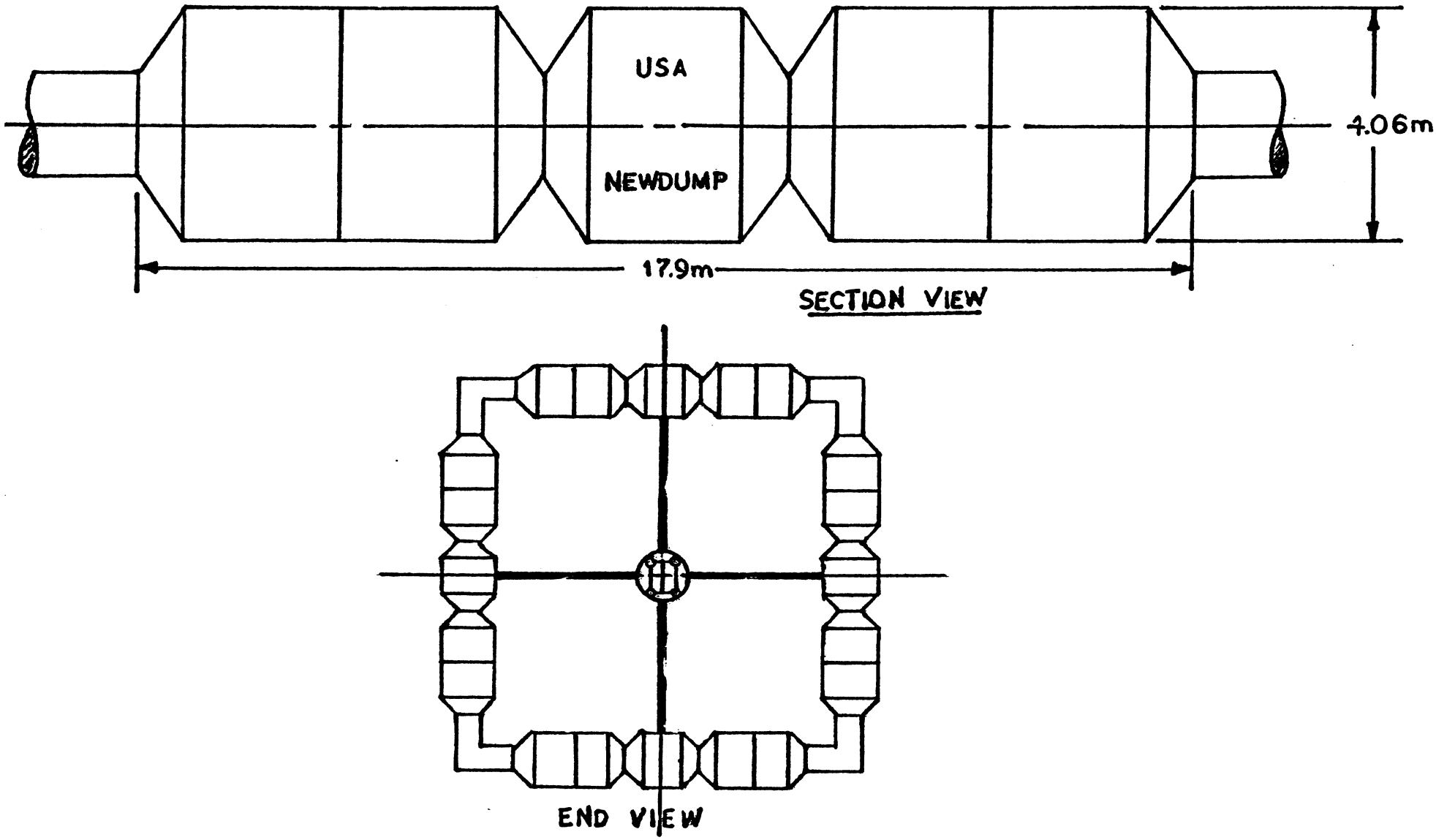

Figure 7.9 Schematic of Double Module Space Lab Configuration of Canisters

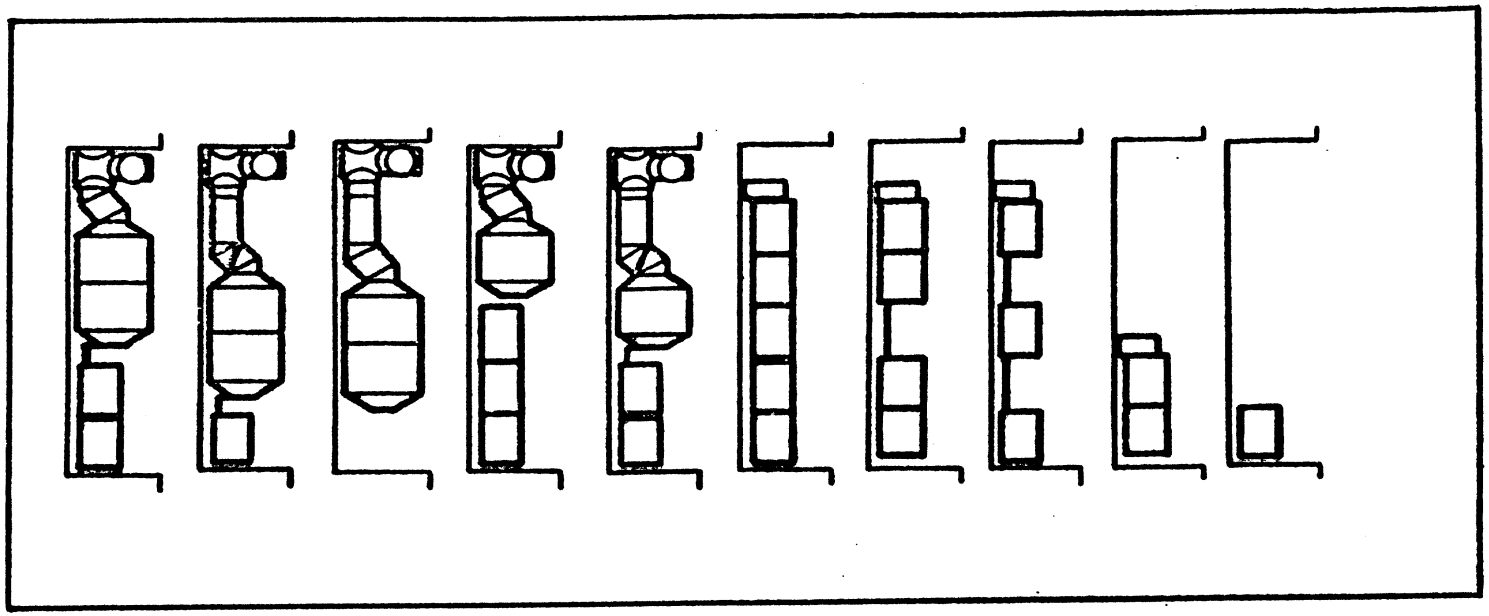

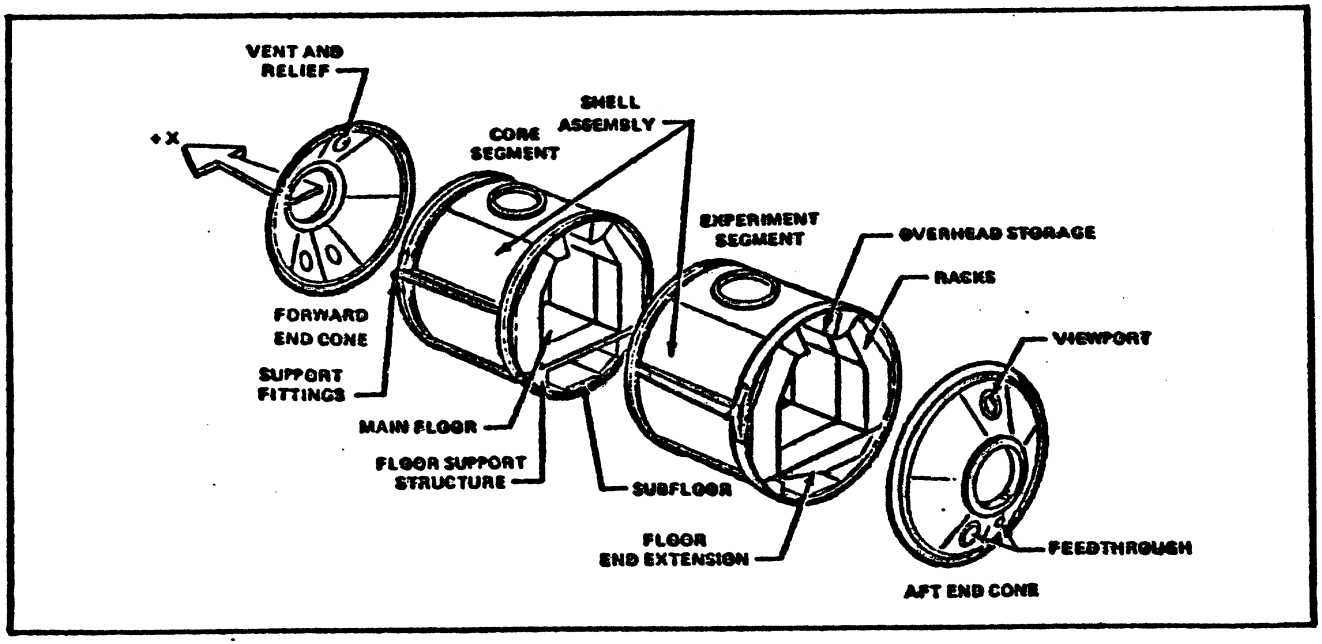

Figure 7.10 Present Space Lab Configurations Showing Pallets and Canisters

1) The best launch facility would be Kennedy Space Center, due to launch considerations and its location.
2) There are approximately 70 nuclear power plants now producing and 120 projected plants. Also 3 reprocessing plants have been built and 1 permit to build a plant has been requested.
3) A facility must be constructed at the present reprocessing plants to package the waste in containers which will be sent in space. This will minimize contact with containers.
4) Waste will be transported by way of the rail system. Interior to the launch facility, the package will be handled in a special manner.
5) A handling system at KSC must be constructed for holding and checkout of waste packages.
6) The environmental impact if a breech in containment occurs would be directly related to the severity of the accident.
7) The tracking system used will be the Tracking and Data Relay Satellite System because it is projected to be used on Space Shuttle and Spacelabs.
8) A preliminary design of Spacelab modules could be constructed to house a life support system.
9) More research must be done on adapting the Spacelab modules to use for a life support system, and adapting it for use on a mass driver.

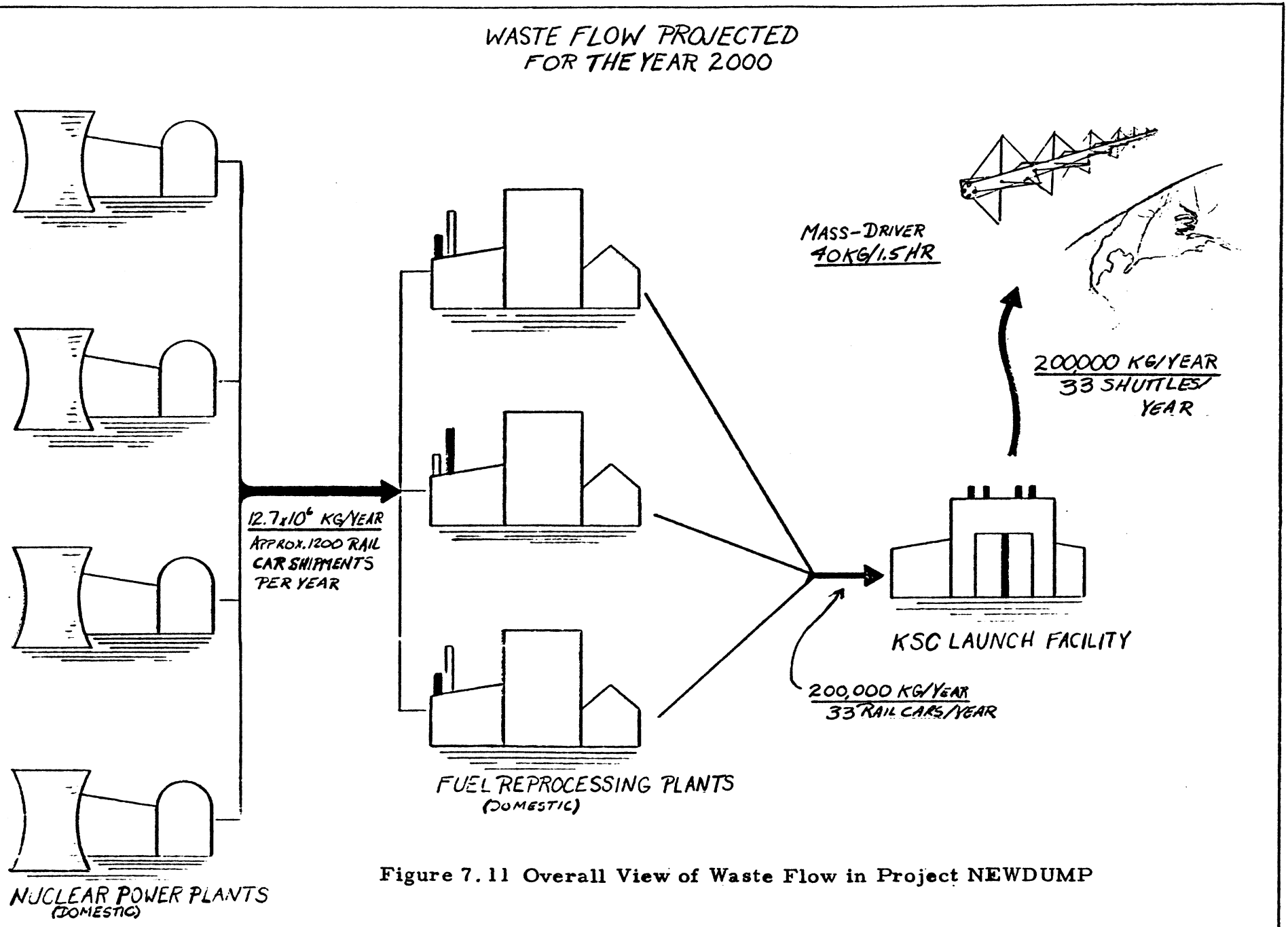

Figure 7.11 Overall View of Waste Flow in Project NEWDUMP

7.10 REFERENCES

1. Deutsch, R. W., Nuclear Power, General Physics Corporation, Columbia, Maryland, 1976, p. 7.
2. Environmental Information Center, Inc., "The Energy Index '78", Energy Reference Department, New York, N. Y., 1978.
3. Gilmore, William R., Editor, "Radioactive Waste Disposal," Noyes Data Corporation, Park Ridge, N. J., 1977.
4. Dickinson, W. B., "The Spaceflight and Tracking Data Network Data Handling System in the 1980's," EASCON '75; Electronics and Aerospace Systems Convention, NASA Goddard Space Flight Center; Electronics and Aerospace Systems Convention, Washington, D. C. September 29-October 1, 1975, Record.
5. Deerkoski, L. F., "Tracking and Data Relay Satellite System (TDRSS) Telecommunication Services," EASCON '75; Electronics and Aerospace Systems Convention, NASA Goddard Space Flight Center; Washington, D. C., September 29-October 1, 1975, Record.
6. National Aeronautics and Space Administration, Space Transportation System Users Handbook, June 1977.
7. Aviation Week and Space Technology, January 29, 1979
8. U. S. Atomic Energy Commission, "Environmental Survey of Transportation of Radioactive Materials to and from Nuclear Power Plants," December 1972.
9. Bodansky, A and Schmidt, F. H., The Nuclear Power Controversy, Prentice, Hall.
10. National Energy Transportation Vol. 1, Current Systems and Movements Committee of Commerce, Science, and Transportation, No. 95-15.
11. Nuclear Safety; Transport of Radioactive Materials in the United States, Vol. 18, No. 3, May-June 1977.
12. Battelle Columbus Laboratories, Preliminary Evaluation of the Space Disposal of Nuclear Waste; Contract No. NAS8-32391, August 30, 1977.
13. Battelle Columbus Laboratories, Evaluation of Space Disposal of Defense Nuclear Waste, Final Review, NASA Marshall Space Flight Center, January 29, 1979, Columbus, Ohio.
14. United States Atomic Energy Commission, "Shipping Radioactive Material at the National Reactor Testing Station," Washington, D. C., AEC Headquarters Bld., Germantown, Maryland, October 1960.

8
COST ANALYSIS

8.1 INTRODUCTION

This chapter is devoted to a cost estimate of Project NEWDUMP and its impact on the electric utility and the consumer industry.

8.2 SUMMARY

The total cost is broken down into three categories; construction of the mass driver in space, operating costs of Project NEWDUMP, and a storage facility at Cape Kennedy. The cost of constructing the mass driver is 11.567 billion dollars. This includes research and development work still to come and Space Shuttle transportation to orbit.

The operating costs are 2.974 billion dollars per year. This includes reprocessing of the waste, ground transportation to Cape Kennedy, and thirty-six Space Shuttle flights each year.

All figures are in 1980 dollars.

Item	Cost $\$ \times 10^6$	Percent of Total Cost
Cape Handling Facility	123	0.8
Mass Driver	11,444	78.7
Waste Disposal Operations (yearly)	2,974	20.5
	14,541	100.0

Table 8.2.1

8.2.1 Mass Driver

The mass driver costs were figured by extrapolation of other predictions made on smaller mass drivers. These predictions were then related to large space satellites. They are listed in Table 8.2.2.

8.2.2 Handling Facility

An estimate of a wast facility at Cape Kennedy was assessed as a nuclear waste storage site meeting NRC safety reuglations. This facility was estimated at 123 million dollars.

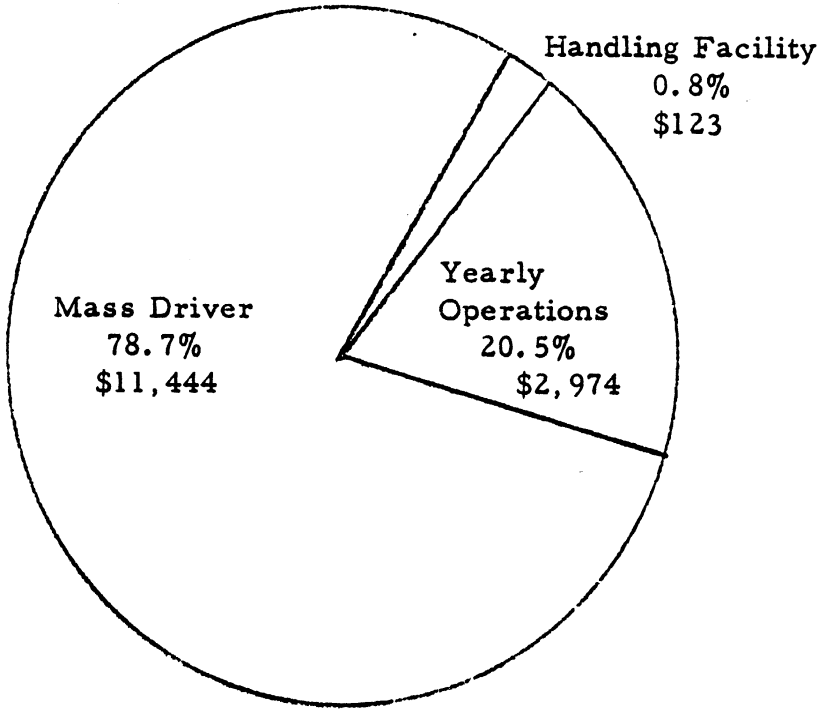

FIGURE 8.2.1 TOTAL PROJECT COST (MILLIONS)

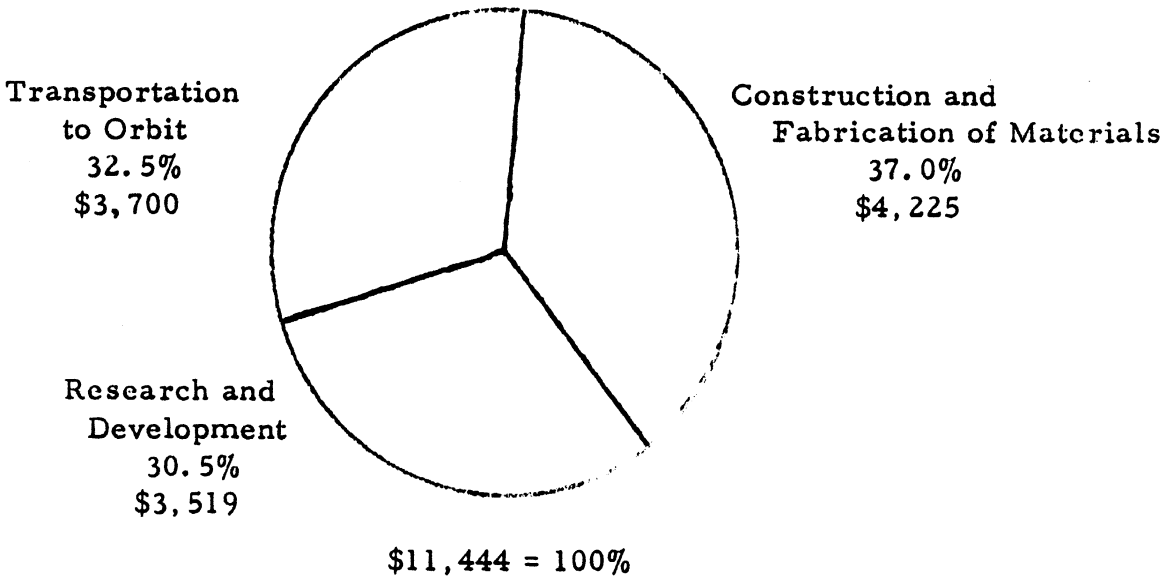

FIGURE 8.2.2 TOTAL MASS DRIVER COST (MILLIONS)

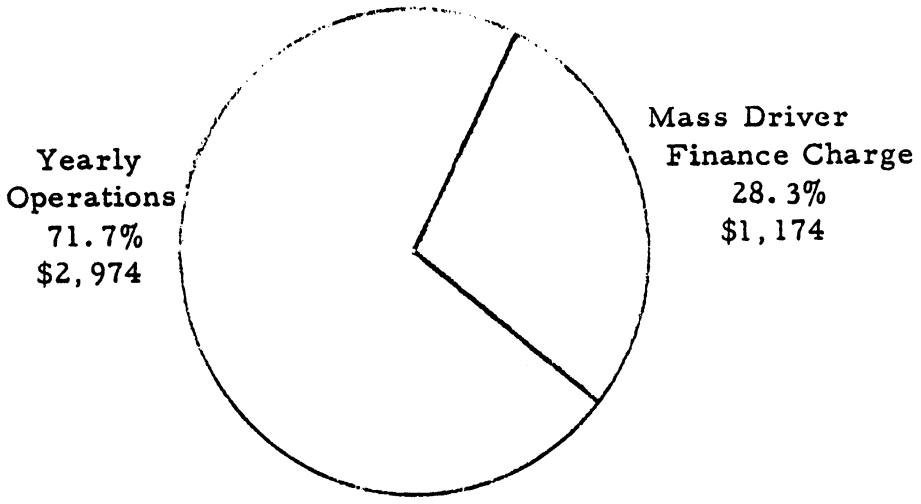

$4,148 = 100%

FIGURE 8.3.1 FINANCES (MILLIONS)

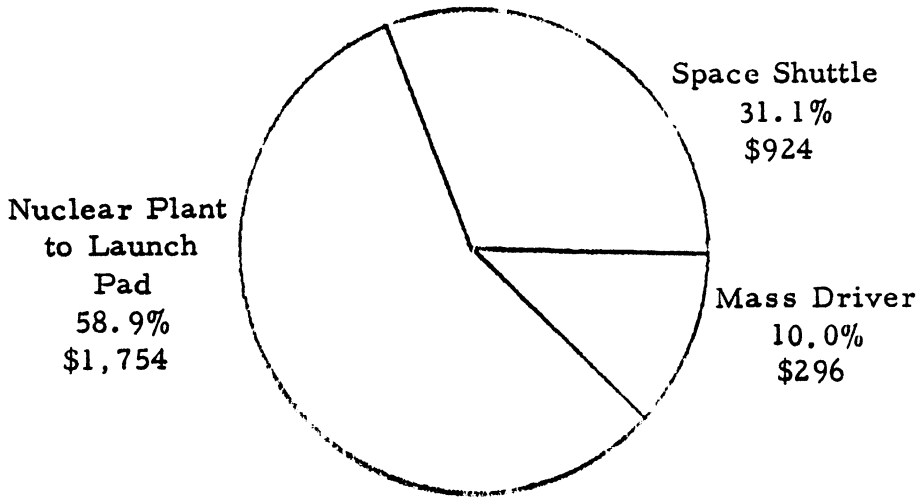

$2,974.6 = 100%

FIGURE 8.2.3 YEARLY OPERATIONS COST (MILLIONS)

	Cost $ x 10^6	Percent of Total
Research and Development		
Mass driver	3,270	28.6
Batteries	205	1.8
Attitude Control Engines	44	0.1
Subtotal	3,519	30.5
Construction and Fabrication of Materials		
Electronics	1,699	14.8
Structures	2,021	17.7
Batteries	223	1.9
Solar Cells	117	1.0
Attitude Control Engines	5	.1
Computers	5	.1
Crew Station	155	1.4
Subtotal	4,225	37.0
Transportation to Orbit		
Space Shuttle	1,940	17.0
Developmental Testing	1,760	15.5
Subtotal	3,700	32.5
Total	11,444	100.0

Table 8.2.2

8.2.3 Yearly Operations

The yearly operations were estimated based on a yearly waste disposal of two hundred thousand kilograms after reprocessing. These are broken down in Table 8.2.3.

	Cost $ x 10^6	Percent of Total
Nuclear Plant to Launch Pad		
Reprocessing	1,305	43.9
Transporting Spent Fuel	95	3.2
High Level Waste Transportation	25	0.8
High Level Waste Management	253	8.5
Safeguards	76	2.5
Subtotal	1,754	58.9
Space Shuttle		
Transportation	874	29.4
Waste Packages	50	1.7
Subtotal	924	31.1
Mass Driver		
Maintenance and Operations	296	10.0
Total	2,974	100.0

Table 8.2.3

8.3 UTILITY IMPACT

The yearly cost of 2.974 billion dollars can be covered by an increase of 5.12% to the electric utilities annual revenue. In order to keep the program operating and pay for the mass driver in a twenty-five year nine percent loan the increase in annual revenue would be 7.15%. This constitutes 4.148 billion dollars per year to remove nuclear waste into space. After the first year 71.4% of the utility bill increases go directly to nuclear waste disposal.

The yearly costs are outlined in Table 8.3.1

	Cost $ x 10^6	Percent of Total
Mass Driver and Handling		
Facility Finance Charge	1,174	28.3
Yearly Operations	2,974	71.7
Total	4,148	100.0

Table .3.1

The consumer will receive an increase in rates of only 0.4¢ per 5¢ kw-hr. This translates to $4.37 per month per family in America.

8.4 CONCLUSIONS

The cost of nuclear waste disposal into space is not prohibitive. The cost to remove 1 kg permanently is $20,074 which is in the realm of ground disposal ($9427/lb).

8.5 REFERENCES

1. Space Planner Guide, USAF, Air Force System Commands, July 1965, pp. VII 1 - VII 27.
2. Project OASIS, The University of Michigan 1978 Senior Aerospace Design Project.
3. Edison Electric Institute, "Statistical Year Book of the Utility Industry," for 1975 published Oct '76 No. 43, No. 76-51.
4. Environment; Volume 17, No. 5, July-Aug '75, "Expensive Enrichment," Marvin Resnikoff.
5. Astronautics and Aeronautics, March 1978, "The Low (Profile) to Space Manufacturing" Gerard O'Neill.
6. Space Transportation System User Handbook NASA June 1977.
7. Steven Rasch, Bechtel Corporation, personal communication.

APPENDIX A
NUCLEAR

A.1 MAGNETIC SUSCEPTIBILITIES

Element	10^{-6} cgs	Element	10^{-6} cgs
Hydrogen (H)	-22	Bismuth (Bi)	-83.0
Lithium (Li)	14.2	Polomium (Po)	----
Iron (Fe)	7200.0	Astatine (At)	----
Carbon (C)	-6.0	Radon (Ra)	----
Cobalt (Co)	4900.0	Francina (Fr)	----
Nickel (Ni)	660.0	Radium (Ra)	----
Copper (Cu)	267.3	Actinium (Ac)	----
Zinc (Zn)	-46.0	Thorium (Th)	-16.0
Gallium (Ga)	-34.0	Protactinium (Pa)	----
Germanium (Ge)	-28.8	Uranium (U)	2360.0
Arsenic (As)	-5.5	Neptunium (Np)	----
Selenium (Se)	-27.2	Plutonium (Pu)	730.0
Bromine (Br)	-56.4	Americium (Am)	-48.1
Krypton (Kr)	-28.8	Curium (Cm)	----
Rhenium (Re)	50.2	Berkelium (Bk)	----
Strontium (Sr)	-106.0	Californium (Cf)	----
Vttrium (Y)	44.4	Einsteinium (Es)	----
Zitconium (Zs)	-13.8	Idium (In)	-47.0
Niobium (Nb)	-10.0		
Molybdenum (Mo)	41.0		
Technetium (Tc)	244.0		
Ruthenium (Ru)	162.0		
Rhodium (Rh)	104.0		
Palladium (Pd)	567.4		
Silver (Ag)	-24.0		
Cadium (Cd)	-159.0		
Tin (Sn)	-41.0		
Antimony (Sb)	-69.4		
Tellurium (Te)	-39.5		
Iodine (I)	-79.4		
Xenon (Xe)	-42.9		
Cesium (Cs)	1534.0		
Basium (Ba)	-29.1		
Lanthanum (La)	-78.0		
Cerium (Ce)	26.0		
Psaseodymium (Ps)	8994.0		
Helium (He)	-1.88		
Thallium (Tl)	-32.0		
Lead (Pb)	-42.0		

A.2 NUCLEAR WASTE MASS

Total Mass BPW
1.83299×10^5 g

Mass of Removed Elements BRW

U = 1.765×10^5 g
Pu = 1.482×10^3 g
Br = 3.311 g
Kr = 5.429 g
Zr = 5.528×10^2 g
Nb = 1.051×10^{-3} g
Mo = 5.084×10^2 g
I = 3.594×10^1 g
Xe = 8.017×10^2 g
Total = 1.798895811×10^5 g

Percent of weight removed

98.14%

Total Mass BPW
4.6141×10^5 g

Mass of Removed Elements BRW

U = 4.412×10^5 g
Pu = 4.016×10^3 g
Br = 9.984 g
Kr = 1.650×10^2 g
Zr = 1.672×10^3 g
Nb = 3.096×10^{-3} g
Mo = 1.535×10^3 g
I = 1.083×10^2 g
Xe = 2.446×10^3 g
Total = 4.511522871 g

Percent of weight removed

97.77%

Total Weight Reduction

97.88%

APPENDIX B
ORBITAL MECHANICS

ΔV requirements for solar system escape for perpendicular launch.

B.1 TEXT AND RESULTS

The following program computes the ΔV_{md} to be provided by the mass driver to escape from the solar system.

The mass driver is placed in a circular parking orbit around the earth at an altitude h; the parking orbit plane coincides with the ecliptic plane. The local circular speed in the parking orbit is found from

$$V_{\ell c} = V_c \sqrt{\frac{R_o}{R_o + h}} \quad , \tag{1}$$

where V_c is the characteristic speed of the earth, R_o its radius.

At an arbitrary point P in the parking orbit the mass driver imparts a ΔV_{md} to the payload. The ΔV_{md} is perpendicular to the orbital plane and since the payload at least must escape the earth's gravity $\Delta V_{md} > V_{\ell c}$. After this velocity change the payload is in an escape trajectory plane which makes an angle ϕ with the parking orbit plane (Figure 1(a))

$$\phi = \arctan \left(\frac{\Delta V_{md}}{V_{\ell c}} \right) \quad . \tag{2}$$

The hinge line between these two planes is the line $\overline{OP}$, where O is the center of the earth.

In the escape trajectory plane the payload is initially at the perigee (point P) of the hyperbolic escape trajectory. The perigee velocity, V_p, is

$$V_p = \sqrt{(\Delta V_{md})^2 + (V_{\ell c})^2} \quad , \tag{3}$$

and the residual velocity the payload has when having escaped the earth's field is found from the energy equation* to be (Figure 1(b))

$$V_\infty = \sqrt{V_p^2 - 2(V_{\ell c})^2} \tag{4}$$

At that time the payload is at a true anomaly θ_∞ given by

---

* $\frac{V_\infty^2}{2} = \frac{V_p^2}{2} - \frac{\mu_e}{R_o + h} = \frac{V_p^2}{2} - (V_{\ell c})^2$

$$\theta_\infty = \arccos\left(-\frac{1}{e}\right), \tag{5}$$

where e is the eccentricity of the escape hyperbola. The eccentricity can be expressed in terms of V_p and h via the energy, E, and angular momentum, H

$$e = \sqrt{\frac{2EH^2}{\mu_e^2} + 1}, \tag{6}$$

where

$$E = \frac{V_\infty^2}{2}, \quad H = V_p(R_o + h) \tag{7}$$

The following transformations serve to find the components of $\vec{V}_\infty$ in the ecliptic plane coordinate system, where x is along V_s, the orbital speed of the earth around the sun, y is in the ecliptic plane radially outward from the sun, and z completes the right-handed axis system. All axis systems have their origin at 0.

Consider first the x_1, y_1, z_1 system. x_1 i along the extension of the line $\overline{PO}$, y, is parallel to $\vec{V}_p$ (Figure 1(b), (c))

$$V_{x_1} = V_\infty \cos(\pi - \theta_\infty), \tag{8}$$

$$V_{y_1} = V_\infty \sin(\pi - \theta_\infty), \tag{9}$$

$$V_{z_1} = 0; \tag{10}$$

Next consider the x_2, y_2, z_2 system obtained from the previous system by rotation through the angle ϕ about the x_1 axis (Figure 1(d))

$$V_{x_2} = V_{x_1}, \tag{11}$$

$$V_{y_2} = V_{y_1} \cos\phi, \tag{12}$$

$$V_{z_2} = V_{y_1} \sin\phi. \tag{13}$$

The $x_2 - y_2$ plane already is the ecliptic plane and to move the x_2, y_2, z_2 system to coincide with the final x, y, z system it must be rotated about the z_2 axis through the angle $(-\beta)$ according to the r. h. rule. Now the payload velocity relative to earth is (Figure 1 (e), see Figure 1(a) for definition of β)

$$V_x = V_{x_2} \cos\beta - V_{y_2} \sin\beta, \tag{14}$$

$$V_y = V_{x_2} \sin\beta + V_{y_2} \cos\beta \ , \tag{15}$$

$$V_z = V_{z_2} \ . \tag{16}$$

The magnitude of the payload velocity relative to the sun is

$$V_T = \sqrt{(V_x + V_s)^2 + (V_y)^2 + (V_z)^2} \tag{17}$$

and this is to be compared to $V_{esc_s} = \sqrt{2}\ V_s$, (18)

the escape speed from the solar system.

The excess speed V_{ex},

$$V_{ex} = V_T - V_{esc_s} \tag{19}$$

is computed. If it is negative, the mass driver ΔV_{md} is increased by .1 km/sec and the process is repeated, for each value of β.

Once lowest ΔV_{md} (to the nearest .1 km/s) is determined to give a positive V_{ex}, the program calculated the inclination of the escape plane to the ecliptic plane

$$i_s = \arctan\left(\frac{-V_z}{V_x}\right), \tag{20}$$

and the initial flight path angle relative to the sun

$$\gamma_s = \arctan\left(\frac{V_y}{\sqrt{V_x^2 + V_z^2}}\right) \tag{21}$$

The program finally prints out β, ΔV_{md}, V_{es}, i_s and γ_s.

Results

1) Figure 2 gives ΔV_{md} vs β

2) The minimum inclination is $28^o = i_{s_{min}}$

3) The minimum flight path angle is $-10.1^o = \gamma_{s_{min}}$

APPENDIX C

C.1 MASS DRIVER

The following mass driver parameters are based on the equations developed for the optimized Mass Driver Reaction Engine (MDRE) from the 1977 NASA Ames summer study on space colonization.

The caliber or "bore", D, is computed from the equation

$$D = \left(\frac{m_l}{6.538 \times 10^{-2} \rho_p} \right)^{\frac{1}{3}}$$

where m_l is the payload mass in kg and ρ_p is the payload density in kg/m^3

With m_l = 1 kg and $\rho_p = 4 \times 10^3$ kg/m^3 D was found to equal .156 meters

Payload Geometry

payload length = .925D = .144 meters
payload diameter = .3D = .047 meters
payload volume = 2.5×10^{-4} m^3

Drive Coil Geometry

ℓm = inductance length = drive coil spacing = .185D = .0289 meters
ℓp = phase length of drive coil oscillation = $4\ell m$ = .1156 meters bucket coil spacing = $6\ell m$ = .1734 meters

Bucket Coil Weight and Geometry

W_B = bucket coil width = .1D = .0156 meters
r = effective radius of bucket coil = .26D = .0407 meters
V_{BC} = volume of individual bucket coil

$$= \pi W_B \left[\left(r + \frac{W_B}{2} \right)^2 - \left(r - \frac{W_B}{2} \right)^2 \right] = 6.2 \times 10^{-5} \ m^3$$

ρ_s = density of bucket coil = 4.53×10^3 kg/m^3 (niobium tin)
m_{Bc} = mass of bucket coil = $V_{Bc}\rho_s$ = .281 kg
m_{super} = total coil mass per bucket = $2\ m_{Bc}$ = .562 kg
m_B = empty bucket mass = $2\ m_{super}$ = 1.123 kg
m_{BL} = loaded bucket mass = $m_B + m_l$ = 2.123 kg

ratio of unloaded to loaded bucket mass = $\frac{m_B}{m_{BL}}$ = .529

i_B = current in each bucket coil = $2.5 \times 10^6 D^2 = 6.084 \times 10^4$ ampere

Mass Driver Geometry

S_a = acceleration length = $V^2/2a = 4.133 \times 10^3$ meters

S_d = deceleration length = $\left(\frac{m_B}{m_{BL}}\right) V^2/2a = 2.186 \times 10^3$ meters

total length = $S_a + S_d = 6.319 \times 10^3$ meters

C.2 PAYLOAD TRAJECTORY

After the payload has been released from the bucket the magnetic guide forces will no longer be acting on it. It will be in free fall inside a moving container and an analysis was done to determine the trajectory.

Call the mass driver acceleration length "a" and the deceleration length "b". The rotation rate is ω and time of flight t.

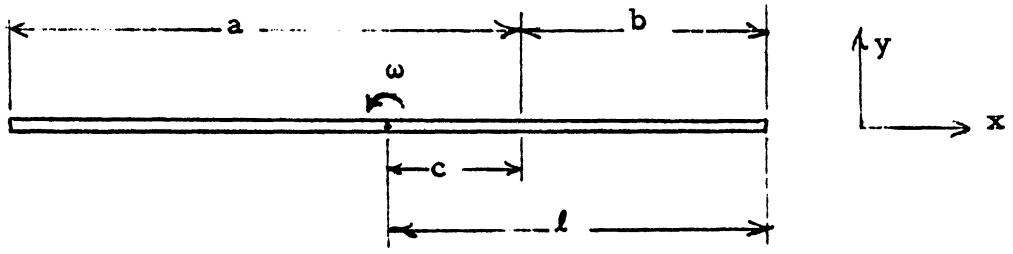

In a time t the end of the mass driver will have moved a distance $\ell\omega t$

where $\ell = \frac{a + b}{2}$

The payload will shift in the same time a distance b sin θ where θ is the angle of the velocity vector with respect to the structure orientation at t = 0

$$\tan \theta = \frac{V_y}{V_x}$$

$$V_x = \Delta V$$

$$V_y = \omega c$$

where $c = \frac{a - b}{2}$

or $\theta = \tan^{-1} \frac{\omega c}{\Delta V}$

in addition to this the payload will fall a distance $1/2\ g\ t^2$ under the influence of gravity

$$d_1 = \ell\omega t$$
$$d_2 = b \sin \theta + \frac{1}{2}\ g t^2$$

The difference between these distances is the amount of clearance required in the tubes.

For $a = 4.2$ km $b = 2.1$ km

$\omega = 1/92.5$ min x 1 min/60 sec x 2π rad $= 1.13 \times 10^{-3}$ rad/sec

$t = .24$ sec

$g = 867$ cm/sec^2

gives $\ell = 3.15$ km $\quad c = 1.05$ km $\quad \theta = 1.3 \times 10^{-4}$ rad

$$d_1 - d_2 = 85.43 - 52.65 = 32.77 \text{ cm}$$

This distance is clearly much larger than the launch tube, therefore some means must be found to assure adequate clearance.

Probably the best solution is the method used in the design of Mass Driver Reaction Engines (MDRE). Here, the payload is released from the launch tube at the same time as release from the bucket; the bucket is snapped away from the payload magnetically and decelerated in a separate, but parallel tube.

APPENDIX D
STRUCTURES

D.1 MASS DRIVER TUBES

From Reference 4, the maximum tension in the subsonic range is ~ 800 N.

Thus, the axial stress, σ, will be given by (assuming that the tubes may be modeled as thin-walled pressure vessels):

$$\sigma = \frac{F_t}{2\pi r t} \qquad (5.1.1)$$

where

F_t = maximum tensile force (= 800N)
r = 1/2 the bore of the mass driver's drive coils
t = tube thickness (meters)

We wish to hold $\sigma \leq \sigma_{ys}$, where σ_{ys} is the yield stress of the tube material (Al 7075-T6). For Al 7075-T6, $\sigma_{ys} = 4.4814 \times 10^8$ N/m^2. Therefore, from (5.1.1),

$$t = \frac{F_t}{2\pi r (\sigma_{ys})} = 3.6425 \times 10^{-6} \text{ m } (.0001434")$$

The maximum compression in the mass driver tubes is 500 N. In this compressive state, we may model the tubing section between adjacent drive coils as a thin-walled shell.

We wish to prevent buckling of this shell.

From Reference 5, the buckling stress of such a shell depends upon the magnitudes of the terms:

A) $(\frac{\pi a}{\ell})^2$ and B) $\frac{2a}{t}\sqrt{3(1-\nu^2)}$

If A) and greater than B), we may use the "Euler-strip" formula. If vice versa, we may use Donnell's empirical relation:

"Euler-strip" formula: $\sigma_{cr} = \frac{\pi^2 E t^2}{12(1-\nu^2)\ell^2}$

Donnell's relation: $\sigma_{cr} = E \frac{.6(t/a) - 10^{-7}(a/t)}{1 + .004(E/\sigma_{ys})}$

where

σ_{cr} = critical buckling stress (of shell)
t = tube thickness
ν = Poisson's ratio

ℓ = shell length (distance between drive coils)
E = Young's modulus
σ_{ys} = yield strength
a = 1/2 bore of mass driver coils (radius of shell).

We have,

a = .078 meters
ℓ = .02892 meters

as determined from an optimization relation included in the Mass Driver report.

$$\therefore \left(\frac{\pi a}{\ell}\right)^2 = 71.8$$

Thus, to use Donnell's relation, we require that

$$\frac{2a}{t}\sqrt{3(1-\nu^2)} \geq 71.8$$

which implies that $t \leq .35$ cm.

For handling and construction purposes, it is desirable to have t somewhat larger than .35 cm.

To yield a conservative design (and also to account for the effects of the accelerating payload), t = 5.0 cm will be used.

Thus, we use the "Euler-strip" formula:

$$\sigma_{cr} = \frac{\pi^2 E t^2}{12(1-\nu^2)\ell^2}$$

(Note: for longer cylinders, σ_{cr} is independent of ℓ)

where

E $\cong$ 10,000 psi (= 6.8944×10^{10} N/m^2)
t = .05 m
ν = .33
ℓ = .02892 m

We obtain

$$\sigma_{cr} = 1.9021 \times 10^{11} \text{ N/m}^2.$$

The actual compressive stress experienced in the subsonic range is:

$$\sigma_c = \frac{500 \text{ N}}{\pi[(a+t)^2 - a^2]} = \frac{500 \text{ N}}{\pi[(.128)^2 - (.078)^2]\text{m}^2} = 1.55 \times 10^4 \text{ N/m}^2.$$

The actual tensile stress experienced in the subsonic range is:

$$\sigma_t = \frac{800\ N}{\pi[(a+t)^2 - a^2]} = 2.472 \times 10^4\ N/m^2.$$

Thus

$$\frac{\sigma_{cr}}{\sigma c} = 1.23 \times 10^7$$

and

$$\frac{\sigma_{cr}}{\sigma t} = 7.695 \times 10^6$$

and

$$\frac{\sigma_{ys}}{\sigma t} = 1.813 \times 10^4$$

and

$$\frac{\sigma_{ys}}{\sigma c} = 2.89 \times 10^4$$

Thus, we see that both plastic yielding and buckling are avoided within very considerable safety margins for t = .05 m.

This thickness yields a tube mass (4 tubes), m, equal to:

$$m = 4\ \rho\pi\ [(a+t)^2]\ \ell \qquad (5.1.2)$$

where

ρ = density of Al 7075-T6 (= 2800 kg/m^3)
ℓ = length of mass driver (= 6320 m)

Therefore, the total tube mass (from (5.1.2)) is:

$$m = 2.29 \times 10^6\ kg$$
$$= 5.04 \times 10^6\ lbm.$$

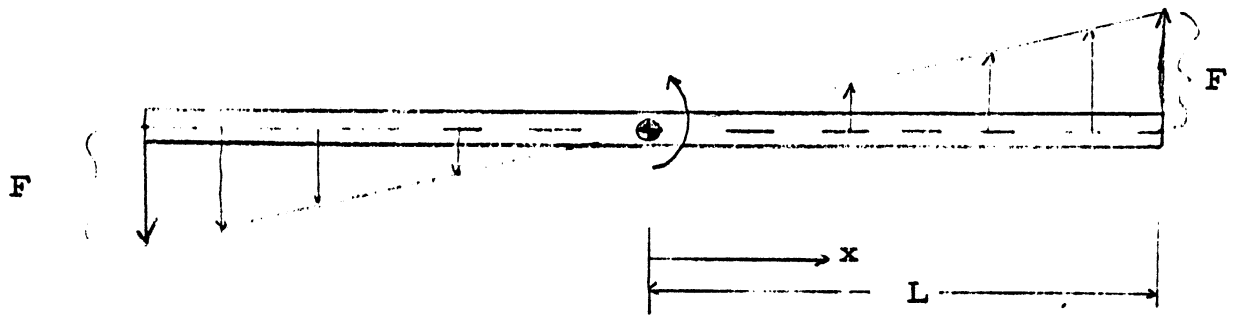

Figure D.1 Thrust Distribution on Mass Driver

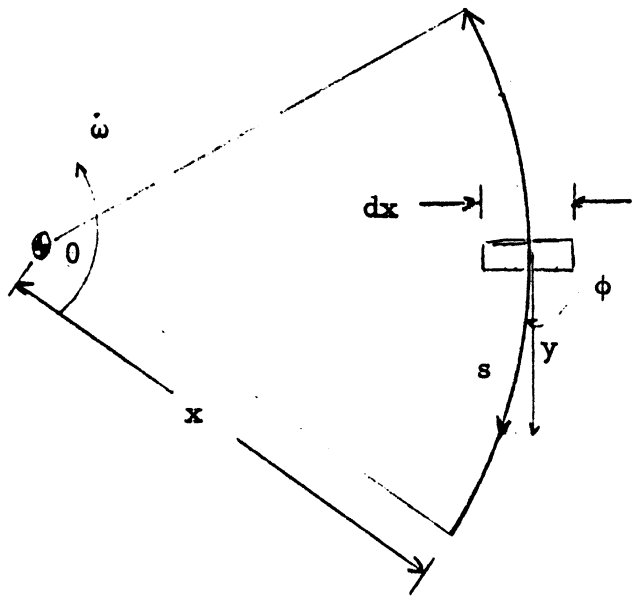

Figure D.2 Geometry of Rotating Mass Driver

D.2 VERIFICTION OF ZERO MOMENT AND SHEAR FORCE DISTRIBUTIONS IN THE MASS DRIVER DUE TO ATTITUDE CONTROL THRUSTING

A linear distribution of thrust per unit length is used for attitude control thrusting as shown in Figure 5.2.1. It is assumed, for this analysis, that this distribution is perfectly continuous.

From Figure 5.2.1,

$$dT = \left(\frac{F}{L}\right) x\, dx \quad ; \quad \left(\frac{F}{L}\right) \text{ is the slope of the thrust distribution.}$$

$$\therefore T = \frac{1}{2} \frac{F}{L} x^2$$

where

T = thrust, F = thrust per unit length at x = L.

Therefore, thrust per unit length is proportional to x. That is, the thrust distribution is linear in x.

The resultant thrust acting over one-half of the mass driver is given by

$$T = \int_0^L dT = \frac{1}{2} FL.$$

Alternate derivation of resultant thrust:

$$T \equiv \int\int dy\, dx = \int_0^L \int_0^{(F/L)x} dy\, dx = \frac{F}{L} \int_0^L x\, dx = \frac{1}{2} FL.$$

Now, consider the inertial loading on an infinitesimal element of the mass driver, as shown in Figure 5.2.2.

We see that, for small ϕ, $y/s = \cos\phi \cong 1$.

Thus,
$$y \cong s = x\,\theta$$
$$\therefore\ y \cong x\,\theta$$

The D'Alembert inertial force (F_D) on the element is given by

$$d(F_D) \cong mij\, dx \text{ , where } m \equiv \frac{\text{mass}}{\text{unit length}}$$

But,

$$y \cong x\,\theta$$

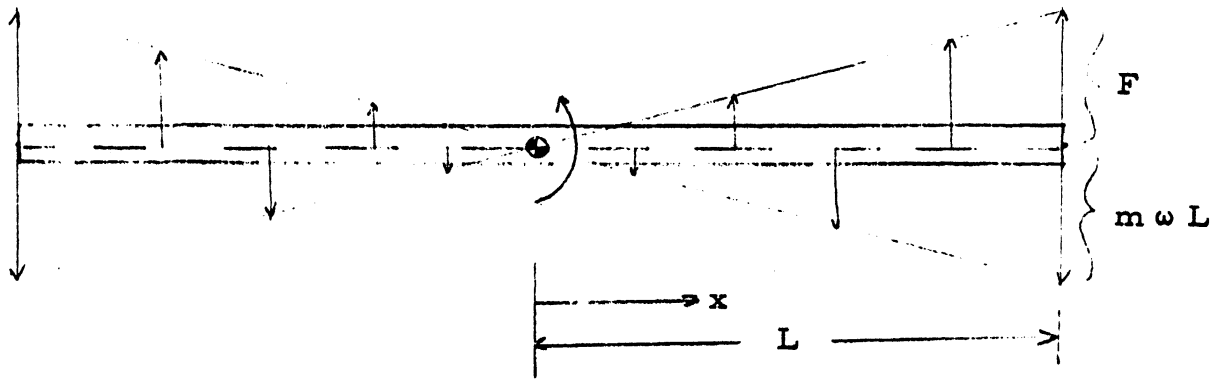

Figure D.3 Loading on Mass Driver Due to Attitude Control Maneuvers

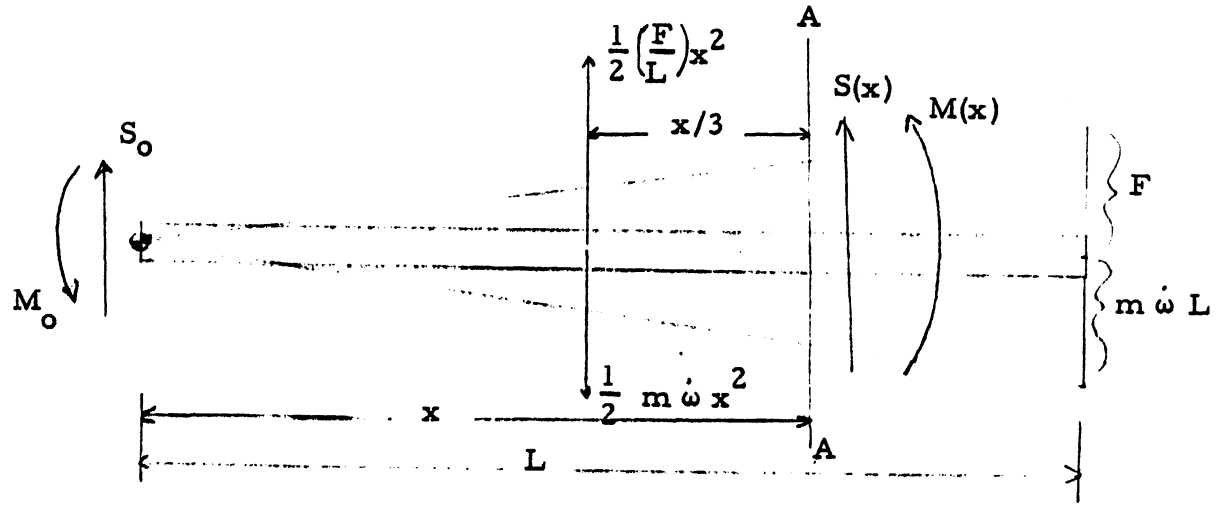

Figure D.4 Equivalent Loading on One-Half of the Mass Driver

Thus,

$$\ddot{y} \cong x\,\ddot{\theta} = x\,\dot{\omega}$$

Therefore, $d(F_D) \cong m\,\dot{\omega}\,x\,dx$, for small ϕ

where,

$\omega \equiv$ angular velocity
$(\dot{})\equiv$ time derivative
$(\ddot{})\equiv$ second time derivative.

Thus, the resultant inertial force on the mass driver is given by

$$F_D = \int d(F_D) = \int m\,\dot{\omega}\,x\,dx = \frac{1}{2} m\,\dot{\omega}\,x^2.$$

Therefore, the D'Alembert reaction per unit length is proportional to x (linear with respect to x).

The total reaction over one-half the mass driver's length is

$$F_D = \int_0^L d(F_D) = \int_0^L m\,\dot{\omega}\,x\,dx = \frac{1}{2} m\,\dot{\omega}\,L^2.$$

Thus, attitude control firing exposes the mass driver to the loading shown in Figure 5.2.3.

This loading is equivalent to that shown in Figure 5.2.4 over one-half the mass driver's length, where:

$$M_o = \frac{1}{3}\,(m\,\dot{\omega}\,L^3 - F\,L^2)$$

and

$$X_o = \frac{1}{2}\,(m\,\dot{\omega}\,L^2 - F\,L)$$

From equilibriu, we have (at section A-A)

$$M(x) = \frac{1}{6}\,(\frac{F}{L} - m\,\dot{\omega})x^3 + \frac{1}{2}\,(m\,\dot{\omega}\,L^2 - F\,L)\,x + \frac{1}{3}(F\,L^2 - m\,\dot{\omega}\,L^3) \qquad (5.2.1)$$

and

$$S(x) = \frac{1}{2}(m\,\dot{\omega} - \frac{F}{L})x^2 + \frac{1}{2}\,(F\,L - m\,\dot{\omega}\,L^2) \qquad (5.2.2)$$

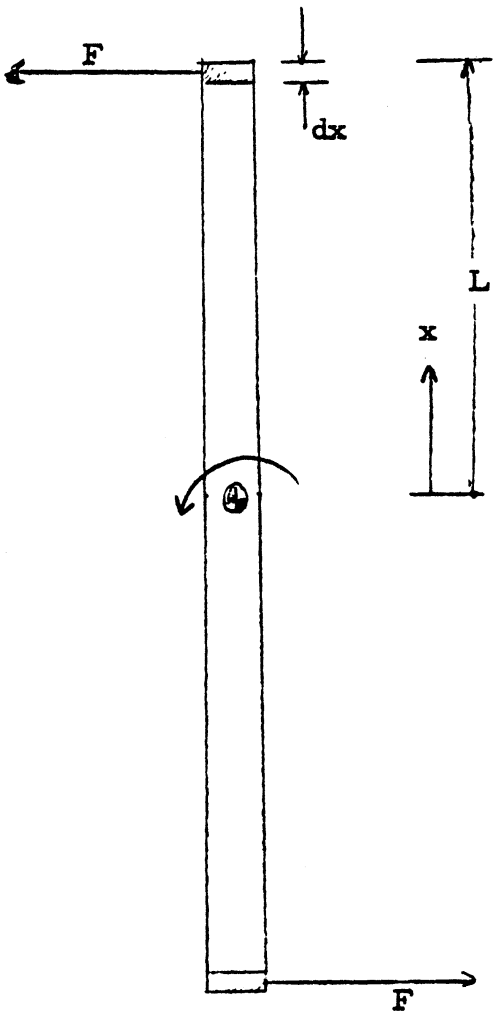

Figure D.4 Rotation of Mass Driver

where

m(x), S(x) are the moment and shear respectively.

From Figure 5.2.4, we see that the applied tangential force (due to thrusting), f, on the element located at $x = \pm L$ is given by

$$f = F\,dx = (m\,dx)\,a_T,$$

where a_T = tangential acceleration.

But, $a_T = \dot{\omega} L$

$$\therefore \quad F\,dx = (m\,dx)\,\dot{\omega} L$$

$$\therefore \quad \underline{F = m \dot{\omega} L} \qquad (5.2.3)$$

From Eq. 5.2.3 it is seen that the coefficients of Eqs. 5,2,1, 5.2.2 vanish identically.

Thus, there are no stresses in the mass driver due to attitude control firing.

D.3 FLEXURAL VIBRATIONAL MODES AND FREQUENCIES OF THE MASS DRIVER STRUCTURE

Since the attitude control thrusters are very closely spaced (10.08 meters) and all fire simultaneously, the mass driver will experience a global force. That is, the mass driver will be induced to vibrate flexurally on a global scale. Thus, it may be modeled as a free beam of small stiffness.

The following assumptions are made in this analysis:

1) The entire mass driver can be modeled as a continuous beam (i.e., no concentrated masses)
2) No nuclear waste (or other) payload is launched during attitude control maneuvers.

The governing differential equation for the motion of the mass driver is (from Reference 7)

$$EI \frac{\partial^4 \omega}{\partial x^4} + m \frac{\partial^2 \omega}{\partial t^2} = 0 \qquad (5.3.1)$$

where

E = Young's modulus
I = moment of inertia of cross section
m = mass/length of mass driver
ω = transverse (flexural) displacement
x = distance from end of mass driver
t = time

To solve this partial differential equation, the technique of "Separation of Variables" is employed.

$\therefore \omega(x, t) = W(x)\, T(t)$, from which are obtained the following equations.

$$\ddot{T} + \omega^2 T = 0 \tag{5.3.2}$$

$$EIW'''' - m\omega^2 W = 0 \tag{5.3.3}$$

where

ω = "natural" vibrational frequencies
$(\dot{})$ = second time derivation
$()''''$ = 4th x-derivative

The solution of Eq. 5.3.3 yields the fundamental and harmonic mode shapes.

Eq. 5.3.3 can be written as:

$$W'''' - \lambda^4 W = 0 \tag{5.3.4}$$

where

$$\lambda^4 = \frac{m\omega^2}{EI} \tag{5.3.4a}$$

The solution to this equation is

$$W(x) = C \sinh \lambda x + D \cosh \lambda x + E \sin \lambda x + F \cos \lambda x \tag{5.3.5}$$

Upon substitution of the boundary conditions into Eq. 5.3.5, and the expansion of the determinant of the coefficients of the resulting set of simultaneous equations, we obtain

$$f(\lambda \ell) = \cos \lambda \ell - \frac{1}{\cosh \lambda \ell} \tag{5.3.6}$$

where

ℓ = mass driver's length

from which the values of $\lambda \ell$ (roots of $[f(\lambda \ell) = 0]$ are obtained).

A plot of $f(\lambda \ell) = 0$ is shown in Figure 5.3.1, from which it is observed that the roots are

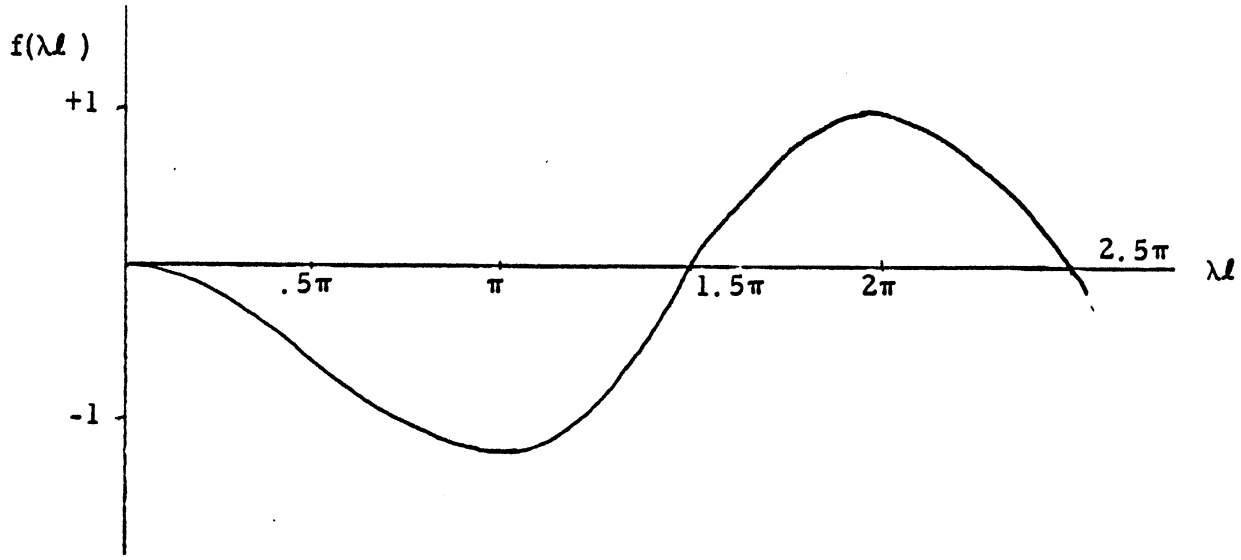

Figure D.3.1 f(λℓ) vs. λℓ

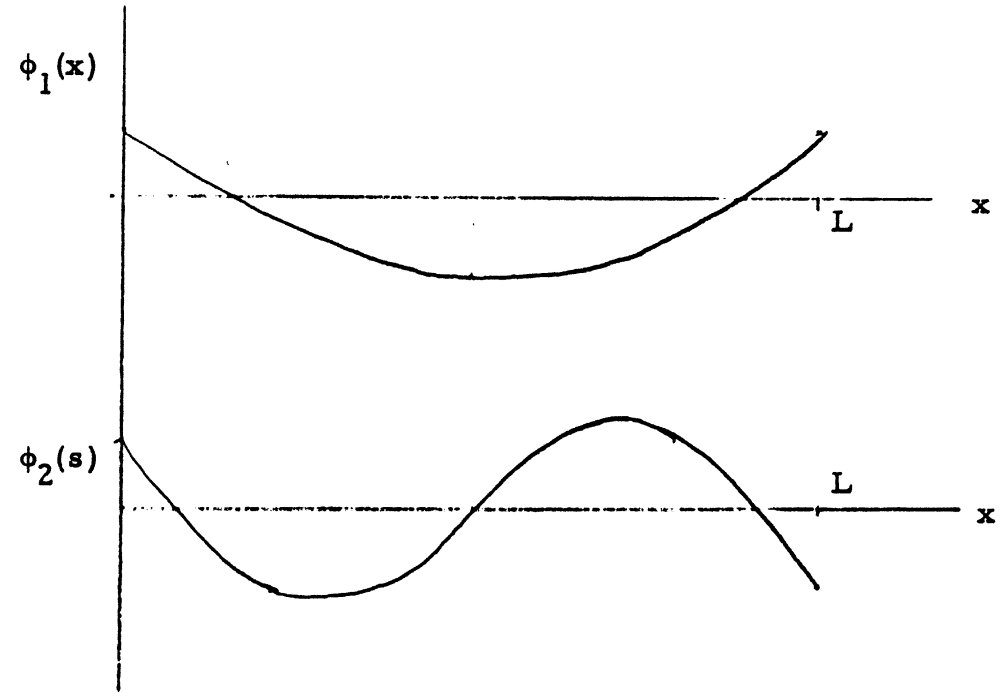

Figure D.3.2 First and Second Vibrational Modes

$$\lambda\ell = 0,\ 1.5\pi,\ 2.5\pi,\ \ldots\ .$$

The first root ($\lambda\ell = 0$) corresponds to $\omega = 0$ (rigid body translation and rotation) and is not of interest here.

Thus, the fundamental vibrational frequency is given by $\lambda\ell = 1.5\pi$

$$\therefore\ \lambda^4 = (1.5)^4 \left(\frac{\pi}{\ell}\right)^4 = \frac{m\omega^2}{EI} \qquad \text{from 5.3.4a}$$

$$\therefore\ \omega = (1.5)^2 \left(\frac{\pi}{\ell}\right)^2 \sqrt{\frac{EI}{m}}$$

Thus, the fundamental frequency is

$$\underline{\omega_1 = 22.2 \sqrt{\frac{EI}{m\ell^2}}} \ . \qquad (5.3.7)$$

The first harmonic is given by $\lambda\ell = 2.5\pi$

$$\therefore\ \lambda^4 = (2.5)^4 \left(\frac{\pi}{\ell}\right)^4 = \frac{m\omega^2}{EI}$$

$$\therefore\ \underline{\omega_2 = 61.69 \sqrt{\frac{EI}{m\ell^4}}} \qquad (5.3.8)$$

The mode shapes corresponding to these frequencies are given by

$$\phi_1(x) = \left[(-.205)\left(\sinh 1.5\frac{\pi x}{\ell} + \sin 1.5\frac{\pi x}{\ell}\right) + \cosh 1.5\frac{\pi x}{\ell} + \cos\frac{1.5\pi x}{\ell}\right]$$

and

$$\phi_2(x) = \left[-\left(\sinh\frac{2.5\pi x}{\ell} + \sin\frac{2.5\pi x}{\ell}\right) + \cosh\frac{2.5\pi x}{\ell} + \cos\frac{2.5\pi x}{\ell}\right]$$

Plots of $\phi_1(x)$, $\phi_2(s)$ appear in Figure 5.3.2.

In general, the ends of the mass driver will contain nuclear waste payloads while the attitude control thrusters are firing. Thus, the vibrational frequencies and modes must be recalculated in the case of concentrated masses at the ends.

The resulting equation for finding the values of $\lambda\ell$ (roots of $f(\lambda\ell)$ is

$$f(\lambda\ell) = (\lambda\ell)\sinh\lambda\ell\ \cos\lambda\ell\ \left[\frac{M_1+M_2}{m\ell}\right] - (\lambda\ell)\sin\lambda\ell\ \cosh\lambda\ell\ \left[\frac{M_1+M_2}{m\ell}\right]$$

$$-2(\lambda\ell)^2\sin\lambda\ell\ \sinh\lambda\ell\ \left[\frac{M_1M_2}{(m\ell)^2}\right] + \cos\lambda\ell\ \cosh\lambda\ell\ - 1 \qquad (5.3.9)$$

where M_1, M_2 are the masses of the payloads at the two ends of the mass driver respectively.

Note that Eq. 5.3.9 reduces to the continuous mass (Eq. 5.3.6) case when M_1, $M_2 = 0$.

Eq. 5.3.9 must be solved graphically with M_1, M_2 specified.

The crew living quarters located at $x = \ell/2$ represents another concentrated mass. An exact solution to this problem involves the expansion of an 8 x 8 determinant. It is therefore desirable to use an energy method to obtain an approximate solution in this case.

However, none of these concentrated masses will alter the fact that the bivrational frequencies are very small (large periods) due to the influence of ℓ^2 in the denominator of the frequency expressions.

Thus, attitude control thrusting frequencies and tension cable forcing frequencies will not cause the mass driver to resonate.

D.4 ANALYSIS OF OUTER RINGS (see Reference 3)

It is assumed that the outer rings may be modeled as four separate circular arcs, each built-in at the points where they are welded to the mass driver tubes, as shown in Figure 5.4.1.

From Reference 3, the slope of the arc at the point of the applied load is given by

$$\frac{dy}{d\theta} = \frac{Wr^3}{2EI}\left[\left(\frac{1-\sin\phi}{2\cos\phi} + \frac{T_A}{Wr}\tan\phi\right)\ \{\alpha\cos\alpha + \sin\alpha\}\right.$$
$$\left.-\left(\frac{1}{2} - \frac{T_A}{Wr}\right)\ \alpha\cos\phi\right] + \frac{Wr^3}{2CI}\left[\left(\frac{T_A}{Wr} - \frac{1}{2}\right)\ \alpha\cos\phi\right.$$
$$\left.+ 1 - \sin\phi - \left(\frac{1-\sin\phi}{2\cos\phi} + \frac{T_A}{Wr}\tan\phi\right)\ \{\sin\alpha - \alpha\cos\alpha\}\right] \qquad (5.4.$$

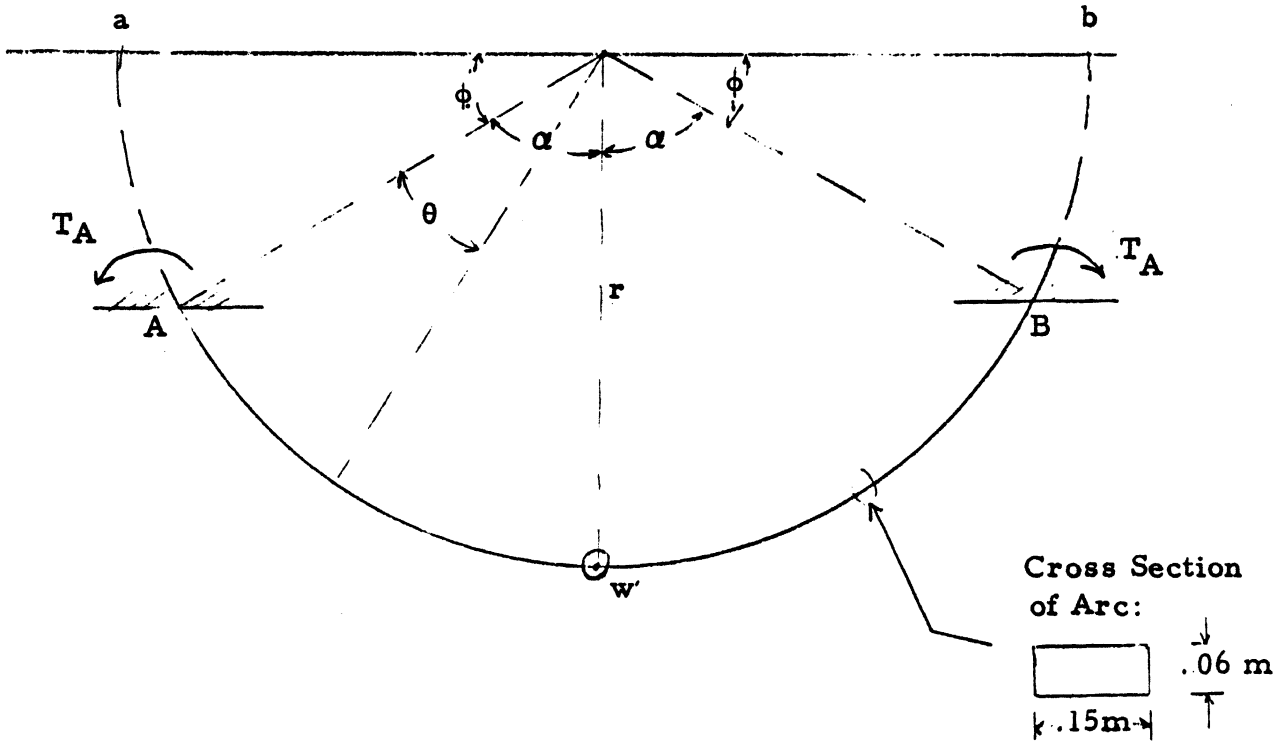

Figure D4.1 Representation of Circular Arc Section of Outer Ring

Eq. 5.4.1 accounts for the reaction forces at the supports.

Also,

W = applied force (related to cable tension)
y = deflection of arc
r = radius of arc
θ = coordinate location on arc
ϕ = (π - angle subtended)/2
α = (π - 2ϕ)/2
T_A = reaction moment at arc support
C = shear modulus of elasticity
J = polar moment of inertia of cross-section (rectangular)
E = Young's modulus
I = moment of inertia (2nd moment of area) or (rectangular) cross-section

In this case,

$$W = 2\ (1000\ \text{lbf})\left(\frac{4.448\ \text{N}}{1\ \text{lbf}}\right)\cos 45^\circ = \underline{6290.4\ \text{N}}$$

2 cables per attachment point; design limit for cable tension; angle between cables and mass driver

Also,

$r \cong .5308$ m
$\phi = 45^\circ = .785$ rad
$\alpha = 45^\circ = .785$ rad
$E = 10{,}400{,}000$ psi $= 7.171 \times 10^{10}$ N/m^2 (Al 7075-T6)
$C \equiv E/2(1+\nu)$ where ν = Poisson's ratio = .33 (Al 7075-T6)

$\therefore C = 3{,}910{,}000$ psi $= 2.696 \times 10^{10}$ N/m^2.

From symmetry, the reaction forces at A, B are given by

$$R_A = R_B = W/2 \tag{5.4.2}$$

The moment about A, B is given by

$$M_A = M_B = \frac{Wr}{2\cos\phi}(1 - \sin\phi) + T_A \tan\phi \tag{5.4.3}$$

From symmetry, $dy/d\theta$ (Eq. 5.4.1) must be zero. Therefore, for a given arc thickness, T_A can be found. Thus, M_A is known and the displacement at the point of applied load is given by

$$y = \frac{r^2}{2EI}\left[M_A\,\alpha\sin\alpha - (R_A r - T_A)(\sin\alpha - \alpha\cos\alpha)\right]$$

$$+\frac{r^2}{2CJ}\left[(T_A - R_A r)(\sin\alpha - \alpha\cos\alpha) + 2R_A r\,(\alpha - \sin\alpha)\right.$$

$$\left. + M_A\,(\alpha\sin\alpha + 2\cos\alpha - 2)\right] \qquad (5.4.4)$$

Now, a rectangular cross-section arc is used (Figure 5.4.1)

$$\therefore\ I\ (= Iy) = \frac{bt^3}{12}$$

where

b = width of cross-section
t = thickness of cross-section

and

$$J \equiv Iy + Iz = \frac{bt^3}{12} + \frac{tb^3}{12} = \frac{1}{12}\,(bt^3 + tb^3)$$

These values of I, J are substituted into Eq. 5.4.1 for b = .15 meters. This yields T_A as a function of t. From Eq. 5.4.3, we have M_A as a function of t.

Substitution into Eq. 5.4.4 yields y (displacement) as a function of t.

The following FORTRAN program computer this displacement for various values of t. It was decided to use t = .06 meters because this results in a very small displacement (y = .2025 millimeters) for cable tension of 1000 lbf (4448 N).

Also, it is desirable to use this value of t to provide a firm support to resist twisting induced by perturbations of the tension cable support rods.

The cross-sectional area of each ring is therefore

$$\pi\,(.5308\ \text{m} + .06\ \text{m})^2 - \pi\,(.5308\ \text{m})^2 = .2114\ \text{m}^2.$$

The mass of each ring is $(2800\ \text{kg/m}^3)(.2114\ \text{m}^2)(.15\ \text{m}) = 88.8\ \text{kg}$.

Now, there are 628 rings.

$\therefore$ total outer ring mass = 55,758.9 kg

$= 1.2267 \times 10^5$ lbm.

The inner cylinders (which contain the storage batteries, as indicated in Figure 5.1) are welded to the mass driver tubes and thus impart extra torsional rigidity to the mass driver.

The cylinders have an outer radius of .2748 meters, a thickness of .0025 meters, and a length of 1.272 meters.

Therefore, the solid cylinder volume is $\cong$

$$2\pi\,(.2748\text{ m})(.0025\text{ m})(1.272\text{ m}) = .0055\text{ m}^3.$$

The cylinders are constructed of 7075-T6 Aluminum (density $\cong$ 2800 kg/m^3).

$\therefore$ each cylinder has a mass of 15.37 kg.

There are 628 cylinders.

$\therefore$ the total cylinder mass = 9,655 kg

$$= 21{,}240.5\text{ lbm.}$$

D.5 MAXIMUM PITCH RATE ALLOWED FOR ATTITUDE CONTROL MANEUVERS

From Figure 5.2.4, the outward radial force which is "felt" by an element dx is given by

$$df = m\,\omega^2\,x\,dx \qquad (5.5.1)$$

This follows from the centripetal force relation

$$f = (\text{mass})\,\frac{(\text{velocity})^2}{(\text{radius})}$$

and

$$\text{velocity} = (\text{angular rate})\,(\text{radius})$$

Thus, the total outward radial force exerted by one-half of the mass driver is given by

$$f = \int_0^{\ell} m\,\omega^2\,x\,dx = \frac{1}{2}\,m\,\omega^2\,\ell^2 \qquad (5.5.2)$$

(m = mass/unit length,
ω = angular velocity,
ℓ = mass driver's length).

Therefore, the total tension, T, felt at the mass driver's midpoint is

$$T = 2f = m\omega^2 \ell^2 \qquad (5.5.3)$$

We wish to ensure that T does not exceed the limit of elastic proportionality (the mass driver does not undergo permanent deformation) with an imposed safety factor of 1.2.

Thus, $1.2T = \sigma_{ys} A$ (5.5.4)

where

σ_{ys} = yield strength
A = total solid cross-sectional area of mass driver tubes (assumed to withstand all tension).

From Section .1:

$$A = 4\pi [(a + t)^2 - a^2] = .1294 \text{ m}^2.$$

Also, $\sigma_{ys} = 4.4814 \times 10^8 \text{ N/m}^2$ (7075-T6 Al)

and $\ell = 6320$ m.

from Eq. 5.5.4,

$$1.2\, m\omega^2 \ell^2 = \sigma_{ys} A$$

$$\therefore \omega_{max} = \sqrt{\frac{\sigma_{ys} A}{1.2\, m \ell^2}}$$

$$\therefore \omega_{max} = 1.10/\sqrt{m} \quad , \quad [m] = \frac{kg}{meter} \; .$$

D.6 THERMAL EFFECTS

If the mass driver structure is not rotated about its longitudinal axis, thermal gradients will induce a bending moment which acts over the mass driver's length. To determine this moment it is necessary to obtain the temperature distribution over the mass driver's cross-section. Due to the rather complex geometry of the mass driver's cross-section (Figure 5.2), the problem of obtaining this temperature distribution becomes a very involved exercise in heat transfer. The problem is of such complexity that a meaningful analytical result is virtually impossible to obtain.

Even if an accurate model of this temperature distribution were available, it would need to be continually revised for each sunlit point in the mass driver's orbit because of the constantly changing angle between the mass driver's longitudinal axis and the incoming solar radiation.

In view of these difficulties, no quantitative result was obtained for this time dependent temperature distribution.

However, the equations which lead to the thermally induced bending moment are developed below. It is assumed that the tension cables described elsewhere (5. 6) in this report will counteract the bending moment (as well as the moment resulting from gravitational effects) and maintain the mass driver in a straight configuration. (It should be noted that the same thermal irregularities will incude bending moments in the tension cable support rods. This would have an adverse effect on the stability analysis used in the design of these rods. However, it is assumed that this effect is sufficiently small to justify its exclusion in design calculations.)

If the deflection components are w, v, we have

$$\left.\begin{aligned} \frac{d^2 w}{dx^2} &= -\frac{1}{E}\left(\frac{I_z M_{Ty} - I_{yz} M_{Tz}}{I_y I_z - I^2_{yz}}\right) \\ \frac{d^2 v}{dx^2} &= -\frac{1}{E}\left(\frac{I_y M_{Tz} - I_{yz} M_{Ty}}{(_y I_z - I^2_{yz}}\right) \end{aligned}\right\} \text{thermally induced curvatures}$$

Since the mass driver cross-section has an axis of symmetry (Figure 5.2), the product of inertia (I_{yz}) vanishes.

$$\therefore \quad \frac{d^2 w}{dx^2} = -\frac{M_{Ty}}{E I_y}$$

and

$$\frac{d^2 v}{dx^2} = -\frac{M_{Tz}}{E I_z}$$

where

$I_{y,z}$ = moments of inertia about the cross-sections bending axes

$M_{Ty,z}$ = thermally induced moments about the bending axes

E = Young's modulus

$$\therefore M_{Tz} = - EI_z \frac{d^2 v}{dx^2}$$

$$M_{Ty} = - EI_y \frac{d^2 w}{dx^2}$$

From Reference 10,

$$M_{Ty} = \int\int [\alpha (E T) z] \, dy \, dz$$

where

α = coefficient of thermal expansion
T (= T(y, z)) = temperature distribution over the cross-section
y, z = centroidal axes of the cross-section

and

$$M_{Tz} = \int\int [\alpha (T y)] \, dy \, dz.$$

To find M_{Ty}, M_{Tz} it is necessary to determined T(y, z).

Furthermore, αE Ty, αE Tz must be integrable functions if one is to obtain an analytical solution. Otherwise, one must resort to numerical methods.

Following this procedure, the bending moments M_{Ty} and M_{Tz} are known functions of x (longitudinal mass driver coordinate). These moments can be superimposed on the gravitational moment (see Apppendix Section 11) to give the total moment (which must be exerted by the tension cable-support rod assembly in the opposite direction) acting on the mass driver.

D.7 OPTIMIZATION OF PACKAGE SIZE

I. Small nuclear waste containers

Dimensions

r (= radius) = 2.34 cm (.921 in)
ℓ (= length) = 14.43 cm (5.68 in)
m (= loaded mass) = 1 kg (2.2 lbm)

Material

Stainless steel, ρ (= density) = 8.0 grms/cm^3.

A. To determine the thickness, t, of the container, it is assumed that the container may be modeled as a thin-walled pressure vessel.

From Figure 5.7.1, the sume of the forces in the vertical direction is given by

$$\xi F_v = -2\sigma_c t\ell + \int_0^{\pi} r P\ell \sin\theta \, d\theta = 0$$

where P is the interval pressure arising from the acceleration of the nuclear material during launch. It is assumed that the pressure is uniform and equal to that which occurs at the bottom of the container during launch. Thus, the design will be conservative, since this pressure actually decreases elsewhere in the container.

$$\therefore 2\sigma_c t\ell = \int_0^{\pi} r (Ma/\pi r^2) \ell \sin\theta \, d\theta$$

where

M = mass of waste in each container (= 1 kg)

and

a = space shuttle's maximum acceleration ($\tilde{=}$ 29.4 m/sec^2)

$$\therefore 2\sigma_c t\ell = \int_0^{\pi} \frac{Ma\ell}{\pi r} \sin\theta \, d\theta$$

$$= -\frac{Ma\ell}{\pi r} [\cos\theta]_0^{\pi}$$

$$= \frac{2Ma\ell}{\pi r}$$

$$\therefore \sigma_c t\ell = \frac{Ma\ell}{\pi r}$$

and

$$\sigma_c = \frac{Ma}{\pi r t}$$

From Reference 1, $\sigma_c = 2\sigma_\ell$ (see Figure 5.7.1)

$\therefore$ σ_c will be the largest stress in the container

$\therefore$ we wish to ensure that σ_c does not exceed the yield strength of stainless steel.

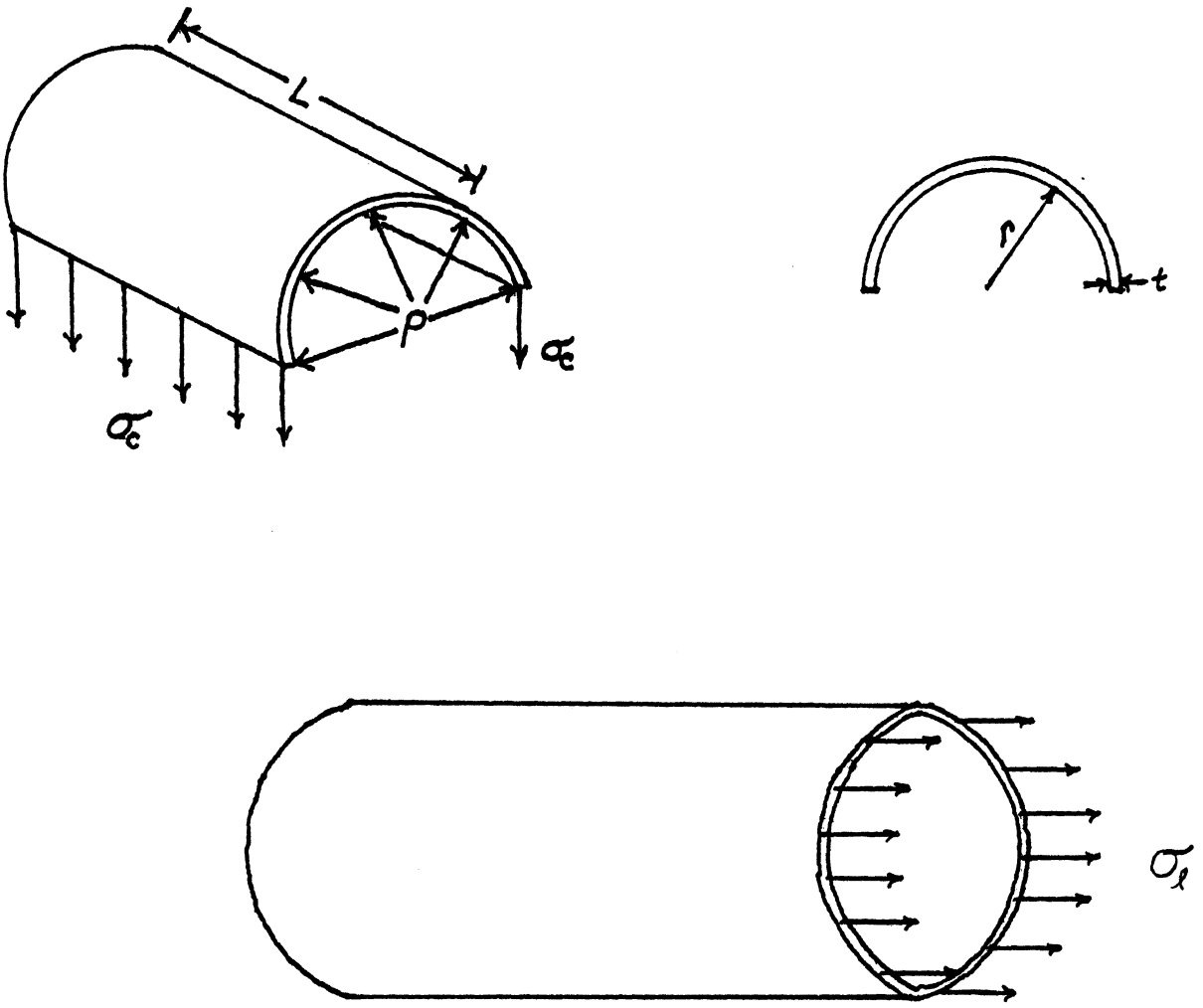

Figure D.7.1 Stresses on Small Cylindrical Container

For a safety factor of 1.2, we have

$$1.2\,\sigma_c = \sigma_{ys} \qquad (\sigma_{ys} = \text{yield strength of stainless steel} = 2.8957 \times 10^8\ N/m^2)$$

$$\therefore\ 1.2\,\frac{Ma}{\pi r t} = \sigma_{ys}$$

$$\therefore\ t = \frac{1.2\,Ma}{\pi r \sigma_{ys}}$$

$$\therefore\ t = 1.66 \times 10^{-6} \text{ meters.}$$

B. To find the mass of each container,

$$m = \rho\,\{(2\pi r^2 + 2\pi r \ell)t\}$$

$$= .327 \text{ grams} = 3.27 \times 10^{-4} \text{ kg}$$

(see Figure 5.5)

II. Numerical example of package size optimization for the large cannisters.

We know that the mass (loaded) of each small container is 1 kg. Now, we assume a ratio of package weight to the weight of the contents for the large cannister:

assume, $\dfrac{\omega_T \text{ package}}{\omega_T \text{ contents}} = 3.$

[Now, the total (cannister + waste) payload is conservatively restricted to weight 40,000 lbs (18181.818 kg)]

$\therefore$ total weight = ω_T pkg + ω_T contents = 4 (ω_T contents)

$\therefore\ \omega_T$ contents = 4545.45 kg

and each container weighs 1 kg, so there are 4545 containers.

A. Assuming 100% packing efficiency (n = 1),

$$4545 \text{ kg} = \rho V = (4 \text{ gms/cm}^3)(\pi R_I^2 L)$$

where

ρ = density of nuclear material
V = interior volume of cannister
R_I = inner radius of cannister)

$$= (4 \text{ gms/cm}^3)(\pi)(2 R_I^3), \text{ for } L = 2R$$

$$R_I = 56.55 \text{ cm (for } \omega_T \text{ package}/\omega_T \text{ contents} = 3).$$

B. Assuming 80% packing efficiency (n = .8),

$$(n)\,\pi\,(R_1)^2 = \pi\,(R_I)^2$$

$$\therefore\ R_1 = \left(\frac{1}{n}\right)^{1/2} R_I \qquad (5.7.1)$$

$$\therefore \text{ for } n = .8,\ R_1 = 63.225 \text{ cm}$$

where

R_1 = the new estimate of the cannister's inner radius.

Now, the containers are packaged in concentric rings, as shown in Figure 5.7.2. From the figure, $R_1 - r_c$ is the radial distance to the center of the outermost ring, and

$$\text{circumference} = 2\pi\,(R_1 - r_c)$$

and

$$\frac{\text{circumference}}{2r_c} = \text{number of containers in each ring.}$$

Thus, for n = .8,

$$\text{number containers in outer ring} = \frac{2\pi(63.275 \text{ cm} - 2.34 \text{ cm})}{2\,(2.34 \text{ cm})}$$

$$= 81.742 = 81 \text{ containers in the outer ring.}$$

number containers in the next innermost ring =

$$\frac{2\pi\,[63.225 \text{ cm} - 3(2.34 \text{ cm})]}{2\,(2.34 \text{ cm})}$$

$$= 75.459 = 75 \text{ containers.}$$

So, in general (for a given n);

$$\text{number containers per ring} = \frac{\pi\,(R_i - Ir_c)}{r_c} \quad \text{rounded down to an integer value} \qquad (5.7.2)$$

where

R_i = inner radius of cannister (a function of n); i = 1, 2, 3, . . .
r^c = radius of small container
I^c = (2N - 1), for the N^{th} ring, I = 3 for the 2^{nd} ring, etc.)

Now, for n = .8, ω_T package/ω_T contents = 3, we have (from Eq. 5.7.2);

I	No. containers
1	81
3	75
5	69
7	62
9	56
11	50
13	44
15	37
17	31
19	25
21	18
23	12
25	6
	= 566 containers per shelf

There are (ω_T package/ω_T contents = 3) 4545 containers and 566 containers per shelf. Therefore, we have 8.03 = 9 shelves requires.

Now, to determine whether or not n = .8 is realistic, we compare the total container height [= (No. of shelves) (height of each container)] with the total inner height of the large cannister:

$\therefore$ total container height = (9) (14.43 cm) = 129.87 cm
cannister height (L = 2R) = (2) (63.275 cm) = 126.45 cm.

We see that it is not possible to fit all the containers in the cannister for n = .8. Indeed, we cannot fit the shelves either (see Section 8 of Appendix).

C. So, we will now assume a decreased packing efficiency. Assume

$$n = .75 \left(\frac{\omega_T \text{ package}}{\omega_T \text{ contents}} = 3, \text{ again}\right)$$

from Eq. 5.7.1, R_2 = inner radius of cannister = 65.298 cm.

from Eq. 5.7.2,

I	No. containers
1	84
3	78
5	71
7	65
9	59
11	53
13	46
15	40
17	34
19	27
21	21
23	15
25	9
27	2

$\therefore$ there are 603 containers per shelf

$\therefore$ there are 8 shelves.

$\therefore$ total container height = (8 shelves) (14.43 cm/shelf) = 115.44 cm
cannister height = 2 (65.298 cm) = 130.596 cm.

This allows a clearance of 1.89 cm per shelf, which is insufficient (see Section 8 of the Appendix).

D. For the 5th iteration, we obtain (for n = .68, and (ω_T package/ω_T contents = 3);

from Eq. 5.7.1, R_5 = 68.58 cm

and from Eq. 5.7.2

I	No. containers
1	88
3	82
5	76
7	70
9	63
11	57
13	51
15	44
17	38
19	32
21	26
23	19
25	13
27	7

$\therefore$ there are 666 containers per shelf.

Again, there are (for ω_T package/ω_T contents = 3) 4545 containers

$\therefore$ there are $\frac{4545}{666} = 7$ shelves

and, total container height = (7 shelves) (14.43 cm/shelf) = 101.01 cm
cannister height = 2 (68.58 cm) = 137.16 cm

which gives 5.16 cm/shelf (which is sufficient).

E. Calculation of actual package weight for R = 68.58 cm.

1) Tungsten layer (5 cm thick)

$\underline{R\ (\equiv \text{radius})} \cong 68.58\ \text{cm} + 2.5\ \text{cm} = 71.08\ \text{cm}$

$\underline{\text{surface area}} \cong 2\pi RL + 2\pi R^2$ (but $L = 2R$)

$\cong 6\pi R^2$

$= 9.523 \times 10^4\ \text{cm}^2.$

$\underline{\text{mass}} = (\rho)(V) = (19.3\ \text{gms/cm}^3)(9.523 \times 10^4\ \text{cm}^2)(5\ \text{cm})$
$= 9.19 \times 10^6\ \text{gms}$

2) Lithium hydride layer (12 cm thick)

$R = (68.58 + 5 + 6)\ \text{cm} = 79.58\ \text{cm}$

$\text{mass} = (.775\ \text{gm/cm}^3)(6\pi)(79.58\ \text{cm})^2(12\ \text{cm}) = 1.110 \times 10^6\ \text{gms}.$

3) Stainless steel shell (.5 cm thick, from Section 9)

$R = 68.58 + 5 + 12 + .25 = 85.83\ \text{cm}$

$\text{mass} = (8.0\ \text{gms/cm}^3)\ (6\pi)(85.83\ \text{cm})^2(.5\ \text{cm}) = 5.554 \times 10^5\ \text{gms}.$

4) $\therefore$ total cannister (package) mass (excluding shelves)

$= 1.086 \times 10^7\ \text{gms} = 1.086 \times 10^4\ \text{kg}.$

Again, the mass of the contents is (4545 containers) (1 kg/container)
$= 4545\ \text{kg}$

$\therefore$ the ratio of package weight to contents weight is

$$\frac{1.086 \times 10^4}{4545} = 2.39.$$

F. Now, reiterate the entire process, using an estimated weight ratio of 2.39. This gives a smaller 'true' weight ratio, so continue the iterations using each preceding iteration's 'true' ratio, until:

G. ω_T package/ω_T contents = 1.88

$\therefore$ ω_T package + ω_T contents = 2.88 ω_T contents

$\therefore$ 2.88 ω_T contents = 18181.81 kg

$\therefore$ ω_T contents = 6313 kg.

Again, each container weighs 1 kg, so there are 6313 containers.

H. Assuming n = 1.0, the inside volume of the cannister is

$$V = 2\pi R^3 = \frac{\text{mass}}{\text{density}} = \frac{6.313 \times 10^6 \text{ gms}}{4.0 \text{ gms/cm}^3}$$

$\therefore$ R_I (first estimate of cannister's inner radius) = 63.15 cm.

I. For n = .65, R_I = 78.33 cm, and from Eq. 5.7.2,

I	No. containers
1	102
3	95
5	89
7	83
9	76
11	70
13	64
15	58
17	51
19	45
21	39
23	32
25	26
27	20
29	14
31	7
33	1

$\therefore$ there are 882 containers/shelf.

for this efficiency, there are 6174 containers in total.

$\therefore$ we have $\frac{6174}{882}$ = 7 shelves

and, total container height = (7 shelves)(14.43 cm/shelf) = 100.38 cm

cannister height = $2R_I$ = 156.66 cm.

This gives 8.04 cm/shelf.

J. Real package weight (for R = 78.33 cm)

1) Tungsten:

$$\text{mass} = (19.3 \text{ gms/cm}^3)(6\pi)(80.83 \text{ cm})^2(5 \text{ cm}) = 1.188 \times 10^7 \text{ gms.}$$

2) Lithium hydride:

$$\text{mass} = (.775 \text{ gms/cm}^3)(6\pi)(89.33 \text{ cm})^2(12 \text{ cm}) = 1.399 \times 10^6 \text{ gms.}$$

3) Stainless steel shell:

$$\text{mass} = (8.0 \text{ gms/cm}^3)(6\pi)(95.58 \text{ cm})^2(.5 \text{ cm}) = 6.888 \times 10^5 \text{ gms.}$$

4) $\therefore$ total package mass = 1.397×10^7 gms.

5) The shelves (see Section 8) have the following dimensions:

- R ($\equiv$ radius) = 78.33 cm
- mass resting on each shelf = 882 kg (882 containers)
- thickness (Section 8) = .507 cm
- mass of each shelf = 77.5 kg
- total mass of shelves = (7 shelves)(77.5 kg/shelf)
  $= 5.425 \times 10^5$ gms
  = 542.5 kg.

6) Total mass inside package $\tilde{=} \omega_T$ contents + ω_T shelves

$$= 6.174 \times 10^6 \text{ g} + 5.424 \times 10^5 \text{ g}$$

$$= 6.717 \times 10^6 \text{ gms}$$

Therefore, the weight ratio = 1.90, which is very close to the estimated value of 1.88. So, this is the optimum design.

D.8 ANALYSIS OF THE SHELVES IN THE NUCLEAR WASTE CANNISTER (see Reference 8)

The small payload containers will be resting on shelves in the large cannister.

We may assume that these shelves can be modeled as thin circular plates which are 'built-in' at their edges, as shown in Figure 5.8.1.

We also assume that the weight of the cans can be modeled as a uniformly distributed load, as shown in Figure 5.8.1.

Thus, the load per unit area (a function of radial distance for circularly symmetric plate and loading) is given by

$$q(r) \cong \frac{1}{\pi R^2} [M(\ddot{y}_{max})] = q_o, \text{ a constant} \qquad (5.8.1)$$

where

M = total mass on plate (mass of containers which are resting on it)
$\ddot{y}_{max}$ = maximum shuttle acceleration along its longitudinal axis (= 3g's, or 29.4 in/sec^2)

The governing differential equation for the transverse deflection of the plate is:

$$D \nabla^4 \omega(r) = q(r) \qquad (5.8.2)$$

where

D = flexural rigidity of the plate
$= Eh^3/12(1 - \nu^2)$ E = Young's modulus
h = plate thickness
ν = Poisson's ratio

$\nabla^4(\ )$ = biharmonic operator
$\omega(r)$ = plate deflection (a function of radial distance)
$q(r)$ = applied load/unit area.

For axisymmetric geometry and loading, and statically determinate plates, Eq. 5.8.2 reduces to (in polar coordinates)

$$D \frac{d}{dr} [\frac{1}{r} \frac{d}{dr} (r \frac{d\omega}{dr})] = - Q(r)$$

where

$$Q(r) = - \frac{1}{r} \int_0^r q(r)\, \xi\, d\xi$$

where

ξ = variable of integration.

The solution is

$$\omega(r) = - \frac{1}{D} I_3(r) + B r^2 + \cancel{c \ln r} + e \qquad (5.8.3)$$

(c must be zero due to the singularity at r = 0. This is the 'regularity condition').

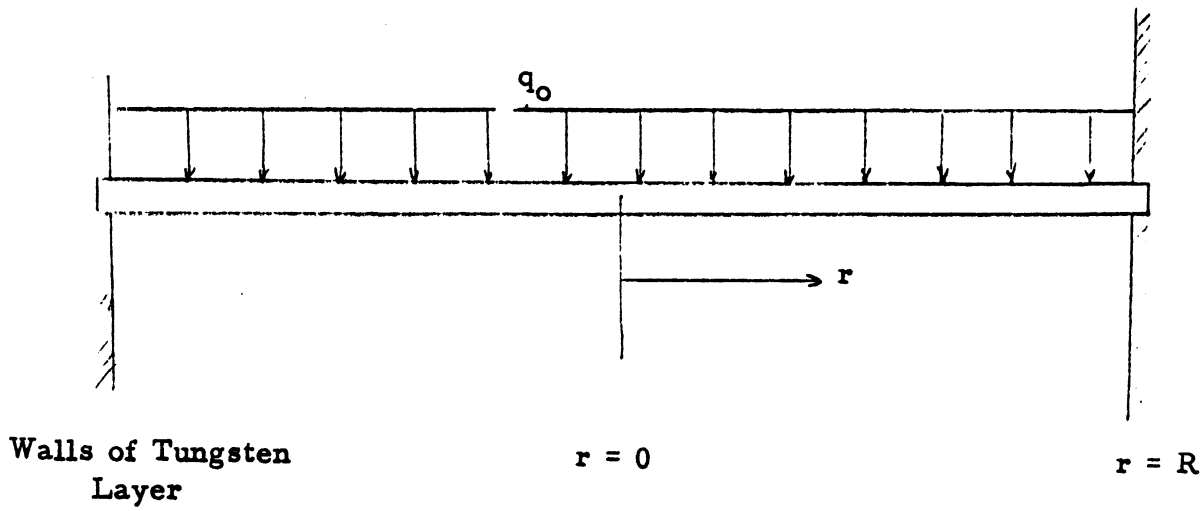

Figure D. 8. 1 Model of Cannister Shelves (Edge View)

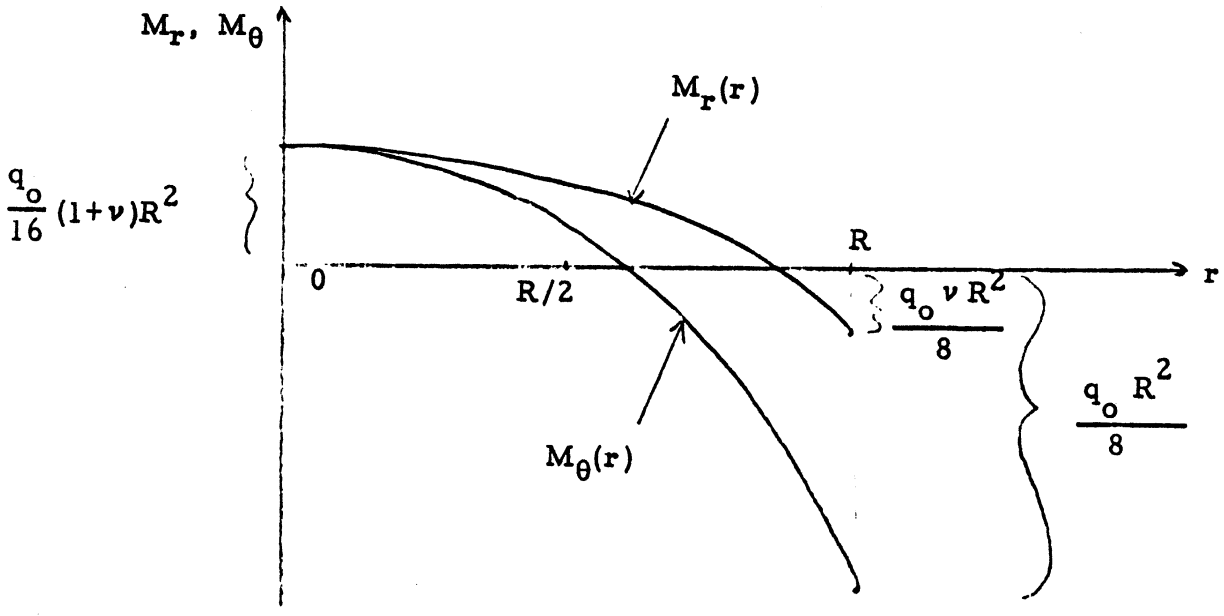

Figure D. 8. 2 Moment Distribution in Shelf as a Function of Radius

$$\therefore \omega(r) = -\frac{1}{D} I_3(r) + B r^2 + E$$

$I_3(r)$ is determined from the following sequence:

a) $$Q(r) = -\frac{1}{r} \int_o^r q(r)\xi \, d\xi = -\frac{1}{r} \int_o^r q_o \xi \, d\xi = -\frac{q_o}{r}\left[\frac{\xi^2}{2}\right]_o^r = -\frac{q_o r}{2}$$

b) $$I_1(r) \equiv \int_o^r Q(\xi) d\xi = -\frac{q_o}{2} \int_o^r \xi \, d\xi = -\frac{q_o}{2}\left[\frac{\xi^2}{2}\right]_o^r = -\frac{q_o r^2}{4}$$

c) $$I_2(r) \equiv \int_o^r \xi I_1(\xi) d\xi = -\frac{q_o}{4} \int_o^r \xi^3 \, d\xi = -\frac{q_o}{16} r^4$$

d) $$I_3(r) \equiv \int_o^r \left(\frac{1}{\xi}\right) I_2(\xi) d\xi = -\frac{q_o}{16} \int_o^r \xi^3 \, d\xi = -\frac{q_o r^4}{64}$$

$$\therefore \omega(r) = \frac{q_o}{64D} r^4 + B r^2 + E \qquad (5.8.3a)$$

We have two unknowns (B, E). Therefore, we need two boundary conditions to completely specify the problem. In this case, the boundary conditions are

$$\omega(r)\Big|_{r=R} = \frac{d\omega}{dr}\Big|_{r=R} = 0$$

Thus, Eq. 5.8.3a becomes

$$\omega(r) = \frac{q_o}{64D}(r^4 - 2R^2 r^2 + R^4) \qquad (5.8.4)$$

We wish to limit the stress on the plate so that it will deform elastically (no permanent deformation).

To establish the appropriate design, the Von Mises yield criterion is used (Reference 9) which states (for plane stress):

$$\sigma_1^2 - \sigma_1 \sigma_2 + \sigma_2^2 = \sigma_{ys}^2 \text{ , for yield} \qquad (5.8.5)$$

σ_1, σ_2 are the principal stresses and σ_{ys} is the yield stress.

In this case, $\sigma_1 = \sigma_r$ (stress in radial direction)

$\sigma_2 = \sigma_\theta$ (stress in circumferential direction).

Thus Eq. 5.8.5 becomes

$$\sigma_r^2 - \sigma_r \sigma_\theta + \sigma_\theta^2 = \sigma_{ys}^2 \qquad (5.8.5a)$$

Thus σ_r, σ_θ must be determined:

1. $\sigma_r = \dfrac{M_r z_{max}}{I}$

where

M_r = moment in the radial direction
$z_{max} = h/2$
$I = h^3/12$.

$$\therefore \sigma_r = -\frac{6 M_r}{h^2} .$$

Now $M_r = -D\left\{\dfrac{d^2\omega}{dr^2} + \dfrac{\nu}{r}\dfrac{d\omega}{dr}\right\}$

$$= -\frac{q_o}{16}(3+\nu)r^2 + \frac{q_o}{16}(1+\nu)R^2, \text{ from Eq. 5.8.4.}$$

2. $\sigma_\theta = -\dfrac{6 M_\theta}{h^2}$, M_θ = moment in circumferential direction

and

$$M_\theta = -D\left\{\frac{1}{r}\frac{d\omega}{dr} + \nu\frac{d^2\omega}{dr^2}\right\}$$

$$= \frac{q_o}{16}\left[(1+\nu)R^2 - (1+3\nu)r^2\right], \text{ from Eq. 5.8.4}$$

M_r, M_θ are plotted in Figure 5.8.2.

From the figure, we see that the maximum biaxial (r, θ) stress state occurs either at r = 0 or at r = R because M_r, M_θ have their extreme values at r = 0, r = R.

Consider r = 0:

$$\sigma_r = -6\left[\frac{q_o}{16}(1+\nu)R^2\right]/h^2 = -.375\, q_o (1+\nu)R^2/h^2$$

$$\sigma_\theta = -6\left[\frac{q_o}{16}(1+\nu)R^2\right]/h^2 = -.375\, q_o (1+\nu)R^2/h^2.$$

Thus, at r = 0, $\sigma_r = \sigma_\theta$.

Consider r = R:

$$\sigma_r = -\frac{6}{h^2}\left(-\frac{q_o R^2}{8}\right) = .75\, q_o R^2/h^2$$

$$\sigma_\theta = -\frac{6}{h^2}\left(-\frac{q_o \nu R^2}{8}\right) = .75\, q_o \nu R^2/h^2.$$

Thus, at r = R, $\sigma_r \neq \sigma_\theta$ (they differ by a factor of ν).

Now, at r = 0, the Von Mises criterion becomes (from Eq. 5.8.5a)

$$\sigma_r \ (= \sigma_\theta) = \sigma_{ys}$$

$$\therefore \ .375 \ q_o \ (1 + \nu) \ (\frac{R}{h})^2 = \sigma_{ys}.$$

Now, at r = R, the criterion becomes (from Eq. 5.8.5a),

$$.75 \ q_o \ (R/h)^2 \ (\nu^2 - \nu + 1)^{1/2} = \sigma_{ys} \ .$$

Stainless steel (347) is used (ν = .31).

Therefore, the biaxial stress at r = 0 gives

$$.49125 \ q_o \ (\frac{R}{h})^2 = \sigma_{ys},$$

and, at r = R:

$$.589575 \ q_o \ (\frac{R}{h})^2 = \sigma_{ys}.$$

Therefore, the plate would yield at r = R.

To prevent yielding, a safety factor of 1.2 is used:

$$\therefore \ 1.2 \ (.589575) \ q_o \ (\frac{R}{h})^2 = \sigma_{ys}$$

For stainless steel, $\sigma_{ys} = 33,000 \ lbf/in^2$

$$\tilde{=} 2.275 \times 10^8 \ N/m^2$$

and ρ (density) = 7930 kg/m^3.

$$\therefore \ h^2 = 1.2 \ (.589575) \ q_o \ R^2/\sigma_{ys}.$$

But, $q_o = \frac{M}{\pi R^2} \ (\ddot{y}_{max})$

$$\therefore \ h = 1.7059 \times 10^{-4} \sqrt{M} \ \text{ meters},$$

where

[M] = kg.

From Section 7, the mass on each shelf is 882 kg.

$$\therefore \ h = .506 \text{ cm to avoid yielding.}$$

A value of $h \cong .507$ cm is chosen. The corresponding deflection at $r = 0$ (maximum deflection) is given by Eq. 5.8.4 and is found to be only 3.18 for $R = 78.33$ cm. This is compatible with the design developed in Section 7. Thus, each shelf has a mass of $\pi R^2 h \rho = 77.5$ kg (170.5 lbs).

D.9 ANALYSIS OF CANNISTER OUTER SHELL (see Reference 5)

We wish to prevent elastic buckling of the stainless steel outer cylinder.

This structure can be modeled as a unity aspect ratio (length/diameter = 1) circularly cylindrical shell.

The appropriate expression for the critical load depends upon the magnitudes of the terms:

$$1)\ \left(\frac{\pi a}{\ell}\right)^2 \text{ and } 2)\ \frac{2a}{t}\ \sqrt{3(1-\nu^2)}$$

where

a = mean cylinder radius
ℓ = cylinder's length
t = wall thickness
ν = Poisson's ratio.

If 1) is the greater quantity, we may use the "Euler-strip" expression:

$$\sigma_{cr} = \frac{\pi^2 E t^2}{12(1-\nu^2)\ell^2}$$

[Note: for longer shells the buckling stress is independent of ℓ.]

where

E = Young's modulus
σ_{cr} = critical (buckling) stress.

If 2) is larger, Donnell's empirical relation is used:

$$\sigma_{cr} = \frac{.6\left(\frac{t}{a}\right) - 10^{-7}\left(\frac{a}{t}\right)}{1 + .004\left(\frac{E}{\sigma_{yp}}\right)}$$

where

σ_{yp} = yield stress.

The outer shell is as shown in Figure 5.9.1.

The solid volume is:

$$\text{Vol.} \cong 2\pi a t \ell + 2\pi a^2 t = 2\pi a t (\ell + a)$$

But $\ell = 2a$.

$$\therefore \text{Vol.} \cong 6\pi a^2 t$$

It is assumed that the shell is rigidly supported at its base, y = 0.

Thus, the total applied stress will be

$$\sigma_{tot} = \sigma_c + \sigma_b$$

where

σ_c = compressive axial stress
σ_b = axial stress due to bending

Now, $\sigma_c \cong m(\ddot{y}_{max})/2\pi a t$

where

$\ddot{y}_{max}$ is the shuttle's maximum acceleration along its longitudinal axis, and m is the mass of the load acting on the shell. (= mass of shell contents)

$\sigma_b \cong \frac{Ma}{I}$, where M = maximum bending moment

I = moment of inertia (2^{nd} moment of area) of shell's cross-section

and

$\sigma_b \cong mg(\ell/2)a/I$, where g = acceleration of gravity.

(This corresponds to horizontal flight (which gives the maximum M)).

Calculation of I:

$$I \equiv \int_A z^2 \, dA = \int_0^{2\pi} \int_{a-t/2}^{a+t/2} r^3 \sin^2\theta \, dr \, d\theta$$

$$\vdots$$

(algebra steps deleted)

$$= \frac{\pi}{4}(4a^3 t + a t^3)$$

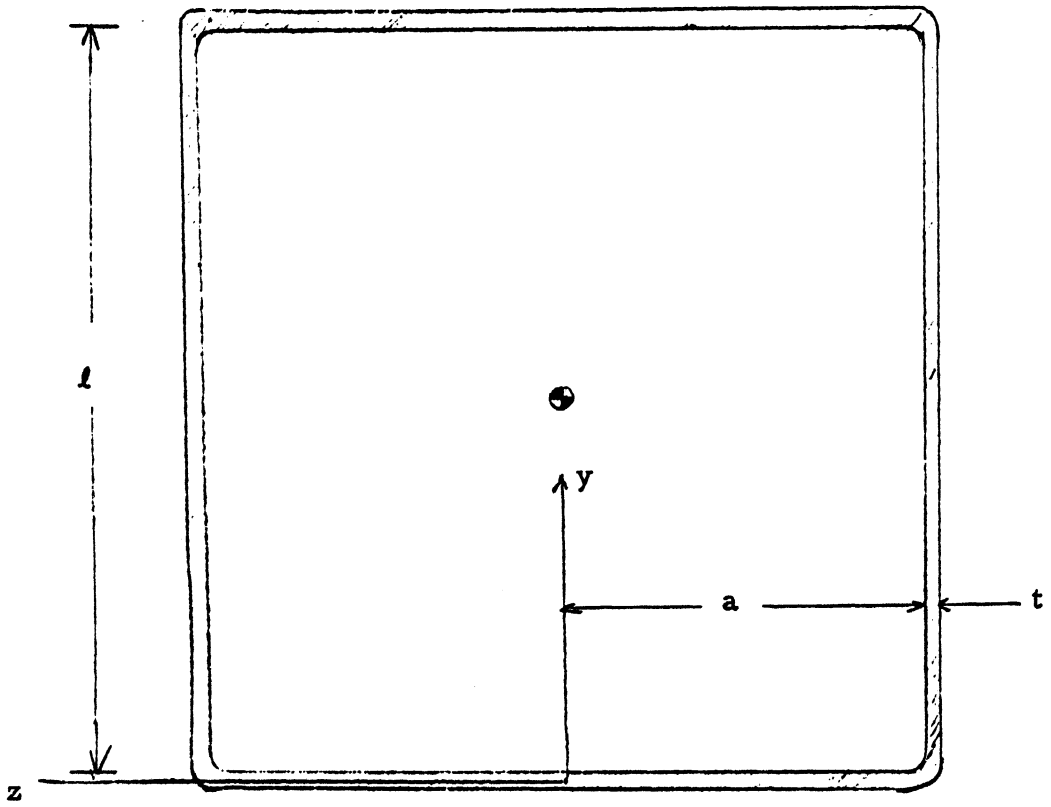

Figure D 9.1 Diagram of Cannister's Outer Shell. (Right Circular Cylinder with ℓ /2a = 1)

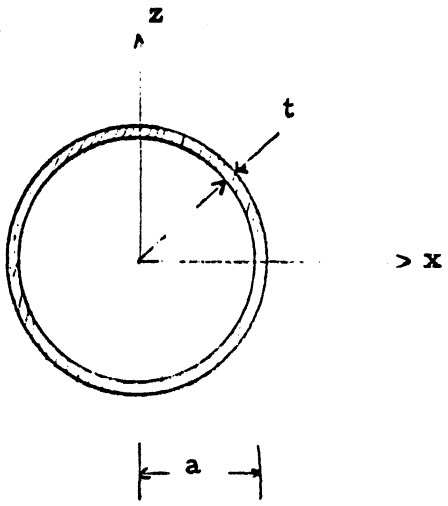

Figure D. 9.2 Diagram for Calculating Moment of Inertia of Shell Cross-Section.

$$\therefore \sigma_b = \frac{mg\,(\ell/2)a}{\pi/4\,a^3t + at^3} = \frac{2mg\ell}{\pi(4a^2t + t^3}$$

$$\therefore \sigma_{tot} = \frac{m(\ddot{y}_{max})}{2\pi at} + \frac{2mg\ell}{\pi(4a^2t + t^3)}$$

$$\therefore \sigma_{tot} = \frac{m[(\ddot{y}_{max})(4a^2 + t^2) + 4agl]}{2\pi at\,(4a^2 + t^2)}$$

(neglecting the mass of the shell).

Now, consider some values of a, t (assume $\nu = .3$)

ℓ	a	t	value of 1)	value of 2)	Appropriate formula
144"	72"	.5"	2.47	475.8	Donnell's

Clearly, for typical shell dimensions, Donnell's is the appropriate formula.

Again, Donnell's formula is:

$$\sigma_{cr} = E\,\frac{.6(t/a) - 10^{-7}(a/t)}{1 + .004\,(E/\sigma_{yp})}$$

A safety factor of 1.2 is used. Therefore, if the total weight of the shell contents is 40,000 lbs (18181.82 kg), we wish to design the shell to withstand the effects caused by,

$$(1.2)(18181.82\text{ kg}) = 21,818.2\text{ kg}\ (1495.4\text{ slugs})$$

Now,

$$\sigma_{tot} = \frac{m[(\ddot{y}_{max})(4a^2 + t^2) + 4agl}{2\pi at\,(4a^2 + t^2)}$$

and

m = 1495.4 slugs, for design purposes.

Our design criterion is given by the equation

$$m\frac{[(\ddot{y}_{max})(4a^2 + t^2) = 4agl]}{2\pi at\,(4a^2 + t^2)} = E\,\frac{.6(t/a) - 10^{-7}(a/t)}{1 + .004\,(E/\sigma_{yp})} \qquad (5.9.1)$$

```
C THIS PROGRAM USES DONNELL'S EQUATION FOR THE BUCKLING STRESS OF A                1.000
C CIRCULARLY SYMMETRIC CYLINDRICAL SHELL. FROM THIS THE SHELL THICKNESS           2.000
C CAN BE FOUND FOR GIVEN PARAMETERS. THE PARAMETERS ARE E(LBS/SQ.IN.),            3.000
C  YP(LBS/SQ.IN.), A(IN.), T(IN.), H(IN.), DENS(GMS/CC), SMASS(SLUGS),            4.000
C HEFT(SLUG)                                                                      4.000
   1  READ(5,100,END=999) E,YP,DENS,A,T,H,ITMAX                                   5.000
      WRITE(6,200) E,YP,DENS,A,H,ITMAX                                            6.000
      DO 2 I=1,ITMAX                                                              7.000
      HEFT=(12*E*(.6*T/A-1.E-07*A/T)/(1.+.004*E/YP))/((1160*(4*A**2               8.000
     1+T**2)+1545.6*A*H)/(2*3.14159*A*T*(4*A**2+T**2)))                           9.000
      IF(HEFT.GE.14954.2) GO TO 3                                                10.000
      T=T+.001                                                                   11.000
   2  CONTINUE                                                                   12.000
   3  SMASS=2*3.14159*A*T*(H+A)*DENS*2.54**3/1000./1.459                         13.000
      WRITE(6,201) I,HEFT,T,SMASS                                                14.000
      GO TO 1                                                                    15.000
 999  STOP                                                                       16.000
 100  FORMAT(F10.1,F10.1,F5.2,F5.2,F5.2,F5.2,I5)                                 17.000
 200  FORMAT('2E     = ',F10.1/'YP   = ',F10.1/'DENS  = ',F5.2/                  18.000
     1'A      = ',F5.2/'H     = ',F5.2/'ITMAX = ',I5)                           19.000
 201  FORMAT('0I     = ',I5/'HEFT  = ',F10.4/'T     = ',F5.3/                   20.000
     1'SMASS = ',F10.4)                                                         21.000
      END                                                                        22.000
```

from which the shell thickness, t, may be determined for a given material.

Note that this expression yields a conservative design because the strengthening effect of the cylinder's end plates has been neglected. Also, the value of σ_{tot} is not likely to be realized in service.

Also, this analysis assumes that the shell carries the entire load of its contents axially (the axial force is transmitted directly to the shell). This axial force, it is assumed, can be replaced by an applied load at the ends of the shell. This leads to a conservative result because the actual load is distributed over the shell's length and has its maximum at the bottom of the shell (the design point).

Once t (thickness) is found from Eq. 5.9.1, the shell mass can be determined from

$$\text{shell mass} = \rho\ (6\pi a^2 t),\ \rho = \text{density of material used.}$$

The values of 't' and shell mass are computed for various values of 'a' (cylinder radius) and for various materials by the following FORTRAN program.

To yield a conservative design, a stainless steel shell, .5 cm thick is used (this value is incorporated into Section 7's design).

.10 DESIGN OF SUPPORT STRUTS FOR THE MASS DRIVER TUBES

The distance between mass driver tubes is .3136 meters.

From Figure 5.10.1, the strut length is given by

$$L = (.3136\ \text{m}) \sin 45^\circ = .4435\ \text{m}$$

and

$$F = (\text{mass of accelerating payload})\ (\text{acceleration of payload})$$

$$= (2.13\ \text{kg})(9,800\ \text{m/sec}^2) = 2.0874 \times 10^4\ \text{Newtons}$$

and

$$FB\ (\text{axial force on strut}) = \frac{2.0874 \times 10^4\ \text{N}}{\cos 45^\circ}$$

$$= 2.9516 \times 10^4\ \text{N.}$$

The buckling load of the strut, Pcr, is

$$Pcr = EI\,(\pi/L)^2$$

For a given cross-sectional area (and hence, mass) of the strut, a square cross-section beam is desirable because it results in a relatively high buckling load.

For a safety factor = 1.2, we have

$$Pcr = \frac{EI(\pi^2/b^2)}{1.2} = \frac{E\,b^4\,\pi^2}{(12)(1.2)L^2} = F_B$$

where

b = length of a side of the strut's corss section.

Thus, for Aluminum 7075-T6 ($E = 7.17 \times 10^{10}$ N/m^2) struts,

b = 1.854×10^{-2} meters and each strut has a mass of
$(2.7 \times 10^3$ kg/m$^3)(1.854 \times 10^{-2}$ m$)^2(.4435$ m$) = \underline{.4116 \text{ kg.}}$

For stainless steel ($E = 2.086 \times 10^{11}$ N/m^2) struts, b = 1.42×10^{-2} m and each strut has a mass of

$$(8.0 \times 10^3 \text{ kg/m}^3)(1.42 \times 10^{-2} \text{ m})^2(.4435 \text{ m}) = .7154 \text{ kg.}$$

Now, there are four struts for every .3136 meters of mass driver length, and the mass driver is 6,320 meters long.

Therefore, there are

$$\left(\frac{4 \text{ struts}}{.3136 \text{ m}}\right)(6320 \text{ m}) = 8.0612 \times 10^4 \text{ struts.}$$

Thus, for Aluminum, the total strut mass is

$$(8.0612 \times 10^4 \text{ struts})(.4116 \text{ kg/strut}) = 3.318 \times 10^4 \text{ kg}$$
$$(7.3 \times 10^4 \text{ lbm})$$

For stainless stell, the total strut mass is

$$(8.0612 \times 10^4 \text{ struts})(.7154 \text{ kg/strut}) = 5.767 \times 10^4 \text{ kg.}$$

Thus, the Aluminum struts result in a more efficient design.

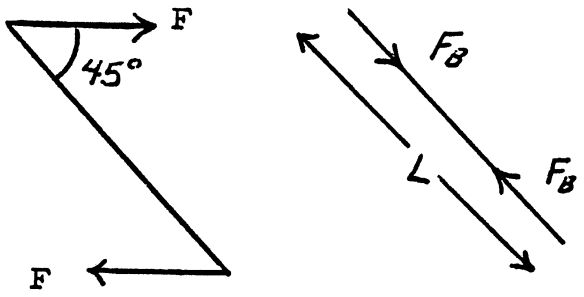

Figure D 10.1

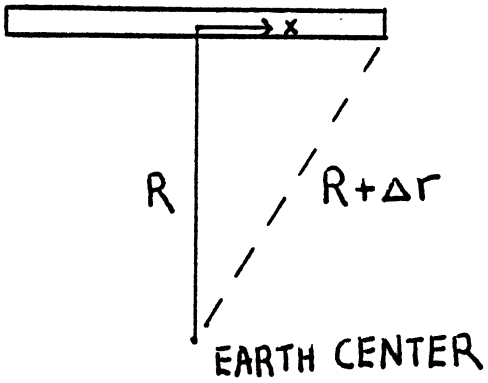

Figure D. 11.1 Geometry of Orbiting Mass Driver

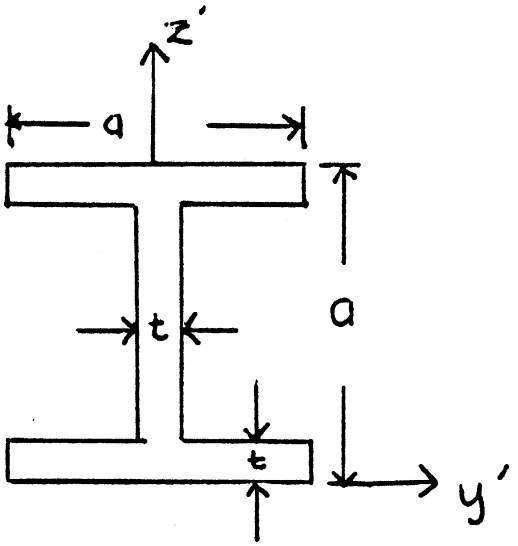

t=.1a

Figure D. 12.1 I-Beam Cross-Section

D.11 INDUCED BENDING MOMENT ON ORBITING MASS DRIVER

The centripetal force, Fc, acting on a body is given by

$$Fa = m v^2/R$$

where

m = mass of body
V = tangential velocity of body
R = radius of circular trajectory

The centripetal force acting on an arbitrary element at a distance x from the mass driver's center of mass is given by (see Figure 5.11.1)

$$d\,Fc = \frac{m\,dx\,(V_c + \Delta V)^2}{R + \Delta R}$$

where

m = mass per unit length

V_c = the circular velocity of the mass driver's e.g. $= \sqrt{\frac{u}{R}}$

where

u = a gravitational constant.

$$\therefore \quad \frac{dv}{dr} = \frac{\sqrt{u}}{R^{3/2}}$$

$$\therefore \quad \Delta V = \frac{\sqrt{u}}{R^{3/2}}\ \Delta R$$

and

$$\Delta R = (R^2 + x^2)^{1/2} - r \quad \text{(Pythagorean theorem).}$$

$$\therefore \quad d\,Fc = m\,dx \left\{ V_c + \frac{\sqrt{u}}{R^{3/2}} [(R^2 + x^2)^{1/2} - R] \right\}^2 / (R^2 + x^2)^{1/2} \qquad (5.11.1)$$

$$\therefore \quad \frac{d\,F_c}{dx} = m \left\{ V_c + \frac{\sqrt{u}}{R^{3/2}} [(R^2 + x^2)^{1/2} - R] \right\}^2 / (R^2 + x^2)^{1/2} \qquad (5.11.2)$$

Eq. 5.11.2 gives the loading distribution on the mass driver and is equal to the 2nd x-derivative off the bending moment distribution, which is the desired quantity.

m = mass/length of the mass driver
V_c = 'local' circular velocity $\cong$ 7.7134 km/sec
u = gravitational parameter $\cong$ 3.986032 km^3/sec^2
R = distance from the center of the earth to the mass driver $\cong$ 6700 km
x = distance to any section of the mass driver from the mass driver's c.g.

If we integrate Eq. 5.11.2 twice and apply the "free-beam" boundary conditions to determine the constants of integration, we obtain the bending moment, M(x).

$$M(x) = 59.1168\, m\left[x\, \ell n\left(x + \sqrt{x^2 + R^2}\right) - \sqrt{x^2 + R^2}\right] + (5.5981 \times 10^{-5})\, m\left(\frac{x^2}{2}\right) + (1.32 \times 10^{-11})\, m\left[\frac{1}{6}\sqrt{(x^2+R^2)^3} + \frac{R^2 m}{2}\left[x\, \ell n\left(x + \sqrt{x^2 + R^2}\right) - \sqrt{x^2 + R^2}\right] - 520.842\, m\, x + 394438.157\, m \right. \quad (5.11.3)$$

where
[M(x)] = kilonewtons - kilometers
[x] = kilometers
[R] = kilometers
[m] = kilograms/kilometer.

This is the induced bending moment which must be counter-acted by the tension-cable support-rod assembly.

D12 ANALYSIS OF TENSION CABLE - SUPPORT ROD SYSTEM

1) Tension cables:

The axial stress, σ_x, in the cables is given by

$$\sigma_x = \frac{T}{A}$$

where
T = tension in cable
A = cable's cross sectional area.

To prevent yielding of the cable, we wish to ensure that the axial stress does not exceed the yield stress (with a safety factor of 1.2)

$$\therefore \quad 1.2\,\sigma_x = (1.2)\,T/A = \sigma_{ys} \qquad \text{where } \sigma_{ys} = \text{yield stress.}$$

$$\therefore \quad A = 1.2\,T/\sigma_{ys} \tag{5.12.1}$$

The length, L, of the cable is given by

$$L = \ell/\cos\theta$$

where ℓ = length of support rod
θ = angle between support rod and cable.

Thus, the mass, M, of each cable is given by

$$M = (LA)\,\rho$$

where ρ = the density of the cable material (stainless steel).

2) Support rods:

The critical (buckling) load of the support rods depends upon cable tension as follows:

$$P_{cr} = 2\,T\cos\theta \tag{5.12.2}$$

where P_{cr} = buckling load
T = maximum allowable cable tension

From beam theory, we find the general expression for a cantilever beam-colum (support rod) to be

$$P_{cr} \cong \frac{1}{4}\left(\frac{\pi}{\ell}\right)^2 EI$$

where E = Young's modulus
I = 2nd moment of area (moment of inertia) of cross-section.

$$\therefore P_{cr} \cong 2.47\,EI/\ell^2.$$

Thus, for a safety factor = 1.2,

$$I = \frac{(1.2)(P_{cr})\ell^2}{(E)(2.47)} \tag{5.12.3}$$

It was determined that a rod with an I-shaped cross section provides a large moment of inertia in relation to its weight. Thus, the I-section is used for the support rods (see Figure 5.12.1).

From the parallel axis theorem, we obtain

$$I_z = .016734\, a^4 \qquad (5.12.4)$$

$$I_y = .1149\, a^4$$

where a is the dimension shown in the figure

and

y, z are the centroidal axes.

Since I_z is smaller than I_y, it is necessary to use I_z in Eq. 5.12.3 to determine 'a', because the rod will seek to buckle about the z-axis, as this mode corresponds to a smaller buckling force.

Now, it is assumed that a maximum cable tension of 1000 lbf (4448 N) is sufficient to counteract the moment outlined in the previous section. Thus, from Eq. 5.12.1 we can determine the cable's cross-sectional area and hence its mass. From Eq. 5.12.2 we have the buckling load and from Eqs. 5.12.3 and 5.12.4 we have the rod's dimensions and hence its mass (the length is known, as explained in Section 5.6).

The following FORTRAN program incorporates these equations to determine, ultimately, the most weight efficient combination of materials, cross-sectional shapes, etc. The results are given in Section 5.6.

D.13 MASS-DRIVER TEMPERATURE CALCULATIONS

Consider the energy-balance equation:

rate of energy absorbed + internal power dissipation = rate at which a body radiates energy.

or

$$\alpha_s\, As\, \dot{q}_s + F\, \alpha_s\, Aa\, \dot{q}_a + F\epsilon\, Ae\, \dot{q}_e + P = \gamma\epsilon\, A_{(surface)}\, T^4 \qquad (5.13.1)$$

where

P = internal power dissipation $\tilde{=}$ 0 by assumption.

α_s = solar absorption of polished aluminum = .20

ϵ = emissivity of polished aluminum = .04

As = mass driver's approximate projected surface area (toward sun) = 3840 m^2

Ae = mass driver's estimated projected surface area (toward earth) = 3840 m^2

$A_{(surface)}$ = estimated surface area of mass driver = 12063.7 m^2

$\dot{q}_s$ = rate of solar flux per unit area = 1396 watts/m^2

SUPPORT ROD AND TENSION CABLE PROGRAM

```
      REAL MOD, MOI, LEN
      DO 500 I = 1, 16
      READ (5, 1000) LEN, TEN, BT
      CBLN = SQRT (2*(LEN**2))
      MOD = 71700000000.0
      YLDST = 289600000.0
      AREA = 1.2* TEN/YLDST
      CBMS = CBLN*AREA*7930
      PCR = 2*TEN*LEN/CBLN
      MOI = PCR*LEN**2/(2.96*MOD)
      IF(BT.EQ.1)GO TO 2
      IF(BT.EQ.2)GO TO 3
    2 STSD=SQRT(SQRT(12*MOI))
      STMS=STSD**2*LEN*2800
      GO TO 4
    3 SIB=SQRT(SQRT(MOI/.016734))
      STMS=.28*SIB**2*LEN*2800
    4 WRITE(6,2000)BT,STMS,CBMS
 1000 FORMAT(F5.2,F10.2,I2)
 2000 FORMAT(I2,2F10.2)
  500 CONTINUE

      END
```

SUPPORT ROD AND TENSION CABLE PROGRAM

PROGRAM TERMINOLOGY

MOD=ELASTICITY MODULUS (ALUMINUM)
MOI=MOMENT OF INERTIA
LEN=DISTANCE BETWEEN STRUTS
TEN=TENSION IN CABLES
BT=BEAM TYPE 1 = SQUARE, 2 = I-BEAM
CBLN=CABLE LENGTH
YLDST=YIELD STRENGTH
AREA=CROSS-SECTIONAL AREA OF CABLE
CBMS=MASS OF CABLE
PCR=CRITICAL BUCKLING LOAD
STSD=SQUARE STRUT DIMENSION
STMS=MASS OF STRUT
SIB=I-BEAM DIMENSION

$\dot{q}_e$ = rate of planetary flux per unit area = 250 watts/m^2
$\dot{q}_a$ = rate of albedo flux per unit area = 502.6 watts/m^2
a = average albedo constant for earth = .36
F = orbit altitude factor = .8854
γ = Boltzman's constant = 5.67×10^{-8} watts/$m^2(^oK)^4$.

From Eq. 5.13.1, the mass driver's surface temperature is

$$T_{surface} = \left[\frac{\alpha_s \, As \, \dot{q}_s + F \, \alpha_s \, Aa \, \dot{q}_a + F \epsilon \, Ae \, \dot{q}_e}{\gamma \epsilon \, A_{(surface)}} \right]^{1/4} \qquad 5.13.2$$

From Eq. 5.13.2, the surface temperatures at positions 1, 2, 3, 4 in Figure 5.8 are

Surface Temp.	^oC	^oF
T_1	206.35	403.43
T_2	161.85	323.33
T_3	-85.45	-121.8
T_4	161.85	323.33

D.14 REFERENCES

1. Nash, William A., Strength of Materials, 21 ed. McGraw-Hill, 1972, p. 42.
2. U.S. NASA Technical Memorandum, TMX-2912.
3. Gibson, A. H., and Ritche, E. G., The Circular Arc Bow Girder, D. Van Nostrand Co, New York, 1915, p. 28.
4. NASA Report (unpublished) on Mass Drivers.
5. Timoshenko, Gene, The Theory of Elastic Stability, McGraw-Hill Book Co., Inc., 1961, Chapter 11.
6. Aerospace Engineering 314 Class Notes (Professor D. L. Sikarskie).
7. Aerospace Engineering 414 Class Notes (Professor J. G. Eisley).
8. Aerospace Engineering 514 Class Notes (Professor D. L. Sikarskie).
9. Applied Mechanics 211 Class Notes, University of Michigan.
10. Boley and Weiner, Theory of Thermal Stress, John Wiley and Sons, Inc. 1960.
11. Space Construction Automated Fabrication Experiment Definition Study (SCAFEDS) Vol. I, General Dynamics, Onvair Division, 1978.
12. Bernstein, I. M., and Pecker, Donald, Handbook of Stainless Steel, McGraw-Hill, 1977.
13. Langton, N. H., Space Research and Technology, Vol. 1: Space Environment American Elsevier Publishing Co., 1969.
14. Mantel, Charles, Engineering Materials Handbook, McGraw-Hill, 1958.
15. Touloukian, Y. S., Thermal Physical Properties of High Temperature Solids, Vol. 1, 5 Collier-Macmillian, 1967.

APPENDIX E

Gravity Gradient Moments

1. General Case

Principal axes at the mass center: x, y, z. α, β, γ are direction cosines of the positive x, y, and z axes relative to the positive direction of $\vec{r}_c$, the position vector of the mass driver center of mass to the center of the force field. Then the gravitational moment is:

$$\vec{M}_g = -\frac{3u}{r_c^3}\left[\beta\gamma(I_{yy} - I_{zz})e_x + \alpha\gamma(I_{zz} - I_{xx})e_y + \alpha\beta(I_{xx} - I_{yy})e_z\right] \qquad (1)$$

2. Long Slender Spacecraft

We consider only pitch rotation about the y-axis so that the structures attitude is in the orbital plane. For this orientation the direction cosines are

$$\alpha = \cos(90 + \phi) = -\sin\phi$$

$$\beta = 0$$

$$\gamma = \cos(180 - \phi) = -\cos\phi$$

From equation (1):

$$\vec{M}_g = -\frac{3u}{r_c^3}\left[\sin\phi\cos\phi\,(I_{zz} - I_{xx})\right] e_y$$

Assuming the mass driver is in the form of a solid homogeneous cylinder of length ℓ and diameter d.

$$I_{yy} = I_{zz} = \frac{M}{12}\left(\frac{3}{4}d^2 + \ell^2\right)$$

$$I_{xx} = \frac{M}{8}d^2$$

$$I_{zz} - I_{xx} = M\left[\frac{3}{48}d^2 + \frac{1}{12}\ell^2 - \frac{1}{8}d^2\right]$$

$$= \frac{M}{12}\left[\ell^2 - \frac{3}{4}d^2\right]$$

This gives us for the moment expression:

$$\vec{M}_g = \frac{3u}{r_c^3} \left[\frac{2 \sin\phi \cos\phi}{2} \frac{M}{12} (\ell^2 - \frac{3}{4} d^2) \right] e_y$$

$$= \frac{1}{8} \frac{u}{r_c^3} m\ell^2 (1 - \frac{3}{4} (\frac{d}{\ell})^2) \sin 2\phi \, e_y$$

or finally

$$\vec{M}_g = \frac{1}{8} \frac{u}{r_c} m (\frac{\ell}{r_c})^2 \left[1 - \frac{3}{4} (\frac{d}{\ell})^2 \right] \sin(2\phi) \, e_y$$

Propulsive Restoring Moment

Let the propulsive force be always linearly distributed as shown.

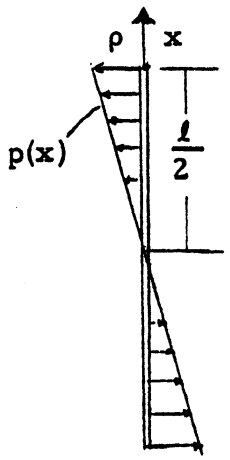

The propulsive "pressure" is then P(N/m) and let the maximum be P at the end of the structure. Thus

$$p = \frac{2P}{\ell} x$$

In terms of P the restoring moment is

$$2 \int_0^{\ell/2} py \, dy = 2 \int_0^{\ell/2} \frac{2P}{\ell} y^2 \, dy = \frac{4P}{\ell} \frac{y^3}{3} \Bigg|_0^{\frac{\ell}{2}} =$$

$$\frac{4P}{3\ell} \cdot \frac{\ell^3}{8} = \frac{1}{6} P\ell^2 \text{ (Nm)}$$

NUCLEAR POWER PLANTS IN THE U.S.

June 30, 1978

The reactor types listed are: Pressurized Water Reactor — PWR; Boiling Water Reactor — BWR; High Temperature Gas-cooled Reactor — HTGR; Liquid Metal Fast Breeder Reactor — LMFBR; Light Water Breeder Reactor — LWBR The reactor manufacturers are: Allis-Chalmers — AC; Babcock & Wilcox — B&W; Combustion Engineering — CE; General Atomic — GA; General Electric — GE; and Westinghouse — W. An asterisk indicates that the plant has been deferred indefinitely and the new start-up date has not been announced. A double asterisk indicates that no start-up date has yet been established.

State and Utility	Plant	Location	Net MWe	Type/Mfr	Operable
ALABAMA					
Alabama Power Co.	**Joseph M. Farley 1**	**Houston County**	**829**	**PWR/W**	**1977**
Alabama Power Co.	Joseph M. Farley 2 (C)	Houston County	829	PWR/W	1980
Tennessee Valley Authority	Bellefonte 1 (C)	Scottsboro	1,235	PWR/B&W	1980
Tennessee Valley Authority	Bellefonte 2 (C)	Scottsboro	1,235	PWR/B&W	1981
Tennessee Valley Authority	**Browns Ferry 1**	**Decatur**	**1,065**	**BWR/GE**	**1973**
Tennessee Valley Authority	**Browns Ferry 2**	**Decatur**	**1,065**	**BWR/GE**	**1974**
Tennessee Valley Authority	**Browns Ferry 3**	**Decatur**	**1,065**	**BWR/GE**	**1976**
ARIZONA					
Arizona Public Service Co. (Salt River Project)	Palo Verde 1 (C)	Wintersburg	1,270	PWR/CE	1982
Arizona Public Service Co. (Salt River Project)	Palo Verde 2 (C)	Wintersburg	1,270	PWR/CE	1984
Arizona Public Service Co. (Salt River Project)	Palo Verde 3 (C)	Wintersburg	1,270	PWR/CE	1986
Arizona Public Service Co.	Palo Verde 4 (O)	Wintersburg	1,270	PWR/CE	1988
Arizona Public Service Co.	Palo Verde 5 (O)	Wintersburg	1,270	PWR/CE	1990
ARKANSAS					
Arkansas Power & Light Co.	**Arkansas Nuclear One—1**	**Russellville**	**850**	**PWR/B&W**	**1974**
Arkansas Power & Light Co.	Arkansas Nuclear One—2 (C)	Russellville	912	PWR/CE	1978
CALIFORNIA					
Pacific Gas and Electric Co.	Diablo Canyon 1 (C)	Avila Beach	1,084	PWR/W	1978
Pacific Gas and Electric Co.	Diablo Canyon 2 (C)	Avila Beach	1,106	PWR/W	1979
Pacific Gas and Electric Co.	**Humboldt Bay**	**Humboldt Bay**	**63**	**BWR/GE**	**1962**
Pacific Gas and Electric Co.	unit 1 (O)	—	1,168	BWR/GE	**
Pacific Gas and Electric Co.	unit 2 (O)	—	1,168	BWR/GE	**
Sacramento Municipal Utility District	**Rancho Seco 1**	**Clay Station**	**918**	**PWR/B&W**	**1974**
Southern California Edison Co. (San Diego Gas and Electric Co.)	**San Onofre 1**	**San Clemente**	**430**	**PWR/W**	**1967**
Southern California Edison Co. (San Diego Gas and Electric Co.)	San Onofre 2 (C)	San Clemente	1,140	PWR/CE	1981
Southern California Edison Co. (San Diego Gas and Electric Co.)	San Onofre 3 (C)	San Clemente	1,140	PWR/CE	1983
COLORADO					
Public Service Company of Colorado	**Fort St. Vrain**	**Platteville**	**330**	**HTGR/GA**	**1973**
CONNECTICUT					
Connecticut Yankee Atomic Power Co.	**Connecticut Yankee**	**Haddam Neck**	**575**	**PWR/W**	**1967**
Northeast Nuclear Energy Co.	**Millstone 1**	**Waterford**	**660**	**BWR/GE**	**1970**
Northeast Nuclear Energy Co.	**Millstone 2**	**Waterford**	**830**	**PWR/CE**	**1975**
Northeast Nuclear Energy Co.	Millstone 3 (C)	Waterford	1,150	PWR/W	1986
FLORIDA					
Florida Power Corp.	**Crystal River 3**	**Red Level**	**825**	**PWR/B&W**	**1976**
Florida Power & Light Co.	**St. Lucie 1**	**St. Lucie County**	**802**	**PWR/CE**	**1976**
Florida Power & Light Co.	St. Lucie 2 (C)	St. Lucie County	842	PWR/CE	1983
Florida Power & Light Co.	**Turkey Point 3**	**Turkey Point**	**693**	**PWR/W**	**1972**
Florida Power & Light Co.	**Turkey Point 4**	**Turkey Point**	**693**	**PWR/W**	**1973**
GEORGIA					
Georgia Power Co. (Oglethorpe Electric Membership Corp.)	Alvin W. Vogtle 1 (C)	Waynesboro	1,100	PWR/W	1984
Georgia Power Co. (Oglethorpe Electric Membership Corp.)	Alvin W. Vogtle 2 (C)	Waynesboro	1,100	PWR/W	1985

Source: Atomic Industrial Forum, June 30, 1978, p. 1-6

Ref. 2, Chapter 7.

State and Utility	Plant	Location	Net MWe	Type/Mfr.	Operable
GEORGIA (continued)					
Georgia Power Co. (Oglethorpe Electric Membership Corp.)	Edwin I. Hatch 1	Baxley	786	BWR/GE	1974
Georgia Power Co. (Oglethorpe Electric Membership Corp.)	Edwin I. Hatch 2	Baxley	795	BWR/GE	1978
ILLINOIS					
Commonwealth Edison Co.	Braidwood 1 (C)	Braidwood	1,120	PWR/W	1981
Commonwealth Edison Co.	Braidwood 2 (C)	Braidwood	1,120	PWR/W	1982
Commonwealth Edison Co.	Byron 1 (C)	Byron	1,120	PWR/W	1981
Commonwealth Edison Co.	Byron 2 (C)	Byron	1,120	PWR/W	1982
Commonwealth Edison Co.	Dresden 1	Morris	200	BWR/GE	1959
Commonwealth Edison Co.	Dresden 2	Morris	794	BWR/GE	1969
Commonwealth Edison Co.	Dresden 3	Morris	794	BWR/GE	1971
Commonwealth Edison Co.	LaSalle 1 (C)	Seneca	1,078	BWR/GE	1979
Commonwealth Edison Co.	LaSalle 2 (C)	Seneca	1,078	BWR/GE	1980
Commonwealth Edison Co.	Zion 1	Zion	1,040	PWR/W	1973
Commonwealth Edison Co.	Zion 2	Zion	1,040	PWR/W	1973
Commonwealth Edison Co. (Iowa-Illinois Gas and Electric Co.)	Quad Cities 1	Cordova	789	BWR/GE	1971
Commonwealth Edison Co. (Iowa-Illinois Gas and Electric Co.)	Quad Cities 2	Cordova	789	BWR/GE	1972
Illinois Power Co.	Clinton 1 (C)	Clinton	950	BWR/GE	1982
Illinois Power Co.	Clinton 2 (C)	Clinton	950	BWR/GE	1988
INDIANA					
Northern Indiana Public Service Co.	Bailly Nuclear 1 (C)	Dunes Acres	660	BWR/GE	1984
Public Service Indiana	Marble Hill 1 (C)	Madison	1,130	PWR/W	1982
Public Service Indiana	Marble Hill 2 (C)	Madison	1,130	PWR/W	1984
IOWA					
Iowa Electric Light and Power Co. (Central Iowa Power Cooperative)	Duane Arnold	Cedar Rapids	538	BWR/GE	1974
Iowa Power and Light Co. (Central Iowa Power Cooperative, Associated Electric Cooperative of Missouri)	Vandalia (O)	Vandalia	1,270	PWR/B&W	•
KANSAS					
Kansas Gas and Electric Co. (Kansas City Power & Light Co.)	Wolf Creek (C)	Burlington	1,150	PWR/W	1983
LOUISIANA					
Gulf States Utilities Co.	River Bend 1 (C)	St. Francisville	934	BWR/GE	1984
Gulf States Utilities Co.	River Bend 2 (C)	St. Francisville	934	BWR/GE	1986
Louisiana Power & Light Co.	Waterford 3 (C)	Taft	1,165	PWR/CE	1981
MAINE					
Maine Yankee Atomic Power Co.	Maine Yankee	Wiscasset	790	PWR/CE	1972
MARYLAND					
Baltimore Gas and Electric Co.	Calvert Cliffs 1	Lusby	845	PWR/CE	1974
Baltimore Gas and Electric Co.	Calvert Cliffs 2	Lusby	845	PWR/CE	1976
MASSACHUSETTS					
Boston Edison Co.	Pilgrim 1	Plymouth	655	BWR/GE	1972
Boston Edison Co.	Pilgrim 2 (O)	Plymouth	1,150	PWR/CE	1985
Northeast Nuclear Energy Co.	Montague 1 (O)	Montague	1,150	BWR/GE	1988-1990
Northeast Nuclear Energy Co.	Montague 2 (O)	Montague	1,150	BWR/GE	1990-1992
Yankee Atomic Electric Co.	Yankee	Rowe	175	PWR/W	1960
MICHIGAN					
Consumers Power Co.	Big Rock Point	Big Rock Point	72	BWR/GE	1962
Consumers Power Co.	Midland 1 (C)	Midland	492	PWR/B&W	1982
Consumers Power Co.	Midland 2 (C)	Midland	818	PWR/B&W	1981
Consumers Power Co.	Palisades	South Haven	805	PWR/CE	1971
Detroit Edison Co.	Enrico Fermi 2 (C)	Lagoona Beach	1,123	BWR/GE	1980
Detroit Edison Co.	Greenwood 2 (O)	St. Clair County	1,208	PWR/B&W	1987
Detroit Edison Co.	Greenwood 3 (O)	St. Clair County	1,208	PWR/B&W	1989
Indiana & Michigan Electric Co.	Donald C. Cook 1	Bridgman	1,054	PWR/W	1974
Indiana & Michigan Electric Co.	Donald C. Cook 2	Bridgman	1,100	PWR/W	1977
MINNESOTA					
Northern States Power Co.	Monticello	Monticello	545	BWR/GE	1970
Northern States Power Co.	Prairie Island 1	Red Wing	530	PWR/W	1973
Northern States Power Co.	Prairie Island 2	Red Wing	530	PWR/W	1974

Source: Atomic Industrial Forum, June 30 1978 p 1-6

State and Utility	Plant	Location	Net MWe	Type/Mfr.	Operable
MISSISSIPPI					
Mississippi Power & Light Co.	Grand Gulf 1 (C)	Port Gibson	1,250	BWR/GE	1981
Mississippi Power & Light Co.	Grand Gulf 2 (C)	Port Gibson	1,250	BWR/GE	1984
Tennessee Valley Authority	Yellow Creek 1 (LWA)	Tishimingo County	1,285	PWR/CE	1985
Tennessee Valley Authority	Yellow Creek 2 (LWA)	Tishimingo County	1,285	PWR/CE	1986
MISSOURI					
Union Electric Co.	Callaway 1 (C)	Callaway County	1,150	PWR/W	1982
Union Electric Co.	Callaway 2 (C)	Callaway County	1,150	PWR/W	1987
NEBRASKA					
Nebraska Public Power District	Cooper	Brownville	778	BWR/GE	1974
Omaha Public Power District	Fort Calhoun 1	Fort Calhoun	457	PWR/CE	1973
NEW HAMPSHIRE					
Public Service Co. of New Hampshire (United Illuminating Co.)	Seabrook 1 (C)	Seabrook	1,194	PWR/W	1982
Public Service Co. of New Hampshire (United Illuminating Co.)	Seabrook 2 (C)	Seabrook	1,194	PWR/W	1984
NEW JERSEY					
Jersey Central Power & Light Co.	Forked River 1 (C)	Lacey Township	1,070	PWR/CE	1983
Jersey Central Power & Light Co.	Oyster Creek	Toms River	650	BWR/GE	1969
Public Service Electric and Gas Co.	Atlantic 1 (O)	Little Egg Inlet (offshore)	1,150	PWR/W	1988
Public Service Electric and Gas Co.	Atlantic 2 (O)	Little Egg Inlet (offshore)	1,150	PWR/W	1990
Public Service Electric and Gas Co.	unit 1 (O)	— (offshore)	1,150	PWR/W	1993
Public Service Electric and Gas Co.	unit 2 (O)	— (offshore)	1,150	PWR/W	1995
Public Service Electric and Gas Co.	Hope Creek 1 (C)	Salem County	1,067	BWR/GE	1984
Public Service Electric and Gas Co.	Hope Creek 2 (C)	Salem County	1,067	BWR/GE	1986
Public Service Electric and Gas Co. (Philadelphia Electric Co.)	Salem 1	Salem	1,090	PWR/W	1976
Public Service Electric and Gas Co. (Philadelphia Electric Co.)	Salem 2 (C)	Salem	1,115	PWR/W	1979
NEW YORK					
Consolidated Edison Co. of N.Y., Inc.	Indian Point 1	Buchanan	265	PWR/B&W	1962
Consolidated Edison Co. of N.Y., Inc.	Indian Point 2	Buchanan	873	PWR/W	1971
Power Authority of the State of New York	Indian Point 3	Buchanan	873	PWR/W	1975
Power Authority of the State of New York	James A. FitzPatrick	Scriba	821	BWR/GE	1974
Power Authority of the State of New York	Greene County (O)	Cementon	1,200	PWR/B&W	1986
Long Island Lighting Co. (New York State Electric & Gas Corp.)	Jamesport 1 (O)	Riverhead	1,150	PWR/W	1988
Long Island Lighting Co. (New York State Electric & Gas Corp.)	Jamesport 2 (O)	Riverhead	1,150	PWR/W	1990
Long Island Lighting Co.	Shoreham (C)	Brookhaven	854	BWR/GE	1980
New York State Electric & Gas Corp. (Long Island Lighting Co.)	unit 1 (O)	—	1,250	PWR/CE	1991
New York State Electric & Gas Corp. (Long Island Lighting Co.)	unit 2 (O)	—	1,250	PWR/CE	1993
Niagara Mohawk Power Corp.	Nine Mile Point 1	Oswego	610	BWR/GE	1969
Niagara Mohawk Power Corp.	Nine Mile Point 2 (C)	Oswego	1,080	BWR/GE	1983
Rochester Gas and Electric Corp.	Robert E. Ginna	Rochester	490	PWR/W	1969
Rochester Gas and Electric Corp. (Orange & Rockland Utilities, Niagara Mohawk Power Corp., Central Hudson)	Sterling (C)	Sterling	1,150	PWR/W	1986
NORTH CAROLINA					
Carolina Power & Light Co.	Brunswick 1	Southport	821	BWR/GE	1976
Carolina Power & Light Co.	Brunswick 2	Southport	821	BWR/GE	1974
Carolina Power & Light Co.	Shearon Harris 1 (C)	New Hill	915	PWR/W	1984
Carolina Power & Light Co.	Shearon Harris 2 (C)	New Hill	915	PWR/W	1986
Carolina Power & Light Co.	Shearon Harris 3 (C)	New Hill	915	PWR/W	1990
Carolina Power & Light Co.	Shearon Harris 4 (C)	New Hill	915	PWR/W	1988
Carolina Power & Light Co.	S.R. 1 (O)	—	1,150	PWR/B&W	1989
Carolina Power & Light Co.	S.R. 2 (O)	—	1,150	PWR/B&W	1991
Duke Power Co.	Thomas L. Perkins 1 (O)	Davie County	1,280	PWR/CE	1988
Duke Power Co.	Thomas L. Perkins 2 (O)	Davie County	1,280	PWR/CE	1991
Duke Power Co.	Thomas L. Perkins 3 (O)	Davie County	1,280	PWR/CE	1993
Duke Power Co.	William McGuire 1 (C)	Cowans Ford Dam	1,180	PWR/W	1979
Duke Power Co.	William McGuire 2 (C)	Cowans Ford Dam	1,180	PWR/W	1981
OHIO					
Cincinnati Gas & Electric Co. (Columbus and Southern Ohio Electric Co., Dayton Power and Light Co.)	Wm. H. Zimmer 1 (C)	Moscow	810	BWR/GE	1979

Source: Atomic Industrial Forum, June 30, 1978, p. 1-6

State and Utility	Plant	Location	Net MWe	Type/Mfr	Operable
OHIO (continued)					
Cincinnati Gas & Electric Co. (Columbus and Southern Ohio Electric Co., Dayton Power and Light Co.)	Wm. H. Zimmer 2 (O)	Moscow	1,150	BWR/GE	•
Central Area Power Coordination Group (CAPCO) [Cleveland Electric Illuminating Co. (operating utility), Duquesne Light Co., Ohio Edison Co., Pennsylvania Power Co., Toledo Edison Co.]	Perry 1 (C)	North Perry	1,205	BWR/GE	1981
Central Area Power Coordination Group (CAPCO) [Cleveland Electric Illuminating Co. (operating utility), Duquesne Light Co., Ohio Edison Co., Pennsylvania Power Co., Toledo Edison Co.]	Perry 2 (C)	North Perry	1,205	BWR/GE	1983
Central Area Power Coordination Group (CAPCO) [Ohio Edison Co. (operating utility), Cleveland Electric Illuminating Co., Duquesne Light Co., Pennsylvania Power Co., Toledo Edison Co.]	Erie 1 (O)	Berlin Heights	1,267	PWR/B&W	1986
Central Area Power Coordination Group (CAPCO) [Ohio Edison Co. (operating utility), Cleveland Electric Illuminating Co., Duquesne Light Co., Pennsylvania Power Co., Toledo Edison Co.]	Erie 2 (O)	Berlin Heights	1,267	PWR/B&W	1988
Central Area Power Coordination Group (CAPCO) [Toledo Edison Co. (operating utility), Cleveland Electric Illuminating Co.]	**Davis-Besse 1**	**Oak Harbor**	**906**	**PWR/B&W**	**1977**
Central Area Power Coordination Group (CAPCO) [Toledo Edison Co. (operating utility), Cleveland Electric Illuminating Co., Duquesne Light Co., Ohio Edison Co., Pennsylvania Power Co.]	Davis-Besse 2 (LWA)	Oak Harbor	906	PWR/B&W	1985
Central Area Power Coordination Group (CAPCO) [Toledo Edison Co. (operating utility), Cleveland Electric Illuminating Co., Duquesne Light Co. Ohio Edison Co., Pennsylvania Power Co.]	Davis-Besse 3 (LWA)	Oak Harbor	906	PWR/B&W	1987
OKLAHOMA					
Public Service Co. of Oklahoma (Associated Electric Cooperative)	Black Fox 1 (O)	Inola	1,150	BWR/GE	1984
Public Service Co. of Oklahoma (Associated Electric Cooperative)	Black Fox 2 (O)	Inola	1,150	BWR/GE	1986
OREGON					
Portland General Electric Co. (Eugene Water & Electric Board)	**Trojan**	**Tainier**	**1,130**	**PWR/W**	**1975**
Portland General Electric Co. (Pacific Power & Light Co., Puget Sound Power & Light Co.)	Pebble Springs 1 (O)	Arlington	1,260	PWR/B&W	1986
Portland General Electric Co. (Pacific Power & Light Co., Puget Sound Power & Light Co.)	Pebble Springs 2 (O)	Arlington	1,260	PWR/B&W	1989
PENNSYLVANIA					
Department of Energy (Power distributed by Duquesne Light Co.)	**Shippingport**	**Shippingport**	**60**	**LWBR/W**	**1977[a]**
Central Area Power Coordination Group (CAPCO) [Duquesne Light Co. (operating utility), Ohio Edison Co., Pennsylvania Power Co.]	**Beaver Valley 1**	**Shippingport**	**852**	**PWR/W**	**1976**
Central Area Power Coordination Group (CAPCO) [Duquesne Light Co. (operating utility), Cleveland Electric Illuminating Co., Ohio Edison Co., Pennsylvania Power Co., Toledo Edison Co.]	Beaver Valley 2 (C)	Shippingport	852	PWR/W	1982
Metropolitan Edison Co. (Jersey Central Power & Light Co., Pennsylvania Electric Co.)	**Three Mile Island 1**	**Londonderry Township**	**819**	**PWR/B&W**	**1974**
Metropolitan Edison Co. (Jersey Central Power & Light Co., Pennsylvania Electric Co.)	**Three Mile Island 2**	**Londonderry Township**	**906**	**PWR/B&W**	**1978**
Pennsylvania Power & Light Co.	Susquehanna 1 (C)	Berwick	1,050	BWR/GE	1981
Pennsylvania Power & Light Co.	Susquehanna 2 (C)	Berwick	1,050	BWR/GE	1982
Philadelphia Electric Co.	Limerick 1 (C)	Limerick Township	1,065	BWR/GE	1985
Philadelphia Electric Co	Limerick 2 (C)	Limerick Township	1,065	BWR/GE	1987
Philadelphia Electric Co. (Public Service Electric and Gas Co.)	**Peach Bottom 2**	**Peach Bottom Township**	**1,065**	**BWR/GE**	**1973**
Philadelphia Electric Co. (Public Service Electric and Gas Co.)	**Peach Bottom 3**	**Peach Bottom Township**	**1,065**	**BWR/GE**	**1974**

[a]Although the original Shippingport core first began to produce power in 1957, the LWBR core went into operation in 1977.

Source: Atomic Industrial Forum, June 30, 1978, p. 1-6

State and Utility	Plant	Location	Net MWe	Type/Mfr	Operable
RHODE ISLAND					
New England Power Co	NEP-1 (O)	Charlestown	1,150	PWR/W	1986
New England Power Co	NEP-2 (O)	Charlestown	1,150	PWR/W	1988
SOUTH CAROLINA					
Carolina Power & Light Co.	H.B. Robinson 2	Hartsville	700	PWR/W	1970
Duke Power Co	Catawba 1 (C)	York County	1,145	PWR/W	1981
Duke Power Co	Catawba 2 (C)	York County	1,145	PWR/W	1983
Duke Power Co	Cherokee 1 (C)	Cherokee County	1,280	PWR/CE	1985
Duke Power Co	Cherokee 2 (C)	Cherokee County	1,280	PWR/CE	1987
Duke Power Co	Cherokee 3 (C)	Cherokee County	1,280	PWR/CE	1989
Duke Power Co	Oconee 1	Lake Keowee	887	PWR/B&W	1973
Duke Power Co.	Oconee 2	Lake Keowee	887	PWR/B&W	1973
Duke Power Co	Oconee 3	Lake Keowee	887	PWR/B&W	1974
South Carolina Electric & Gas Co (South Carolina Public Service Authority)	Virgil C. Summer 1 (C)	Parr	900	PWR/W	1980
TENNESSEE					
Tennessee Valley Authority	Hartsville A-1 (C)	Hartsville	1,205	BWR/GE	1983
Tennessee Valley Authority	Hartsville A-2 (C)	Hartsville	1,205	BWR/GE	1984
Tennessee Valley Authority	Hartsville B-1 (C)	Hartsville	1,205	BWR/GE	1983
Tennessee Valley Authority	Hartsville B-2 (C)	Hartsville	1,205	BWR/GE	1984
Tennessee Valley Authority	Phipps Bend 1 (C)	Surgoinsville	1,220	BWR/GE	1984
Tennessee Valley Authority	Phipps Bend 2 (C)	Surgoinsville	1,220	BWR/GE	1985
Tennessee Valley Authority	Sequoyah 1 (C)	Daisy	1,140	PWR/W	1979
Tennessee Valley Authority	Sequoyah 2 (C)	Daisy	1,140	PWR/W	1980
Tennessee Valley Authority	Watts Bar 1 (C)	Spring City	1,165	PWR/W	1979
Tennessee Valley Authority	Watts Bar 2 (C)	Spring City	1,165	PWR/W	1980
Tennessee Valley Authority (Commonwealth Edison Co.) U.S. Department of Energy)	Clinch River Breeder Reactor Plant (O)	Oak Ridge	350	LMFBR/W	1984
TEXAS					
Gulf States Utilities Co	Blue Hills 1 (O)	Jasper	950	PWR/CE	1989
Gulf States Utilities Co	Blue Hills 2 (O)	Jasper	950	PWR/CE	1991
Houston Lighting & Power Co	Allen's Creek 1 (O)	Wallis	1,150	BWR/GE	1985
South Texas Project (Houston Lighting & Power Co. (project manager) Central Power and Light Co., City Public Service Board of San Antonio City of Austin)	South Texas Project 1 (C)	Matagorda County	1,250	PWR/W	1980
South Texas Project (Houston Lighting & Power Co. (project manager) Central Power and Light Co., City Public Service Board of San Antonio City of Austin)	South Texas Project 2 (C)	Matagorda County	1,250	PWR/W	1982
Texas Utilities Generating Co (Dallas Power & Light Co., Texas Electric Service Co., Texas Power & Light Co.)	Comanche Peak 1 (C)	Somervell County	1,150	PWR/W	1981
Texas Utilities Generating Co (Dallas Power & Light Co., Texas Electric Service Co., Texas Power & Light Co.)	Comanche Peak 2 (C)	Somervell County	1,150	PWR/W	1983
VERMONT					
Vermont Yankee Nuclear Power Corp	Vermont Yankee	Vernon	514	BWR/GE	1972
VIRGINIA					
Virginia Electric and Power Co	North Anna 1	Mineral	907	PWR/W	1977
Virginia Electric and Power Co	North Anna 2 (C)	Mineral	907	PWR/W	1979
Virginia Electric and Power Co	North Anna 3 (C)	Mineral	907	PWR/B&W	1983
Virginia Electric and Power Co	North Anna 4 (C)	Mineral	907	PWR/B&W	1984
Virginia Electric and Power Co.	Surry 1	Gravel Neck	822	PWR/W	1972
Virginia Electric and Power Co	Surry 2	Gravel Neck	822	PWR/W	1973
WASHINGTON					
Puget Sound Power and Light Co (Portland General Electric Co., Pacific Power & Light Co.)	Skagit 1 (O)	Sedro Woolley	1,288	BWR/GE	1985
Puget Sound Power and Light Co. (Portland General Electric Co., Pacific Power & Light Co.)	Skagit 2 (O)	Sedro Woolley	1,288	BWR/GE	1987
Department of Energy (Power distributed by Washington Public Power Supply System)	Hanford — N	Richland	800	Graphite (NRC)	1966
Washington Public Power Supply System	WPPSS 1 (C)	Richland	1,267	PWR/B&W	1982
Washington Public Power Supply	WPPSS 2 (C)	Richland	1,103	BWR/GE	1980
Washington Public Power Supply System	WPPSS 3 (C)	Satsop	1,242	PWR/CE	1984
Washington Public Power Supply System	WPPSS 4 (C)	Richland	1,267	PWR/B&W	1984
Washington Public Power Supply System	WPPSS 5 (C)	Satsop	1,242	PWR/CE	1985
WISCONSIN					
Dairyland Power Cooperative	LaCrosse	Genoa	50	BWR/AC	1967
Northern States Power Co.	Tyrone 1 (C)	Durand	1,100	PWR/W	1985
Wisconsin Electric Power Co.	Haven 1 (O)	Haven	900	PWR/W	1987
Wisconsin Electric Power Co	Haven 2 (O)	Haven	900	PWR/W	1989
Wisconsin Michigan Power Co. (Wisconsin Electric Power Co.)	Point Beach 1	Two Creeks	497	PWR/W	1970
Wisconsin Michigan Power Co. (Wisconsin Electric Power Co.)	Point Beach 2	Two Creeks	497	PWR/W	1971
Wisconsin Public Service Corp (Wisconsin Power and Light Co.)	Kewaunee	Carlton Township	535	PWR/W	1973
PUERTO RICO					
Puerto Rico Water Resources Authority	Isleta (O)	Arecibo	583	PWR/W	

Source: Atomic Industrial Forum, June 30, 1978, p. 16

U.S. Nuclear Powerplant Operations*

		Maximum Dependable Capacity	Average Power	Percent of Total Domestic Electricity Generation
		Thousands of net kilowatts		
1972	AVERAGE	7,726	6,174	3 1
1973	AVERAGE	13,860	8,760	4.5
1974	AVERAGE	29,921	13,011	6.1
1975	AVERAGE	35,671	19,692	9.0
1976	January	36,750	21,638	9 0
	February	36,879	20,657	9 2
	March	38,072	18,808	8.5
	April	39,763	15,142	7 2
	May	39,902	16,034	7 6
	June	39,781	21,885	9 1
	July	40,168	23,807	9 5
	August	42,067	24,681	9.8
	September	42,896	24,014	10 5
	October	42,877	23,327	10.6
	November	43,673	22,408	9.5
	December	42,877	28,380	11.5
	AVERAGE	40,642	21,756	9.4
1977	January	44,316	29,774	11 1
	February	44,282	29,168	12 0
	March	44,289	27,785	12 2
	April	45,131	27,631	12 7
	May	45,222	27,687	12 2
	June	45,991	29,885	11 9
	July	45,984	29,335	11 0
	August	45,987	30,578	11 6
	September	46,051	27,264	11 1
	October	46,088	25,593	11 4
	November	46,088	27 025	11 6
	December	47,133	31,350	12 9
	AVERAGE	45,564	28,640	11.8
1978	January	47,167	34,722	13 1
	February	48,080	32,480	R12 6
	March	48,062	30,173	13 0
	April	48,926	24,451	11 0
	May	48,924	27,441	R11 6
	June	49,714	R30,813	R11 8
	July	49,719	R31,612	12 3
	August	49,815	34,967	12 7
	AVERAGE (8 months)	48,805	31,096	12 3

*Includes all units authorized to generate commercial electricity, including units in startup testing and those owned by the Government.
**Preliminary data
R Revised data
Sources: Capacity data for units in commercial operation or startup testing and Average Power for August 1978 from Nuclear Regulatory Commission. Remaining data from FPC Form 4, "Monthly Powerplant Report."

Source: Dept of Energy: Monthly Energy Review, Oct. 1978, p. 54

FORECAST OF DOMESTIC URANIUM REQUIREMENTS
Tons U_3O_8 – No Recycle

Year	DOE Domestic Tail Enrichment Feed Contracts* Annual	Cumulative
1978	18,600	18,600
1979	21,200	39,800
1980	28,100	67,900
1981	31,200	99,100
1982	33,300	132,400
1983	34,900	167,300
1984	40,300	207,600
1985	41,100	248,700
1986	43,000	291,700
1987	44,600	336,300
1988	44,500	380,800
1989	44,700	425,500
1990	45,600	471,100

*0.20% tails to October 1, 1980, 0.25% tails thereafter. Tails is the amount of U-235 in the depleted uranium stream after enrichment

Source: *Statistical Data of the Uranium Industry*, GJO-100(78), U.S. Department of Energy, January 1, 1978.

Source: INFO News Release, Aug. 1978, p. 5

DOMESTIC URANIUM RESOURCE ESTIMATES AS OF 1/1/78
Tons U_3O_8

$/lb. U_3O_8 Production Cost	Reserves	Potential Resources: Probable	Possible	Speculative	Total
$15	370,000	540,000	490,000	165,000	1,565,000
$15-30 Increment	320,000	475,000	646,000	250,000	1,690,000
$30	690,000	1,015,000	1,135,000	415,000	3,255,000
$30-50 Increment	200,000	380,000	380,000	150,000	1,110,000
$50	890,000	1,395,000	1,515,000	565,000	4,365,000
By Product 1977-2000*	140,000				140,000
	1,030,000	1,395,000	1,515,000	565,000	4,505,000

*By product of phosphate and copper production

Source: *Statistical Data of the Uranium Industry*, GJO-100(78), U.S. Department of Energy, January 1, 1978.

Source: INFO News Release, Aug. 1978, p. 5

ATTAINABLE WORLD URANIUM PRODUCTION CAPABILITIES
Tons U_3O_8

	1977	1980	1985
North America	24,030	37,450	56,460
United States	16,100	26,900	39,500
Canada	7,930	10,330	16,250
Mexico	0	220	710
Africa	11,840	22,100	30,810
South Africa	8,710	15,210	16,250
Niger	2,090	5,330	11,700
Gabon	1,040	1,560	1,560
Central African Empire	0	0	1,300
Australia	520	650	15,340
Europe	3,350	4,990	7,460
France	2,860	3,700	4,810
Spain	250	880	1,650
Portugal	110	120	350
Italy	0	160	160
Germany, F.R.	130	130	260
Yugoslavia	0	0	230
Asia	300	480	430
India	260	260	260
Japan	40	40	40
Turkey	0	130	130
Philippines	0	50	0
South America	170	970	1,280
Argentina	170	470	780
Brazil	0	500	500
Total (rounded)	40,000	67,000	112,000

Source: *Uranium Resources, Production and Demand*, OECD Nuclear Energy Agency and the International Atomic Energy Agency, December 1977. United States statistics from DOE.

Source: INFO News Release Aug 1978 p 6

WORLD URANIUM REQUIREMENTS[1]
Thousand Tons U_3O_8

	Without Recycle				With Recycle[2]			
	"Accelerated"[3] Power Growth		"Present Trend"[4] Power Growth		"Accelerated" Power Growth		"Present Trend" Power Growth	
Year	Annual	Cumulative	Annual	Cumulative	Annual	Cumulative	Annual	Cumulative
1978	38	68	38	68	38	68	38	68
1979	45	113	45	113	45	113	45	113
1980	56	169	53	166	56	169	53	166
1981	66	235	61	227	66	235	61	227
1982	78	313	69	296	78	313	69	296
1983	90	403	77	373	87	400	74	370
1984	103	506	84	458	96	497	79	450
1985	114	620	92	550	107	603	84	534
1986	127	747	101	651	117	720	90	624
1987	144	892	109	760	127	848	95	719
1988	162	1,054	117	877	138	985	100	819
1989	182	1,236	125	1,002	149	1,135	105	924
1990	203	1,439	133	1,135	164	1,299	110	1,035

[1] Based on 0.25% U-235 enrichment plant tails assay. Tails is the amount of U-235 in the depleted uranium stream after enrichment.
[2] Beginning in 1985.
[3] Assumes the goals of ambitious nuclear power programs, planned in response to the oil embargo, rising costs, and the possible unavailability of conventional fuels.
[4] Perceives current patterns of energy utilization supply as well as present delays in the construction of new reactors and generally assumes a continuation of these trends.

Source: *Uranium Resources, Production and Demand*, OECD Nuclear Energy Agency and the International Atomic Energy Agency, December 1977.

Source: INFO News Release Aug 1978 p 6

WORLD URANIUM RESOURCES
(As of January 1, 1977)
Thousand Tons U_3O_8

	Reasonably Assured			Estimated Additional		
	<$30/lb. U_3O_8 Reserves	$30-50/lb.	Total	<$30/lb. U_3O_8	$30-50/lb.	Total
North America	913	227	1,140	1,633	684	2,317
United States	690	200	890	1,120	330	1,450
Canada	217	19	236	510	343	853
Mexico	6	0	6	3	0	3
Denmark	0	8	8	0	11	11
Africa	680	63	743	196	62	258
South Africa	398	55	453	44	49	93
Niger	208	0	208	69	0	69
Algeria	36	0	36	65	0	65
Gabon	26	0	26	6	6	12
Central African Empire	10	0	10	10	0	10
Zaire	2	0	2	2	0	2
Somalia	0	8	8	0	4	4
Madagascar	0	0	0	0	3	3
Australia	376	9	385	57	6	63
Europe	81	417	498	58	57	115
France	48	19	67	31	26	57
Spain	9	0	9	11	0	11
Portugal	9	2	11	1	0	1
Yugoslavia	6	3	9	6	20	26
United Kingdom	0	0	0	0	10	10
Germany, F.R.	2	1	3	4	1	5
Italy	2	0	2	1	0	1
Austria	2	0	2	0	0	0
Sweden	1	390	391	4	0	4
Finland	2	2	4	0	0	0
Asia	54	4	58	31	0	31
India	39	0	39	31	0	31
Japan	10	0	10	0	0	0
Turkey	5	0	5	0	0	0
Korea*	0	4	4	0	0	0
Philippines	*	0	*	0	0	0
Central & South America	47	31	78	18	1	19
Brazil	24	0	24	11	0	11
Argentina	23	31	54	0	0	0
Chile	0	0	0	7	0	7
Bolivia	0	0	0	0	1	1
Grand Total (rounded)	2,200	700	2,900	2,000	800	2,800

*Less than 1,000 Tons of U_3O_8.

Source: *Uranium Resources, Production and Demand*, OECD Nuclear Energy Agency and the International Atomic Energy Agency, December 1977. United States statistics from DOE.

Source: INFO News Release, Aug 1978, p 7

ACKNOWLEDGEMENTS

Prof. Harm Buning, Aerospace Engineering, University of Michigan
Prof. J. Eisley, Aerospace Engineering, University of Michigan
Mr. Kevin Fine, Francis Bitter National Magnet Laboratory, MIT
Mr. William Gilbrath, NASA, Ames
Mr. Keith Henson, Analog Precision, Inc.
Mr. Lyle Jenkins, NASA Johnson Space Center
Mr. B. R. Klein, Bechtel Associates Professional Corp.
Dr. Henry Kolm, Francis Bitter National Magnet Laboratory, MIT
Mr. Don Kopinski, Bechtel Associates Professional Corp.
Mr. Don McKeon, University of Michigan
Mr. Walter K. Muench, Grumman Aerospace Corp.
Dr. B. E. Schutz, University of Texas
Prof. R. A. Scott, Applied Mechanics, University of Michigan
Prof. David L. Sikarskie, Aerospace Engineering, University of Michigan
Dr. F. J. Stebbins, NASA Johnson Space Center
Dr. Victor Szebehely, Aerospace Engineering, University of Texas
Prof. John E. Taylor, Applied Mechanics, University of Michigan
Mr. Thomas Van Flandern, U. S. Naval Observatory
Mr. Fred Williams, MIT

A special thank you is extended to the following persons for taking the time to lecture to the team and assisting us in our efforts:

Mr. Alan L. Friedlander, Science Applications, Inc.
Prof. Robert M. Howe, Aerospace Engineering, University of Michigan
Prof. C. Kikuchi, Nuclear Engineering, University of Michigan

Most of all we extend a very special thanks to Professor Harm Buning for his guidance throughout the project. We would also like to thank Ann Gee for her typing throughout the term and Caroline Rehberg for her efforts in typing this report.